Waveguide Quasi-Phase-Matched Sum-Frequency Generation Device for High-Efficiency Optical Sampling

T. Suhara, *Senior Member, IEEE*, H. Ishizuki, M. Fujimura, *Member, IEEE*, and H. Nishihara, *Fellow, IEEE*

***Abstract*— A $LiNbO_3$ waveguide quasi-phase-matched sum-frequency generation (SFG) device using a fan-out domain-inverted grating for picosecond optical sampling was designed and fabricated. Sampling of signal waves at 1.5-μm wavelength by 25-ps sampling pulses generated by a gain-switched laser diode is demonstrated in a device of 5 mm length with a normalized SFG efficiency as high as 43%/W.**

***Index Terms*—Nonlinear optics, optical sampling, optical signal processing, optical waveguide, quasi-phase matching, sum-frequency generation, wavelength conversion.**

I. Introduction

NONLINEAR waveguide quasi-phase-matching (QPM) structures can perform wavelength conversion as well as various high-speed optical signal processing. Autocorrelation measurement of picosecond optical pulses [1] and self phase modulation [2] in QPM waveguides have been demonstrated. Optical switching [3] and pulse compression [4] have been demonstrated using bulk QPM structures.

High-speed optical sampling [5] using ultrashort optical pulses is an important technique for optical waveform measurements and demultiplexing of TDM optical signals. Ultrafast sampling based on Type-II phase matched sum-frequency generation (SFG) in bulk KTP and organic crystals has been demonstrated [6], [7]. The SFG efficiencies, however, were in the order of 10^{-2}%/W or less, and the experiments required optical amplifiers for signal and sampling pulses. Waveguide QPM-SFG devices would offer advantages of much higher efficiencies and larger flexibility for signal and sampling wavelengths. In this letter, we present design, fabrication and experimental demonstration of a $LiNbO_3$ waveguide QPM-SFG device for efficient picosecond optical sampling.

II. Device Description and Design

Fig. 1 illustrates a $LiNbO_3$ waveguide QPM-SFG device for optical sampling. The device consists of an array of channel waveguide and a ferroelectric-domain inverted grating of a fan-out pattern [8]. A signal wave of frequency ω_1 (wavelength λ_1) and sampling pulses of ω_2 ($\neq\omega_1$) (λ_2) are combined together and coupled into a waveguide channel. The dependence of the QPM grating period on λ_1, λ_2 in 1.5-μm band calculated by using the extraordinary index dispersion of bulk crystal is shown in Fig. 2 with $\Delta\lambda = \lambda_1 - \lambda_2$ as a parameter. At or near the QPM condition, sum-frequency ($\omega_3 = \omega_1 + \omega_2$) wave ($\lambda_3$) of a power P_3 proportional to the product of the signal and sampling wave powers P_1, P_2 is generated, and therefore the device serves as an optical multiplier for sampling. The SF wave can easily be detected by a near-infrared detector with appropriate time constant to give a sampling signal.

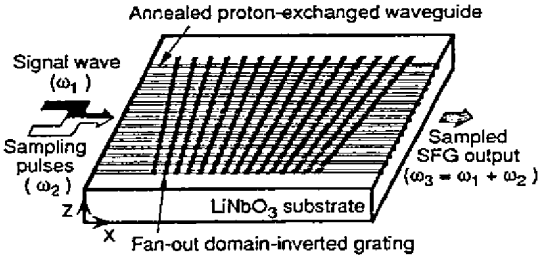

Fig. 1. Schematic illustration of a waveguide QPM-SFG device for optical sampling.

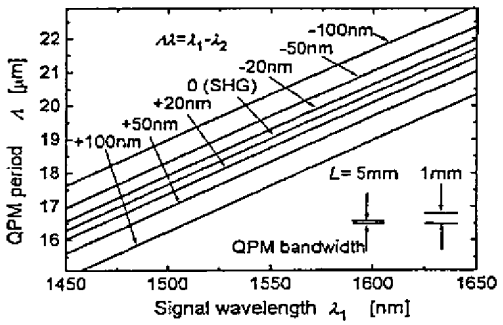

Fig. 2. Dependence of the QPM grating period on the input wavelengths.

For continuous-wave (CW) input waves, the P_3 is given approximately by

$$P_3 = \kappa^2 P_1 P_2 L^2 \{\sin(\Delta L)/\Delta L\}^2,$$
$$2\Delta = 2\pi(N_3/\lambda_3 - N_1/\lambda_1 - N_2/\lambda_2 - 1/\Lambda) \quad (1)$$

where L is the device length, Λ the grating period, κ the SFG coupling coefficient, $N_{1,2,3}$ the effective indexes for $\lambda_{1,2,3}$

Manuscript received February 23, 1999.
This work was supported by a Grant-in-Aid from the Ministry of Education, Science and Culture, and Research for the Future Project of Japan Society for the Promotion of Science.
The authors are with Department of Electronics, Graduate School of Engineering, Osaka University, Osaka 565-0871, Japan.
Publisher Item Identifier S 1041-1135(99)05904-2.

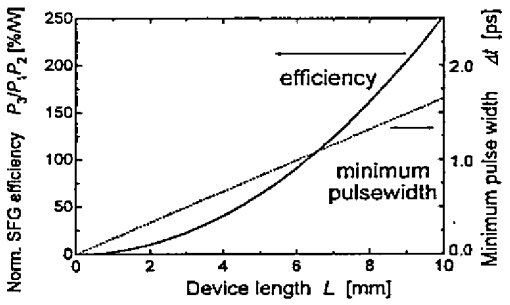

Fig. 3. Calculated dependence of the normalized SFG efficiency and minimum pulsewidth on the device length.

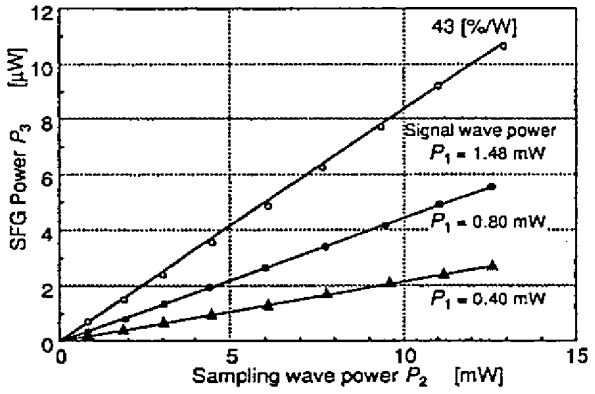

Fig. 4. Measured dependence of the SFG power upon input powers.

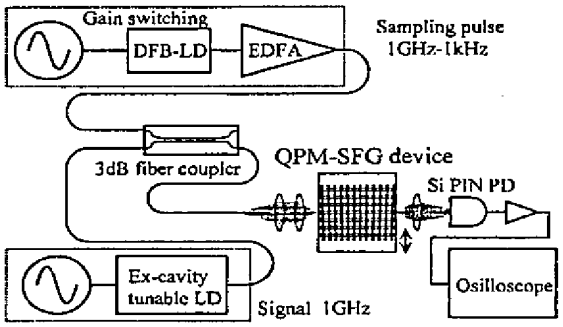

Fig. 5. Experimental setup for optical sampling.

waves, and Δ denotes the deviation from exact QPM. The QPM bandwidth for SFG in terms of the grating period Λ is 0.32, 0.064 μm for $L = 1$, 5 mm, respectively, as shown in Fig. 2. At the QPM-SFG condition ($\Delta = 0$), weak (phase-mismatched) second-harmonic generation (SHG) of λ_1, λ_2 waves may take place, and the SH waves affect the sampling performance as noise. The $\lambda_1/2$ and $\lambda_2/2$ SH powers, P_{11} and P_{22}, are given by formulae similar to (1) with SHG coupling coefficient κ_{SHG} ($\kappa = 2\kappa_{\mathrm{SHG}}$ for $\lambda_1 \sim \lambda_2$) [9]. The extinction ratio may be defined as the ratio of residual SHG maximum (envelope) power to the SFG power $(P_{11\mathrm{env}} + P_{22\mathrm{env}})/P_3$. A large extinction can be obtained by choosing an appropriate wavelength separation $\Delta\lambda$ depending on L.

For SFG of short pulses, wavelength bandwidths of the pulses, pulse broadening in the dispersive waveguide, and walkoff between the input and SF pulses must be considered. Simple calculation assuming Fourier-transform limited picosecond pulses shows that, in a $LiNbO_3$ waveguide of $L \leq 10$ mm, the broadening and walkoff are so small that their effects can be neglected. For efficient SFG, however, the wavelength bandwidth must be within the QPM width which decreases with increasing L. Thus, the QPM width dominates the lower limit for the sampling pulsewidth. Fig. 3 shows the dependence of the normalized SFG efficiency at exact QPM, $P_3/P_1P_2 = \kappa^2L^2$, and the minimum pulsewidth upon L. A $LiNbO_3$ waveguide of 192 μm^2 effective cross section S_{eff} [9] with a grating of 1:1 duty ratio is assumed. The result indicates that picosecond sampling with efficiency higher than 100%/W (~0 dB with 1-W peak sampling pulses) can be obtained. For example, 63%/W SFG efficiency, 1-ps minimum pulsewidth and 18-dB extinction are expected for $L = 5$ mm, $\Delta\lambda = 20$ nm and $P_1/P_2 = 0.1$.

III. Fabrication

A SFG device consisting of a fan-out grating of $\Lambda = 16.0$–18.7 μm and 80 waveguide channels of $L = 5$ mm was fabricated. The fabrication process is similar to that of SHG and difference-frequency generation (DFG) devices reported previously [10], [11]. At first domain-inverted gratings were fabricated in a z-cut $LiNbO_3$ crystal of 0.15 mm thickness by applying a voltage pulse of ~4 kV between a corrugation electrode on the $+z$ surface and a uniform electrode on the $-z$ surface. The pulse duration was automatically controlled to give a predetermined inversion charge. The grating has ~1:1 duty ratio and it continues through the entire crystal thickness. Then the waveguide array was fabricated by proton exchange in benzoic acid at 200 °C for 1.5 h using an Al film mask with 3.5-μm-wide channel openings followed by annealing at 350 °C for 4 h in oxygen atmosphere. Finally, the waveguide input/output ends were polished for end-fire coupling.

IV. Experimental Result

The SFG characteristics were first measured by CW operation. An external-cavity tunable LD and a DFB LD were used as light sources of λ_1 and λ_2. Both waves were combined by a 3-dB fiber coupler and coupled into the waveguide to excite fundamental TM modes. A channel was selected to accomplish QPM, and for λ_1, λ_2 = 1573, 1542 nm, strongest SFG of λ_3 = 779 nm was obtained in a channel of 16.47-μm grating period. The mode sizes (FWHM) were measured as 7.2×6.3 μm^2 for λ_1, λ_2 and 2.4×1.8 μm^2 for λ_3 ($S_{\mathrm{eff}} = 192$ μm^2). Fig. 4 shows the dependence of P_3 upon P_1, P_2 measured at the waveguide output end. A normalized SFG efficiency of 43%/W was obtained. This value compares fairly well with the theoretically estimated value of 63%/W. The SFG bandwidth in terms of λ_1 was 4 nm, which was in good agreement with the theoretical value of 4.2 nm.

Fig. 5 shows the setup for demonstration of optical sampling. A DFB LD was driven by a ~1 GHz sinusoidal

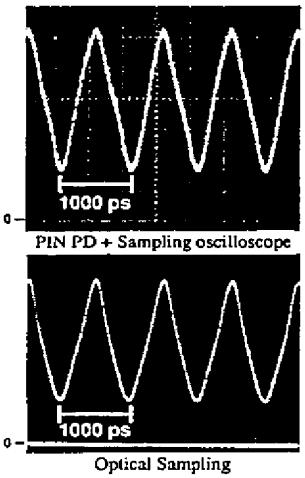

Fig. 6. Obtained sampling signal.

wave with small dc bias to generate sampling pulses by gain switching. The pulses ware amplified by an Er-doped fiber amplifier. The average power of the coupled sampling pulses was roughly 10 mW. The pulsewidth was measured as 25 ps by a SHG autocorrelator. The wavelength and the bandwidth were $\lambda_2 = 1543$ and 0.6 nm, respectively. The external cavity LD was directly modulated by a 1-GHz sinusoidal wave to produce a signal wave of $\lambda_1 = 1577$ nm and 5-mW average power. The SFG output was detected by a Si p-i-n photodiode (insensitive in the 1.5-μm band) and displayed on an oscilloscope of 1-MΩ input impedance. When the repetition frequencies of the signal wave and sampling pulses were set at 1 GHz and 1 GHz–1 kHz, respectively, a sampling signal of 1-kHz repetition, which is a time-converted replica of the signal waveform, was obtained as shown in Fig. 6. The waveform directly observed by a high-speed InGaAs p-i-n photodiode and a sampling oscilloscope of 50-Ω input impedance is also shown for comparison. It should be noted that the level of the optical sampling signal was orders of magnitude higher than that of the direct detection. Observations of several different waveforms showed that the time resolution was consistent with the 25-ps sampling pulsewidth. The residual SHG level was smaller than 5% of the SFG sampling signal level.

V. Conclusion

High-efficiency picosecond optical sampling using a $LiNbO_3$ waveguide QPM-SFG device has been demonstrated for the first time. Obtained efficiency was three orders of magnitude higher than that of sampling by bulk crystals. Experimental work is being continued for improvements of efficiency and time resolution and integration with couplers.

References

[1] A. Galvanauskas, J. Webjorn, A. Krotkus, and G. Arvidsson, "Autocorrelation measurements of picosecond laser-diode pulses by means of quasiphase-matching $LiNbO_3$ channel waveguides," *Electron. Lett.*, vol. 27, pp. 738–740, 1991.

[2] M. Sundheimer, C. Bosshard, E. Van Stryland, G. Stegeman, and J. Bierlein, "Large nonlinear phase modulation in quasiphase-matched KTP waveguides as a result of cascaded second-order processes," *Opt. Lett.*, vol. 18, pp. 1397–1399, 1993.

[3] M. Asobe, I. Yokohama, H. Itoh, and T. Kaino, "All-optical switching by use of cascading of phase-matched sum-frequency-generation and difference-frequency-generation processes in periodically poled $LiNbO_3$," *Opt. Lett.*, vol. 22, pp. 274–276, 1997.

[4] M. Arbore, A. Galvanauskas, D. Harter, M. Chou, and M. Fejer, "Engineerable compression of ultrashort pulses by use of second-harmonic generation in chirped-period-poled lithium niobate," *Opt. Lett.*, vol. 22, pp. 1341–1343, 1997.

[5] T. Kanada and D. Franzen, "Optical waveform measurement by optical sampling with mode-locked laser diode," *Opt. Lett.*, vol. 11, pp. 4–6, 1986.

[6] H. Takara, S. Kawanishi, T. Morioka, K. Mori, and M. Saruwatari, "100 Gbit/s optical waveform measurement with 0.6 ps resolution optical sampling using subpicosecond supercontinuum pulses," *Electron. Lett.*, vol. 30, pp. 1152–1153, 1994.

[7] H. Takara, S. Kawanishi, A. Yokoo, S. Tomaru, T. Kitoh, and M. Saruwatari, "100 Gbit/s optical signal eye-diagram measurement with optical sampling using organic nonlinear optical crystal," *Electron. Lett.*, vol. 32, pp. 2256–2258, 1996.

[8] Y. Ishigame, T. Suhara, and H. Nishihara, "$LiNbO_3$ waveguide second-harmonic generation device phase matched with a fan-out domain-inverted grating," *Opt. Lett.*, vol. 16, pp. 375–377, 1991.

[9] T. Suhara and H. Nishihara, "Theoretical analysis of waveguide second-harmonic generation phase matched with uniform and chirped gratings," *IEEE J. Quantum Electron.*, vol. 26, pp. 1265–1276, 1990.

[10] K. Kintaka, M. Fujimura, T. Suhara, and H. Nishihara, "High- efficiency $LiNbO_3$ waveguide second-harmonic generation devices with ferroelectric-domain-inverted gratings fabricated by applying voltage," *J. Lightwave Technol.*, vol. 14, pp. 462–468, 1996.

[11] M. Fujimura, A. Shiratsuki, T. Suhara, and H. Nishihara, "Wavelength conversion in $LiNbO_3$ waveguide difference frequency generation devices with domain-inverted gratings fabricated by voltage application," *Jpn. J. Appl. Phys.*, vol. 37, pt. 2, no. 6A, pp. L659–L662, 1998.

1.5-μm-Band Wavelength Conversion Based on Cascaded Second-Order Nonlinearity in $LiNbO_3$ Waveguides

M. H. Chou, I. Brener, M. M. Fejer, E. E. Chaban, and S. B. Christman

Abstract—**We report wavelength conversion and spectral inversion using cascaded second-order nonlinearity in periodically poled $LiNbO_3$ waveguides pumped at 1.5 μm. The converter has an internal conversion efficiency of −8 dB, a conversion bandwidth of 76 nm, and a constant conversion efficiency for the 50-dB range of signal powers tested.**

Index Terms—**Nonlinear optics, optical fiber communications, optical frequency conversion, wavelength conversion, wavelength-division multiplexing.**

WAVELENGTH conversion is an important function in wavelengt-division multiplexed (WDM) optical networks. Among numerous demonstrated wavelength conversion techniques, difference frequency generation (DFG) [1] is attractive in several respects: it is an instantaneous process that easily accommodates more than terahertz modulation bandwidths, can simultaneously up and down convert multiple channels with equal efficiencies, has negligible spontaneous emission noise and has no intrinsic frequency chirp.

DFG-based wavelength converters have been demonstrated in AlGaAs [1], [2] and $LiNbO_3$ waveguides [3]–[5], showing promising results for WDM wavelength conversion. However, the use of DFG and current device efficiencies indictate the need for a single mode pump laser with ~50–100 mW of power operating in the 750–800-nm range. Moreover, it is difficult to simultaneously launch the 780-nm pump and 1.5-μm band signals into the fundamental mode of the waveguide, although this has been solved using an integrated mode coupling structure [4] In this letter, we demonstrate wavelength conversion in $LiNbO_3$ waveguides using a cascaded second-order nonlinearity ($\chi^{(2)} : \chi^{(2)}$) [6]–[8], where both the input pump and signals are in the 1.5-μm band. Mode matching in this case is simplified compared to DFG pumped at 780 nm, since all input wavelengths are in the same band and can be launched into a single port.

The $\chi^{(2)} : \chi^{(2)}$-based device for 1.5-μm band wavelength conversion uses a pump in the 1550-nm region. The pump at frequency ω_p is upconverted to frequency $2\omega_p$ by second-harmonic generation (SHG) via the second-order nonlinearity $\chi^{(2)}$. The generated $2\omega_p$ simultaneously mixes with input signals ω_s to generate wavelength shifted outputs $\omega_{out} = 2\omega_p - \omega_s$ by DFG via another $\chi^{(2)}$ process. Phasematching between interacting waves for both SHG and DFG is required, and this can be accomplished by choosing an appropriate quasi-phasematching (QPM) grating period. It is interesting to note that this $\chi^{(2)} : \chi^{(2)}$ process mimics four-wave mixing (FWM) which uses the third-order nonlinearity $\chi^{(3)}$. The effective $\chi^{(3)}$ of such process in $LiNbO_3$ under quasiphase-matching condition is 10^4–10^5 times larger than that of silica glass. The $\chi^{(2)} : \chi^{(2)}$ allows the use of a very short sample when compared to fiber, and has better noise figure compared to FWM in semiconductor optical amplifiers. The converted output is related to pump power and input signal power in the low conversion efficiency approximation by [7]

$$P_{out} \approx \tfrac{1}{4}\eta^2 L^4 P_p^2 P_s \qquad (1)$$

where P_{out}, P_p, and P_s are converted output power, pump power and signal power, respectively. η is the normalized efficiency (the same for SHG and near degenerate DFG) in units of $mW^{-1}\cdot cm^{-2}$ (this number is proportional to both the mode overlap between the interacting waves and the material nonlinearity $\chi^{(2)}$), and L is the interaction length. The conversion efficiency scales with the fourth power of the interaction length, so doubling the device length will increase the conversion efficiency by a factor of 16. In the high-conversion efficiency regime, the exponent of L in 1 is less than 4 due to pump depletion. In an optimized $LiNbO_3$ waveguide with a normalized efficiency of $150\%/W\cdot cm^2$ (or $0.0015\ mW^{-1}\cdot cm^{-2}$) and 6-cm interaction length, one can achieve 0-dB conversion efficiency with ~75 mW of pump power; or 3-dB gain with ~100 mW of pump power.

We fabricated the waveguides by annealed proton exchange in periodically poled $LiNbO_3$ (PPLN) [9]. The device used in this experiment is 4 cm long, has a QPM period of 15 μm, waveguide width of 12 μm, proton exchange depth of 0.7 μm, and was annealed for 26 h at 325 °C. The above parameters allow phasematching at room temperature between the fundamental mode of the pump at 1556 nm and the fundamental mode of SHG wave at 778 nm. We can tune the pump wavelength by using waveguides with different QPM period and/or temperature tuning. The normalized efficiency of this device is $65\%/W\cdot cm^2$. One can achieve a normalized efficiency of $150\%/W\cdot cm^2$ by optimizing the mode overlap

Manuscript received November 24, 1998; revised February 16, 1999. This work was supported by the Office of Naval Research through JSEP, by Lucent Technologies, and by the Defense Advanced Research Projects Agency through the CNOM at Stanford University, Stanford, CA.

M. H. Chou and M. M. Fejer are with E. L. Ginzton Laboratory, Stanford University, Stanford, CA 94305-4085 USA.

I. Brener, E. E. Chaban, and S. B. Christman are with Bell Laboratories, Lucent Technologies, Murray Hill, NJ 07974 USA.

Publisher Item Identifier S 1041-1135(99)04221-4.

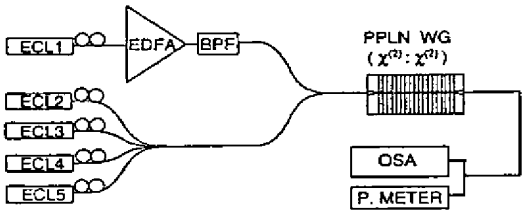

Fig. 1. Experimental setup. ECL: External cavity laser. BPF: Bandpass filter. PPLN WG: Periodically poled $LiNbO_3$ waveguide. OSA: Optical spectrum analyzer. The waveguide is fiber coupled at both the input and the output. The later is analyzed by an OSA and power meter.

between the fundamental mode of the pump and the first high-order mode of the second harmonic. At the input and output of this device, the waveguides are optimized for fiber coupling by tapering a section of 1-mm length to adiabatically transform the modes into and out of the wavelength conversion sections.

Fig. 1 shows a schematic diagram of the experimental setup used in this work. The pump laser is an external cavity laser (ECL) amplified by an erbium-doped fiber amplifier (EDFA) to a level of ~300 mW and filtered through a FBG in order to supress the amplified spontaneous emission (ASE). This pump is combined with signal sources generated in four different ECL's and fiber launched into the waveguides. The output of the waveguide is fiber coupled and later analyzed in an optical spectrum analyzer (OSA) and power meter. The fiber to fiber coupling loss in this configuration is ~4.5 dB due to reflection losses at the uncoated endfaces (~1.7 dB), mode mismatching between the fibers and the waveguide (~1.3 dB), and intrinsic waveguide losses (~1.5 dB, i.e., ~0.35 dB/cm).

We first characterized the device by measuring the SHG power versus pump wavelength. We chose to keep the waveguide at 90 °C (or higher) in order to avoid photorefractive effects. This effectively shifts the phasematching wavelength to 1562 nm, but keeps the other parameters unchanged. The device shows a near-ideal sinc^2 wavelength tuning curve with a peak internal efficiency (output SHG power divided by square of input pump power) of ~500%/W and an FWHM of ~0.27 nm at low pump power. At higher pump power (>100 mW), the device displayed a distorted wavelength tuning curve due to photorefractive effects of the generated second-harmonic waves, which results in waveguide nonuniformity and reduces the effective device length.

We performed simultaneous multichannel wavelength conversion with a pump power of ~110 mW launched inside the waveguide; the results, in Fig. 2, show that the efficiencies are the same (−15 dB) for all the input channels. The best conversion efficiency (−8 dB) was obtained with a pump power of ~175 mW in a similar device with a slightly different QPM period and operated at 120 °C, as shown in the inset of Fig. 2.

For $\chi^{(2)} : \chi^{(2)}$-based wavelength converters, the converted electric field is the complex conjugate of signal electric field, meaning that the output electric field spectrum is the mirror image of input spectrum about the pump wavelength. We show the spectral inversion properties of our device in Fig. 3 using an asymmetric input spectrum, formed by combining an ECL

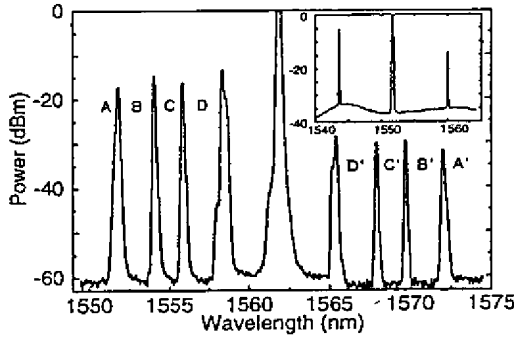

Fig. 2. Simultaneous wavelength conversion of four WDM channels with the same conversion efficiencies. Pump power is ~110 mW inside the PPLN waveguide at a wavelength of 1562 nm. The inset shows a −8-dB conversion efficiency of a similar device operated at 120 °C with 175 mW of pump power.

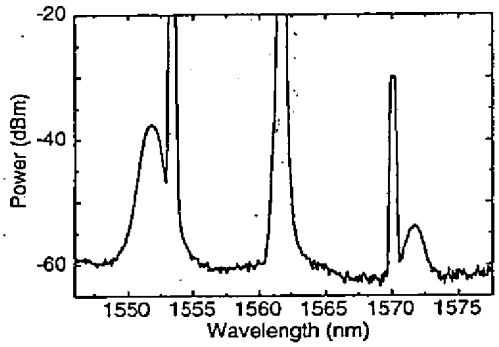

Fig. 3. Spectral inversion of the $\chi^{(2)} : \chi^{(2)}$ wavelength converter. The output electric field spectrum is the mirror image of input spectrum about the pump wavelength, a feature that can be used to invert the signal chirp.

signal and filtered ASE from an EDFA. This feature can be used to invert the signal chirp for dispersion management in a transmission system.

Fig. 4 shows the measured bandwidth of this wavelength converter when tuning the input signal wavelength while keeping the pump wavelength fixed at 1562 nm. This device has a 3-dB signal bandwidth of 76 nm, which is wider than the theoretical bandwidth of an ideal 4-cm-long device due to photorefractive effects at high pump powers.

We tested the linearity of this wavelength converter by varying the input signal power, as shown in Fig. 5. We measure a linear response for more than 50 dB with a maximum input signal power of ~0 dBm. The only saturation mechanism in this device comes from the depletion of SHG or pump power. We estimate a 0.16-dB deviation from linearity for a input power of 0 dBm in an ideal 6-cm-long device with a normalized efficiency of 150%/W·cm^2 and pump power of ~100 mW. For a device with a 2.5-cm interaction length, a normalized efficiency of 65%/W·cm^2, and pumped by ~100 mW, the deviation at 0-dBm signal power should be 0.006 dB, which is smaller than the resolution in this experiment. Our measurements confirm these estimates.

The conversion efficiency of this device currently is limited by photorefractive effects at high pump powers, which can

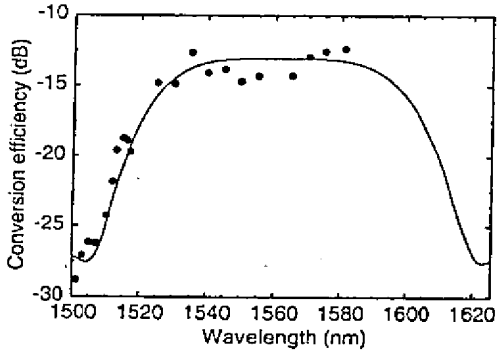

Fig. 4. Conversion efficiency vs. input signal wavelength. The closed circles are the measured results and the solid line is a theoretical fit to a device with an effective interaction length of 2.5 cm. The 1562-nm pump has a power of ~135 mW inside the waveguide.

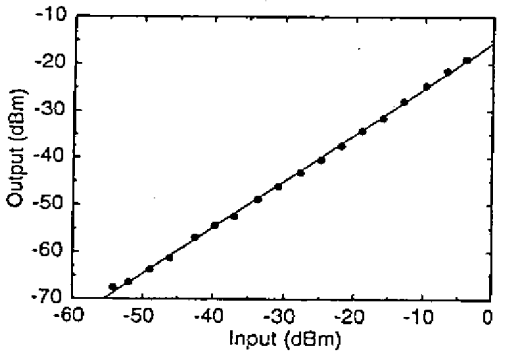

Fig. 5. Single-channel output/input transfer curve of the $\chi^{(2)} : \chi^{(2)}$ wavelength converter. This device has a linear response for more than 50-dB range of input signal powers.

be reduced by operating at higher temperature or annealing samples in an O_2 atmosphere. In addition, it has been shown that MgO:$LiNbO_3$ has several orders of magnitude more resistance to photorefractive effects than congruent $LiNbO_3$, and thus a similar device fabricated on MgO:$LiNbO_3$ would operate more efficiently.

In summary, we have demonstrated wavelength conversion within the 1.5-μm band using $\chi^{(2)} : \chi^{(2)}$ in PPLN waveguides. This approach requires only lasers operating in the 1550-nm region. We have shown spectral inversion and simultaneous conversion of four WDM channels, a static internal conversion efficiency of -8 dB, a conversion bandwidth of 76 nm, and a linearity over an input power range of more than 50 dB. With further improvements, a wavelength converter with 0-dB conversion efficiency or even gain is a feasible goal. In addition, this $\chi^{(2)} : \chi^{(2)}$-based wavelength converter can also function as clock recovery or time gating component by use of a pulsed pump.

ACKNOWLEDGMENT

The authors thank Crystal Technology for donating $LiNbO_3$ substrates and B. Eggleton for providing the fiber Bragg grating.

REFERENCES

[1] S. J. B. Yoo, "Wavelength conversion technologies for WDM network applications," *J. Lightwave Technol.*, vol. 14, pp. 955–966, 1996.

[2] S. J. B. Yoo, M. A. Koza, C. Caneau, and R. Bhat, "Simultaneous wavelength conversion of 2.5-Gbit/s and 10-Gbit/s signal channels by difference-frequency generation in an AlGaAs waveguide," in *1998 OSA Tech. Dig. Ser., Conf. Optical Fiber Communications*, vol. 2, paper WB5.

[3] C. Q. Xu, H. Okayama, and M. Kawahara, "1.5 μm band efficient broadband wavelength conversion by difference frequency generation in a periodically domain-inverted $LiNbO_3$ channel waveguide," *Appl. Phys. Lett.*, vol. 63, pp. 3559–3561, 1993.

[4] M. H. Chou, J. Hauden, M. A. Arbore, and M. M. Fejer, "1.5-μm-band wavelength conversion based on difference-frequency generation in $LiNbO_3$ waveguides with integrated coupling structures," *Opt. Lett.*, vol. 23, pp. 1004–1006, 1998.

[5] C. Q. Xu, H. Okayama, and T. Kamijoh, "$LiNbO_3$ quasiphasematched wavelength converter and its module," in *Proc. Eur. Conf. Optical Communications*, 1998, pp. 173–174.

[6] K. Gallo, G. Assanto, and G. Stegeman, "Efficient wavelength shifting over the erbium amplifier bandwidth via cascaded second order processes in lithium niobate waveguides," *Appl. Phys. Lett.*, vol. 71, pp. 1020–1022, 1997.

[7] G. P. Banfi, P. K. Datta, V. Degiorgio, and D. Fortusini, "Wavelength shifting and amplification of optical pulses through cascaded second-order processed in periodically poled lithium niobate," *Appl. Phys. Lett.*, vol. 7, pp. 136–138, 1998.

[8] G. I. Stegeman, D. J. Hagan, and L. Toner, "$\chi^{(2)}$ cascading phenomena and their applications to all-optical signal processing, mode-locking, pulse compression and solitons," *Opt. Quantum Electron.*, vol. 28, pp. 1691–1740, 1996.

[9] L. E. Myers, R. C. Eckardt, M. M. Fejer, R. L. Byer, W. R. Bosenberg, and J. W. Pierce, "Quasiphase-matched optical parametric oscillators in bulk periodically poled $LiNbO_3$," *J. Opt. Soc. Amer. B*, vol. 12, pp. 2102–2106, 1995.

All-Optical Switching Based on Cascading of Second-Order Nonlinearities in a Periodically Poled Titanium-Diffused Lithium Niobate Waveguide

Hirohisa Kanbara, Hiroki Itoh, *Member, IEEE,* Masaki Asobe, Kazuto Noguchi, *Member, IEEE,* Hiroshi Miyazawa, Tsutomu Yanagawa, and Itaru Yokohama

***Abstract*—We report efficient all-optical switching by using a periodically poled titanium-diffused lithium niobate (Ti:PPLN) waveguide. The periodically domain inversion of the Ti:PPLN waveguide is achieved by electric field poling. The switching is driven by the second-order nonlinear effect of the cascading of phase-matched sum-frequency-generation and difference-frequency-generation processes. It is found that about 12% of the signal is switched by a 20-W gate power.**

***Index Terms*— All-optical switching, cascading, difference-frequency-generation, periodically poled lithium niobate, second-order nonlinearity, sum-frequency-generation.**

I. Introduction

PERIODICALLY POLED lithium niobate (PPLN), which provides large second-order nonlinearity and high transparency, has led to the development of optical devices that are based on the high-yields frequency mixing. Typical examples are blue light sources using second-harmonic-generation and communication-band-wavelength converters using difference-frequency-generation (DFG) [1], [2]. Besides these devices, PPLN is also promising for constructing efficient optically gated optical switches [3]. It has been pointed out that the cascading of the second-order nonlinearities makes possible a lower gate power compared with that for the conventional switch driven by third-order nonlinear effects like a nonlinear change in the refractive index [4]–[6]. As an instance of this, we proposed optical switching that utilizes the cascading of phase-matched sum-frequency-generation (SFG) and DFG, and thereby realized full-switching operation with a gate power of 3 kW using 10-mm-long bulk PPLN [3]. In this study, for further improvement of the switching efficiency, we fabricated a titanium-diffused PPLN (Ti:PPLN) waveguide and examined the optical switching properties based on the cascading of phase-matched SFG and DFG in the waveguide.

Manuscript received September 24, 1998; revised December 8, 1998.

H. Kanbara, H. Itoh, M. Asobe, K. Noguchi, and H. Miyazawa are with NTT Photonics Laboratories, Atsugi, Kanagawa 243-0198, Japan.

T. Yanagawa was with NTT Opto-electronics Laboratories, Atsugi, Kanagawa 243-0198, Japan. He is now with NTT Affiliated Business Headquarters, Shinjuku-ku, Tokyo 163-1419, Japan.

I. Yokohama was with NTT Photonics Laboratories, Atsugi, Kanagawa 243-0198, Japan. He is now with NTT Photonics Laboratories, Tokai, Ibaraki 319-1193, Japan.

Publisher Item Identifier S 1041-1135(99)01880-7.

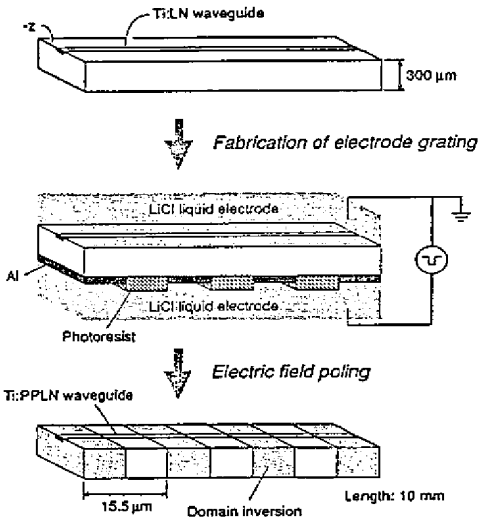

Fig. 1. Preparation process for the Ti:PPLN waveguide. The periodically domain inversion results from electric field poling. We used a 300-μm-thick substrate for the poling.

II. Experimental

The Ti:PPLN waveguide was prepared by using electric field poling [7], [8]. The preparation process is shown in Fig. 1. A titanium-diffused lithium niobate (LN) waveguide was formed on the $-z$ face of the LN substrate [9]. For the poling, an aluminum electrode grating was deposited on the $+z$ face of the substrate, and the insulator was also coated with photoresist on this $+z$ face so that its domain would remain unchanged. The period of the electrode grating was 15.5 μm. A lithium chloride liquid electrode directly touched the $-z$ face of the substrate [7]. After the application of electric field, we found that the domain inversion only occurred in the part where the aluminum grating was deposited. A 10-mm-long waveguide was used to conduct the optical switching experiment.

In optical switching by means of the cascading of SFG and DFG processes, SFG occurs first, when a strong gate beam, ω_{Gate}, and a weak signal beam, ω_{Signal}, are input together, and then DFG yields the switched signal

$$\omega_{\mathrm{Gate}} + \omega_{\mathrm{Signal}} \rightarrow \omega_{\mathrm{SFG}} \tag{1}$$

$$\omega_{\mathrm{SFG}} - \omega_{\mathrm{Gate}} \rightarrow \omega_{\mathrm{Signal}}. \tag{2}$$

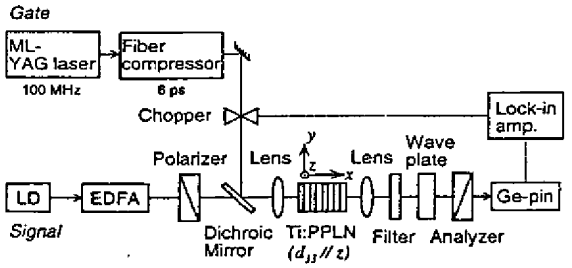

Fig. 2. Setup for the three-terminal optical switching experiment. Unswitched signal cannot pass through the analyzer.

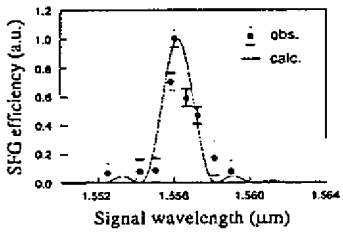

Fig. 3. Signal wavelength dependence of the SFG efficiency. The signal with a wavelength of 1.556 μm provides the largest SFG efficiency for a 1.319-μm gate wavelength.

The experimental setup is illustrated in Fig. 2. We examined a three-terminal switching operation. The configuration is almost the same as that of an optical Kerr shutter switch, which employs a third-order nonlinear process. When there is no gate beam, the signal does not pass through the analyzer. On the other hand, when the gate beam strikes the Ti:PPLN waveguide, the signal passes through the analyzer because the direction of the polarization of the emerging phase-changed signal is effectively rotated [3]. In case the phase change of the signal is π, a 100% switching efficiency is obtained. We constructed a collinear-type switch with a dichroic mirror. For the gate beam, we used a fiber-compressed, mode-locked YAG laser pulse with a wavelength of 1.319 μm. The gate pulses had a duration of 6 ps and a repetition rate of 100 MHz. A CW distributed-feedback laser diode coupled to an erbium-doped fiber amplifier (EDFA) produced the signal beam. The largest second-order nonlinear component, d_{33}, of LN was parallel to the z axis. For the switching experiment, the gate beam was linearly polarized parallel to this z axis, and the polarization of the linearly polarized signal beam is set to $\pi/4$ with respect to that of the gate beam. The optical filter prevented the gate beam from entering the germanium p-i-n photodetector, which was connected to a lock-in amplifier. The waveplate compensated for the birefringence of the waveguide.

III. Results and Discussion

Before trying any switching, we first did the SFG measurement to determine the appropriate signal wavelength. In the SFG measurement, the signal beam was produced by a wavelength-tunable semiconductor CW light source and an EDFA. In Fig. 3, the SFG efficiency is plotted as a function of the signal wavelength. The dots are measured data, and they show that the SFG efficiency strongly depends on the

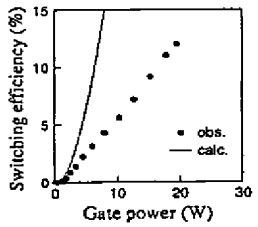

Fig. 4. The dependence of the switching efficiency on the gate peak power. The signal was found to continuously increase with increasing gate power.

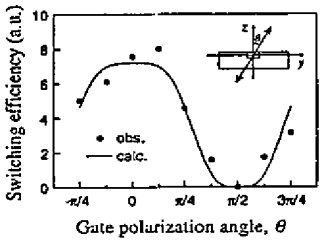

Fig. 5. The dependence of the switching efficiency on the angle of polarization of the gate beam. The z-directional gate beam gives the largest switching efficiency, but no signal was detected for the y-directional gate beam.

signal wavelength. The main peak was found to be at 1.556 μm, so we used that wavelength in the switching experiments. The solid curve was calculated from the Sellmeier coefficient at 300 K [10], but the center wavelength was shifted so that it matched the experimental data. The refractive index difference between LN and Ti:PPLN probably brings about this discrepancy in the center wavelength. Large error bars for experimental data are thought to be due to the instability of the output power of the wavelength-tunable semiconductor CW light source. The measurement revealed that the maximum normalized SFG conversion efficiency for the Ti:PPLN waveguide was 130%/W. This value is more than two orders of magnitude larger than the 0.97%/W for bulk PPLN [3].

The switching property is shown in Fig. 4. This graph shows how the intensity of a switched signal varies with the gate peak power. The gate power was estimated at the output of the waveguide. The lens-to-lens transmittance of the waveguide was 15% for the gate beam and 20% for the signal beam. The extinction ratio of the linear polarization maintenance for the signal beam was over 30 dB. The signal power was 1 mW at the output of the waveguide. We observed clear switching of the signal even when the gate power was less than 20 W. At the gate power of 20 W, the switched signal was approximated to be 12%. This result indicates that the gate power is over two orders of magnitudes smaller than that for the conventional optical Kerr shutter switch using a silica glass fiber [11]. To obtain the same switching efficiency, the needed gate power was found to be 5.5 times larger than the calculated one. This large power consumption is probably caused by nonuniformity of the periodically poled structure, optical damage of the waveguide, and incomplete overlapping of the gate and signal beams. Trials for improvement are in progress.

Fig. 5 shows how the switching efficiency depended on the angle of polarization of the linearly polarized gate beam. The

inset shows the waveguide and the direction of polarization of the gate beam. Here, $\theta = 0$ means that the gate polarization is parallel to the z axis, or in other words, parallel to the d_{33} of LN. The polarization of the signal beam was kept at $\theta = \pi/4$. We obtained the maximum switched signal when the gate beam was polarized parallel to the z axis. And we did not get any signal when the gate beam was polarized in the y direction. For the waveguide we used, the wavelength conversion efficiency is much lower in the y direction, because there is a phase mismatch in this direction and the second-order nonlinearity of d_{31} is small. Assuming zero nonlinearity along the y axis, the calculated curve agrees well with the measured data. This proves that the switching was driven by cascading processes of the second-order nonlinearity governed by d_{33} as well as phase matching, and that the switching did not originate from the third-order nonlinearity where phase matching is irrelevant.

IV. Conclusion

All-optical switching that are based on the cascading of phase-matched SFG and DFG was demonstrated by use of a 10-mm-long Ti:PPLN waveguide. We constructed an optical-Kerr-shutter-type configuration to perform a switching experiment and observed an efficient three-terminal optical switching operation. The switched signal was about 12% at the gate power of 20 W. It was evidenced that a PPLN waveguide will be very useful in producing highly efficient optical switching devices.

Acknowledgment

The authors would like to thank H. Iwamura for his valuable suggestions. The authors are also indebted to Y. Oiso and S. Ishibashi for their helpful advice in fabricating the Ti:PPLN waveguide.

References

[1] K. Mizuuchi, K. Yamamoto, and M. Kato, "Harmonic blue light generation in X-cut MgO:$LiNbO_3$ waveguide," *Electron. Lett.*, vol. 33, pp. 806–807, 1997.

[2] M. H. Chou, J. Hauden, M. A. Arbore, and M. M. Fejer, "1.5-μm-band wavelength conversion based on difference-frequency generation in $LiNbO_3$ waveguides with integrated coupling structures," *Opt. Lett.*, vol. 23, pp. 1004–1006, 1998.

[3] M. Asobe, I. Yokohama, H. Itoh, and T. Kaino, "All-optical switching by use of cascading of phase-matched sum-frequency-generation and difference-frequency-generation processes in periodically poled $LiNbO_3$," *Opt. Lett.*, vol. 22, pp. 274–276, 1997.

[4] G. I. Stegeman, M. Sheik-Bahae, E. Van Stryland, and G. Assanto, "Large nonlinear phase shifts in second-order nonlinear-optical processes," *Opt. Lett.*, vol. 18, pp. 13–15, 1993.

[5] D. C. Hutchings, J. S. Aitchison, and C. N. Ironside, "All-optical switching based on nondegenerate phase shifts from a cascaded second-order nonlinearity," *Opt. Lett.*, vol. 18, pp. 793–795, 1993.

[6] Y. Baek, R. Schiek, G. I. Stegeman, G. Krijnen, I. Baumann, and W. Sohler, "All-optical integrated Mach–Zehnder switching due to cascaded nonlinearities," *Appl. Phys. Lett.*, vol. 68, pp. 2055–2057, 1996.

[7] L. E. Myers, R. C. Eckardt, M. M. Fejer, R. L. Byer, W. R. Bosenberg, and J. W. Pierce, "Quasiphase-matched optical parametric oscillators in bulk periodically poled $LiNbO_3$," *J. Opt. Soc. Amer. B*, vol. 12, pp. 2102–2116, 1996.

[8] K. Kintaka, M. Fujimura, T. Suhara, and H. Nishihara, "High-efficiency $LiNbO_3$ waveguide second-harmonic generation devices with ferroelectric-domain-inverted gratings fabricated by applying voltage," *J. Lightwave Technol.*, vol. 3, pp. 462–468, 1996.

[9] T. Nozawa, K. Noguchi, H. Miyazawa, and K. Kawano, "Water vapor effects on optical characteristics in Ti:$LiNbO_3$ channel waveguides," *Appl. Opt.*, vol. 30, pp. 1085–1089, 1991.

[10] V. G. Dmitriev, G. G. Gurzadyan, and D. N. Nikogosyan, *Handbook Nonlinear Optical Crystals*. Berlin, Germany: Springer-Verlag, 1991.

[11] T. Morioka, H. Takara, K. Mori, and M. Saruwatari, "Ultrafast reflective optical Kerr demultiplexer using polarization rotation mirror," *Electron. Lett.*, vol. 28, pp. 521–522, 1992.

Low-Power All-Optical Gate Based on Sum Frequency Mixing in APE Waveguides in PPLN

K. R. Parameswaran, M. Fujimura, M. H. Chou, and M. M. Fejer

Abstract—**We present an all-optical gate implemented in periodically poled lithium niobate. Efficient mixing is achieved by using a phase-matched guided-wave interaction. A control wave at 1.537 μm is used to gate a signal at 1.552 μm, where a control power of 185 mW is sufficient to achieve 96% depletion of a low-power signal. A simple switch configuration is described whereby high-contrast low-power all-optical switching can be performed.**

Index Terms—**Gated mixer, nonlinear optics, optical fiber communications, optical frequency conversion, optical switching, optical waveguide, periodically poled lithium niobate, quasi-phase-matching, sum frequency generation.**

I. Introduction

ALL-OPTICAL switching is an enabling function for future high-speed fiber communication systems. Previously demonstrated approaches using the third-order material nonlinearity $\chi^{(3)}$ suffer from difficulties such as high-switching powers and/or long devices (due to weak nonlinearities in optical fiber-based four wave mixing [1]) or signal degradation due to additive noise (in four wave mixing in semiconductor optical amplifiers (SOA's) [2]. Cascading of second-order nonlinearities ($\chi^{(2)} : \chi^{(2)}$) has also been used to perform switching [3]. The switching power needed in these configurations is quite high (on the order of several Watts), primarily because they operate far from phase matching in order to simultaneously obtain a large phase shift (required for switching) and flat spectral response.

We demonstrate an all-optical gate based on sum frequency mixing (SFM) using a single $\chi^{(2)}$ interaction in an annealed proton exchanged (APE) waveguide formed in periodically poled lithium niobate (PPLN). This approach exploits the high conversion efficiency available from a phase-matched interaction, resulting in 96% depletion of a CW signal by a 185-mW control beam. A structure using this gate is described with which high-contrast low-power, all-optical switching can be performed.

Manuscript received December 3, 1999; revised March 3, 2000. This work was supported by the Joint Services Electronics Program and by DARPA through the Optoelectronic Materials Center. One of the authors, M. Fujimura, was supported by the Japan Society for the Promotion of Science during this work.

K. R. Parameswaran and M. M. Fejer are with the Edward L. Ginzton Laboratory, Stanford University, Stanford, CA 94305-4085 USA.

M. Fujimura is with the Department of Electronics, Osaka University, Osaka, 565-0871 Japan.

M. H. Chou was with Ginzton Labs/Stanford, he is now with Lucent Technologies, Holmdel, NJ 07733 USA.

Publisher Item Identifier S 1041-1135(00)04608-5.

II. Theory

Coherent three-wave mixing using $\chi^{(2)}$ has several attractive features such as transparency to signal format and the addition of negligible excess noise. Difference frequency mixing (DFM) using $\chi^{(2)}$ has been used to perform efficient wavelength conversion within the 1.55-μm communication band [4] as well as between the 1.3- and 1.55-μm bands [5]. In each case, a strong pump wave is mixed with weak signal waves to produce mixed outputs at frequencies mirrored about half the local oscillator frequency. These same devices can be used to mix a low-power signal with a stronger control wave to generate a signal at the sum frequency. Both phenomena are described by the well-known coupled mode equations for three-wave mixing [6], but with different boundary conditions in each case. In DFM, the low-power signal is *amplified* during the mixing process, whereas in SFM, the signal wave is *depleted* during generation of the sum frequency wave. In the simple case of a phase-matched interaction without loss, where the control wave is much stronger than the signal wave (and can be considered undepleted), the evolution of power in the SFM and signal waves is described by

$$P_{\mathrm{SFM}}(L) = P_{\mathrm{SIG}}(0)\,\frac{\lambda_{\mathrm{SIG}}}{\lambda_{\mathrm{SFM}}}\sin^2\left(\sqrt{\eta_{\mathrm{nor}}P_{\mathrm{CTRL}}}L\right) \tag{1a}$$

$$P_{\mathrm{SIG}}(L) = P_{\mathrm{SIG}}(0)\cos^2\left(\sqrt{\eta_{\mathrm{nor}}P_{\mathrm{CTRL}}}L\right) \tag{1b}$$

where L is the interaction length, P_{CTRL} is the control power, λ_{SFM} and λ_{SIG} are the SFM and signal wavelengths and η_{nor} is the normalized conversion efficiency. Complete depletion of the signal occurs when the argument of the trigonometric functions equals $\pi/2$. Hence, gating of the signal can be accomplished by turning the control power on and off.

III. Experiment

The device used in this work was designed to mix signal and control waves in the 1.55-μm band, with a mixing region designed to be insensitive to variations in waveguide width, which loosens fabrication tolerances [7]. This noncritical design requires a waveguide that supports multiple transverse modes at both input wavelengths in the conversion region, so a mode filter and adiabatic taper at the input are incorporated to facilitate launching of power into the fundamental modes in the conversion region [8]. The optimized widths are 4 μm for the mode filter and 12 μm for the conversion region. The 6.05-cm long sample was diced from a 3-in-diameter wafer of $LiNbO_3$, which had been electric-field poled [9] with a quasi-phasematching

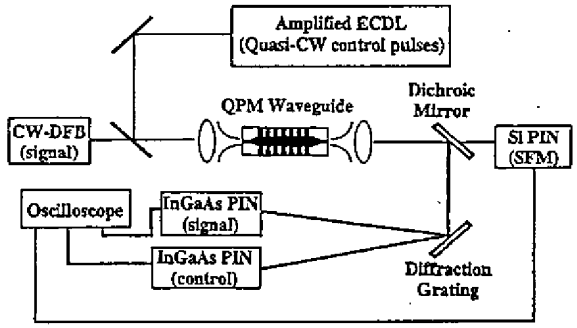

Fig. 1. Experimental setup.

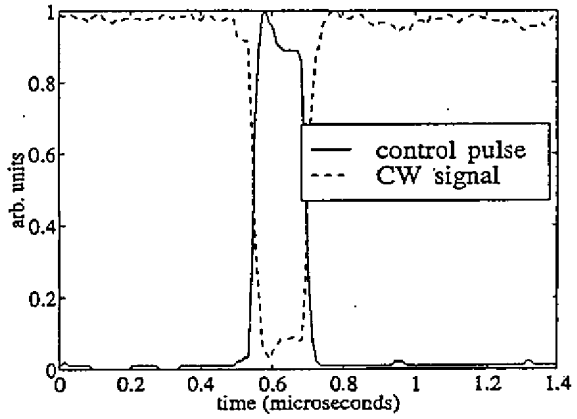

Fig. 2. Typical pulse traces, showing depletion of the signal in the presence of the control pulse.

(QPM) period of 14.7 μm. The QPM grating is 5.55 cm long. Waveguides were formed by proton exchange for 15 h at a temperature of 160 °C (to a depth of 0.71 μm), followed by annealing for 26 h at 328 °C. The end faces of the sample were then polished to permit efficient end fire coupling.

The experimental setup is shown in Fig. 1. Control pulses were produced by a fiber-amplified externally modulated diode laser. A DFB laser diode operating at 1.552 μm produces the CW signal. Phasematching was observed with λ_{CTRL} = 1.537 μm resulting in λ_{SFM} = 0.772 μm. The signal and control beams are combined, then launched into the same waveguide. Output light at the three wavelengths is separated using a dichroic mirror and diffraction grating, then directed onto fast photodiodes for power measurement. The experiment was carried out at room temperature.

IV. Results and Discussion

Fig. 2 shows depletion of the CW signal in the presence of the control pulse. One advantage of the nonlinear transfer function of the SFM process is that distortions in the control pulse are suppressed in the depleted signal pulse, making the switching less sensitive to variations in the control pulse. Fig. 3 shows a plot of normalized signal transmission as a function of control power. The solid line shows the calculated result obtained

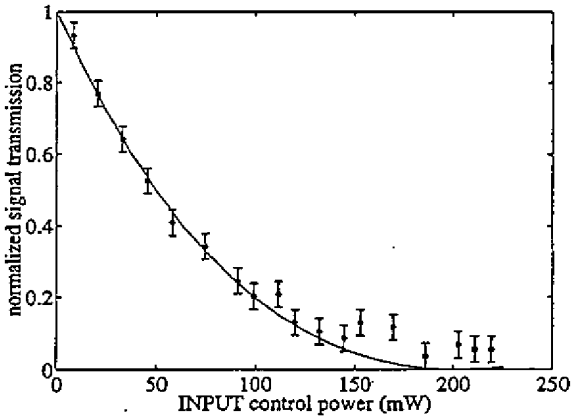

Fig. 3. Measured and calculated variation of signal transmission with control power.

by numerical integration of the coupled mode equations describing the SFM process in waveguides, including the propagation losses neglected in obtaining (1). The calculation used a normalized internal SFM conversion efficiency of 33.9 W^{-1} (as determined by measurement of the second harmonic generation efficiency of 8.47 W^{-1}) and typical values of propagation losses at the three wavelengths (0.35 dB/cm at λ_{SIG} and λ_{CTRL}, and 0.70 dB/cm at λ_{SFM}). Mode profiles used in the calculation were obtained by solution of Maxwell's equations subject to the refractive index profile resulting from the annealed proton exchange process [16]. Nearly complete (96%) extinction of the signal is seen at an input control power of 185 mW, a value in reasonable agreement with theory. The mechanism responsible for the residual 4% is unclear; slight phase mismatch arising from waveguide nonuniformity is one possibility.

V. Future Possibilities

The required gating power in SFM devices can be significantly reduced by several relatively straightforward means. The device used in this experiment had nonuniformities resulting from imperfect fabrication. Optimization of the process would result in a 30% increase in η_{nor}. The conversion efficiency in waveguide QPM interactions is roughly proportional to the square of the grating length. Periodically poled devices as long as 8 cm have been reported [10], hence, moving to this length from the current value of 5.55 cm would increase η_{nor} by about a factor of two. High index cladding layers [11] and buried waveguides [17] have also been used to improve the spatial overlap of modes in waveguides. Calculations indicate that this technique could potentially increase η_{nor} by another factor of two. Combining the above techniques could result in a control power around 40 mW (or 16 dBm, a power level readily available from commercial EDFA's). This corresponds to a gating energy of 1 pJ for 25 ps pulses in a 20-GHz return-to-zero pulse train, which compares very well with similar experiments using SOA's [12]. The bandwidth of the device is limited by group velocity walkoff between the three interacting waves such that the minimum pulsewidth scales inversely with the device length. Hence, efficiency and bandwidth can be traded against

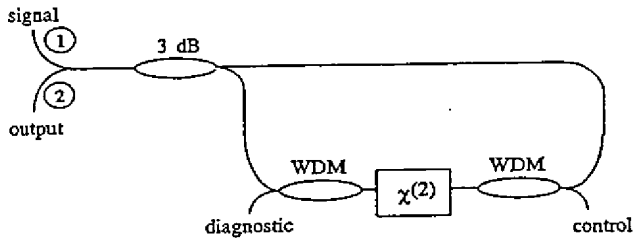

Fig. 4. "AND" gate using $\chi^{(2)}$ in NOLM configuration.

each other. One way to eliminate this tradeoff is known as "quasi-group velocity matching" [8], where after each walkoff length, the faster pulse passes through a delay line integrated into the waveguide structure in order to be resynchronized with the slower pulse. This scheme, currently being investigated, would allow for high efficiency switching of "arbitrarily" short pulses.

VI. Proposed Switch Structure Using $\chi^{(2)}$ Gate

Higher contrast can be achieved by placing this device in an interferometer or in a nonlinear optical loop mirror (NOLM [13], Fig. 4). In the absence of the control pulse, the loop is balanced and all of the signal power exits at port 1. When the control is on, signal power traveling in one direction in the loop gets depleted so that incomplete interference at the 3-dB coupler results in signal power leaving port 2 (at a level 6 dB below the input value). Hence, an "AND" logic function is implemented (there is output only when the signal and control are both on). Power switched to the SFM wave (at 0.772 μm in the current device) can be used for further signal processing. A similar device has been used to perform efficient optical sampling [14].

An attractive feature of SFM is that the signal wavelength acceptance bandwidth is narrow (~0.3 nm for a 6 cm long device) such that individual WDM channels can be switched out of a bit stream in this way. In order to switch multiple wavelengths simultaneously, DFM can be used as the mixing process instead of SFM. Here, the NOLM is unbalanced by *amplifying* the signal rather than switching it out. Parametric gain on the order of 3 dB has been observed in APE waveguides in PPLN [15]. This can be used to create a switch with 0-dB insertion loss and very wide signal bandwidth (around 46 nm, for a 6-cm device).

VII. Conclusion

An optical gate based on phasematched SFM in QPM-APE waveguides in PPLN has been demonstrated. Nearly complete extinction with a control power of 185 mW was observed. Two possible configurations for very high contrast switching have been presented.

Acknowledgment

The authors would like to thank Crystal Technology Inc., Palo Alto, CA, for donation of the $LiNbO_3$ wafers and D. Attanasio of JDS Uniphase Corporation, Bloomfield, CT, for donation of the electrooptic modulator used in the pulsed 1.55-μm source.

References

[1] S. Bigo, O. Leclerc, and E. Desurvire, "All-optical fiber signal processing and regeneration for soliton communications," *IEEE J. Selected Topics Quant. Electron.*, vol. 3, pp. 1208–1223, 1997.

[2] D. F. Geraghty, R. B. Lee, K. J. Vahala, M. Verdiell, M. Ziari, and A. Mathur, "Wavelength conversion up to 18 nm at 10 Gb/s by four-wave mixing in a semiconductor optical amplifier," *IEEE Photon. Technol. Lett.*, vol. 9, pp. 452–454, 1997.

[3] Y. Baek, R. Schiek, G. I. Stegeman, G. Krinjen, I. Baumann, and W. Sohler, "All-optical integrated Mach–Zender switching due to cascaded nonlinearities," *Appl. Phys. Lett.*, vol. 68, pp. 2055–2057, 1996.

[4] M. H. Chou, J. Hauden, M. A. Arbore, and M. M. Fejer, "1.5 μ m band wavelength conversion based on difference frequency generation in $LiNbO_3$ waveguides with integrated coupling structures," *Opt. Lett.*, vol. 23, pp. 1004–1006, 1998.

[5] M. H. Chou, K. R. Parameswaran, M. A. Arbore, J. Hauden, and M. M. Fejer, "Bidirectional wavelength conversion between 1.3- and 1.5-μm telecommunication bands using difference frequency mixing in $LiNbO_3$ wavegudes with integrated coupling structures," *CLEO 1998*, pp. 475–476.

[6] R. W. Boyd, *Nonlinear Optics*. New York: Academic, 1992.

[7] M. L. Bortz, S. J. Field, M. M. Fejer, D. W. Nam, R. G. Waarts, and D. F. Welch, "Noncritical quasiphase matched second harmonic generation in an annealed proton-exchanged $LiNbO_3$ waveguide," *IEEE Trans. Quantum Electron.*, vol. 30, pp. 2953–2960, 1994.

[8] M. H. Chou, "Optical frequency mixers using three-wave mixing for optical fiber communications," Ph.D. dissertation, Stanford Univ., 1999.

[9] L. E. Myers, R. C. Eckardt, M. M. Fejer, R. L. Byer, W. R. Bosenberg, and J. W. Pierce, "Quasiphase-matched optical parametric oscillators in bulk periodically poled $LiNbO_3$," *J. Opt. Soc. Amer. B*, vol. 12, pp. 2102–2116, 1995.

[10] D. Hofmann, G. Schreiber, C. Haase, H. Herrmann, W. Grundkötter, R. Ricken, and W. Sohler, "Quasiphase-matched difference-frequency generation in periodically poled Ti:LiNbO3 waveguides," *Opt. Lett.*, vol. 24, pp. 896–898, 1999.

[11] K. Mizuuchi, H. Ohta, K. Yamamoto, and M. Kato, "Second-harmonic generation with a high-index-clad waveguide," *Opt. Lett.*, vol. 22, pp. 1217–1219, 1997.

[12] B. K. Mathason, H. Shi, I. Nitta, G. A. Alphonse, J. Abeles, J. C. Connolly, and P. J. Delfyett, "Multiwavelength all-optical TDM switching using a semiconductor optical amplifier in a loop mirror," *IEEE Photon. Technol. Lett.*, vol. 11, pp. 331–333, 1999.

[13] K. J. Blow, N. J. Doran, and B. P. Nelson, "Demonstration of the nonlinear fiber loop mirror as an ultrafast all-optical demultiplexer," *Electron. Lett.*, vol. 26, pp. 962–964, 1990.

[14] T. Suhara, H. Ishizuki, M. Fujimura, and H. Nishihara, "Waveguide quasi-phase-matched sum-frequency generation device for high-efficiency optical sampling," *IEEE Photon. Technol. Lett.*, vol. 11, pp. 1027–1029, 1999.

[15] M. H. Chou, I. Brener, G. Lenz, R. Scotti, E. E. Chaban, J. Shmulovich, D. Philen, S. Kosinski, K. R. Parameswaran, and M. M. Fejer, "Efficient, wideband, and tunable mid-span spectral inverter using cascaded nonlinearities in $LiNbO_3$ waveguides," *IEEE Photon. Technol. Lett.*, vol. 12, pp. 82–84, 2000.

[16] M. L. Bortz, "Quasi-phasematched optical frequency conversion in lithium niobate waveguides," Ph.D. dissertation, Stanford Univ., Stanford, CA, 1994.

[17] Y. N. Korkishko, V. A. Fedorov, T. M. Morozova, F. Caccavale, F. Gonella, and F. Segato, "Reverse proton exchange for buried waveguides in $LiNbO_3$," *J. Opt. Soc. Amer. A*, vol. 15, pp. 1838–1842, 1998.

Second harmonic generation in reverse proton exchanged Lithium Niobate waveguides

Annarita Di Lallo, Alfonso Cino*, Claudio Conti and Gaetano Assanto
National Institute for the Physics of Matter INFM-RM3 &
Department of Electronic Engineering, Terza University of Rome
Via della Vasca Navale 84, 00146 Rome - ITALY
Assanto@ele.uniroma3.it

** Permanent address: Center for Electronics Research in Sicily (CRES), Monreale (PA), Italy.*

Abstract: We investigate efficient second harmonic generation in reverse proton exchanged Lithium Niobate waveguides. In z-cut crystals, the resulting buried and surface guides support TM and TE polarizations, respectively, and are coupled through the d_{31} nonlinear element. Numerically estimated conversion efficiencies in planar structures operating at 1.32μm reach 90% in 2cm or a normalized 14% μm/W cm.

OCIS codes: (190.2620) Frequency conversion, (130.3730) Lithium Niobate, (130.4310) Nonlinear

References and links

1. See, for example, A. M. Prokhorov, U. S. Kuz'minov, O. A. Khachaturyan, *Ferroelectric Thin Film Waveguides in Integrated Optics and Optoelectronics*, Cambridge International Science Publ., 1996
2. X. F. Cao, R. V. Ramaswamy, and R. Srivastava, "Characterization of annealed proton exchanged $LiNbO_3$ waveguides for nonlinear frequency conversion," J. Lightw. Technol. **10**, 1302-1315 (1992)
3. J. L. Jackel, and J. J. Johnson, "Reverse exchange method for burying proton exchanged waveguides," Electron. Lett. **27**, 1360-1361 (1991)
4. J. Olivares, J. M. Cabrera, "Modification of proton exchanged $LiNbO_3$ layers for guiding modes with ordinary polarization," Fiber Integ. Optics **12**, 277-285 (1993)
5. J. Olivares, J. M. Cabrera, "Guided modes with ordinary refractive index in proton exchanged $LiNbO_3$ waveguides," Appl. Phys. Lett. **62**, 2468-2470 (1993)
6. P. Baldi, M. De Micheli, K. El Hadi, A. C. Cino, P. Aschieri, and D. B. Ostrowsky, "Proton exchanged waveguides in $LiNbO_3$ and $LiTaO_3$ for integrated lasers and nonlinear frequency converters," Opt. Eng. **37**, 1193-1202 (1998).
7. K. El Hadi, P. Baldi, M. P. De Micheli, D. B. Ostrowsky, Y. N. Korkishko, V. A. Fedorov, and A. V. Kondrat'ev, "Ordinary and extraordinary waveguides realized by reverse proton exchange on $LiTaO_3$," Opt. Commun. **140**, 23-26 (1997)
8. Y. N. Korkishko, V. A. Fedorov, T. M. Morozova, F. Caccavale, F. Gonella, and F. Segato, "Reverse proton exchange for buried waveguides in $LiNbO_3$," J. Opt. Soc. Am. A **15**, 1838-1842 (1998)
9. J. Rams, J. Olivares, and J. M. Cabrera, "SHG-capabilities of reverse PE-$LiNbO_3$ waveguides," Electron. Lett. **33**, 322-323 (1997)
10. A. W. Snyder and J. D. Love, *Optical Waveguide Theory* (Chapman & Hall, London, 1983)
11. G. R. Hadley, "Transparent boundary condition for the beam propagation method," IEEE J. Quantum Electron. **28**, 363-370 (1992)
12. G. J. Edwards and M. Lawrence, "A temperature dependent dispersion for congruently grown lithium niobate," Opt. & Quantum Electron. **16**, 373-374 (1984)
13. K. Chikuma and S. Umegaki, "Characteristics of optical second-harmonic generation due to Cerenkov-radiation-type phase matching," J. Opt. Soc. Am. B **7**, 768-775 (1990)
14. M. De Micheli, "Second harmonic generation in Cerenkov configuration" in *Guided Wave Nonlinear Optics*, D. B. Ostrowsky and R. Reinisch eds. (Kluwer Acad. Publishers., Dordrecht, NL 1992)
15. G. Arvidsson and F. Laurell, "Nonlinear optical wavelength conversion in Ti:$LiNbO_3$ waveguides," Thin Solid Films **136**, 29-36 (1986)

#30076 - $15.00 US
Received January 02, 2001; Revised January 23, 2001

16. N. A. Sanford and J. M. Connors, "Optimization of the Cerenkov sum-frequency generation in proton-exchanged Mg:$LiNbO_3$ channel waveguides," J. Appl. Phys. 65, 1430-1437 (1989)
17. G. Tohmon, J. Ohya, K. Yamamoto, and T. Taniuchi, "Generation of ultraviolet picosecond pulses by frequency-doubling of laser diode in proton-exchanged MgO:$LiNbO_3$ waveguide," IEEE Phot. Techn. Lett. 2, 629-631 (1990)
18. W. Sohler and H. Suche, "Second-harmonic generation in Ti-diffused $LiNbO_3$ waveguides with 25% conversion efficiency," Appl. Phys. Lett. 33, 518-520 (1978)

1. Introduction

Among man-made crystals for electro-optics and nonlinear photonics, Lithium Niobate (LN) is probably the most investigated and employed. It allows efficient phase and amplitude modulation and parametric generation in guided-wave configurations [1]. Several specific technologies have been mastered in order to fabricate LN planar integrated devices, from Titanium in-diffusion to ion-exchange to e-beam implantation, etc. Among them, proton exchange (PE) combines the advantages of a low-temperature process with a substantial surface index increase and a reduced photorefractive sensitivity [2]. Despite their high quality, even with additional improvements such as thermal annealing, soft exchange in diluted solutions, sealed ampoule method, etc., the asymmetric profile of PE waveguides is an obstacle to efficient coupling to/from silica fibers. In order to improve such coupling between waveguide and LP_{01} fiber modes, Reverse PE (RPE) was recently introduced to obtain buried and more symmetric channel waveguides.[3-8]

RPE is a two-step process: a first, deeply penetrating $H^+ \rightarrow Li^+$ exchange followed by a second, weaker $Li^+ \rightarrow H^+$ exchange. Such technique allows to form two superimposed waveguides with graded index profiles, each of them able to confine one of the principal (orthogonal) polarizations. For a z-cut crystal, for instance, an ordinary ray can be confined as a TE guided mode, while an extraordinary ray becomes a TM eigenfields. As sketched in Fig. 1, TE and TM waves can then propagate and carry power along y at different depths, corresponding to the two (ordinary and extraordinary) refractive distributions.

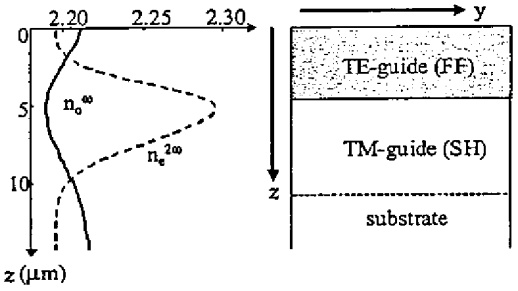

Fig. 1. RPE geometry with graphs of ordinary and extraordinary index distributions in z-cut LN.

These superimposed waveguides can be coupled by a nonlinear interaction involving a non-diagonal element, i. e., thru a polarization field orthogonally polarized with respect to the input electric wave. This is the typical configuration of a Type I phase-matched process of Second-Harmonic Generation (SH-G), whereby the harmonic is orthogonal to the fundamental frequency (FF) field. Furthermore, this is the standard SHG taking place in uniform birefringent phase-matched LN crystals thru the d_{31} element of the quadratic susceptibility, the largest non-diagonal. It is worth underlining that the double exchange tends to recover the quadratic nonlinear response of the surface layer, contrary to single-step PE [9]. Therefore,

#30076 - $15.00 US

Received January 02, 2001; Revised January 23, 2001

using mode coupling between fundamental and second harmonics in the surface and buried guides of an RPE geometry, respectively, one expects the generation of a TM frequency-doubled field by injecting a TE FF wave in the upper waveguide.

In this Paper we investigate numerically SHG in RPE planar waveguides in z-cut propagation-homogeneous (non-periodically-poled) LN, and demonstrate that large conversion efficiencies can be obtained even in those cases when much higher or lower temperatures would be required in the absence of Quasi-Phase-Matching, with good fabrication tolerances and physical separation of the harmonic field distributions at the output.

2. Models

Let us consider a z-cut y-propagating LN crystal. The pertinent non-diagonal elements of the second-order tensor d will couple z and x components of the electric-field. An FF wave propagating in the surface waveguide as a TE mode will radiate a cross-polarized SH field into the buried guide, supporting TM eigenwaves (see the extraordinary -dashed- index profile in Fig. 1). We will assume the upper guide is single-moded at the FF wavelength, whereas the deep guide is multimodal at the SH, the most common situation in a practical realization:

$$E_{TE}^{\omega}(z,y) = A(y)f_{\omega}(z)e^{-ik_0N_{\omega}y} \quad , \quad E_{TM}^{2\omega}(z,y) = \sum_v B_v(y)f_{2\omega}^{v}(z)e^{-i2k_0N_{2\omega}^{v}y} \qquad (1)$$

with k_0 the vacuum wave-number at FF and N the effective index. The generation will then take place through the interaction between the fundamental FF mode and high-order SH modes, whenever phase-matching is accomplished with an appreciable overlap integral $I = \int (f_{2\omega}^{v})^{*} f_{\omega}^{2} dz$, as prescribed by coupled-mode theory (CMT) [10].

In a structure of finite length, however, the interaction is better described by a system of partial differential equations taking into account the details of the geometry and the overall field distributions undergoing nonlinear propagation and energy exchange. For the superposition of cross-polarized (FF and SH) harmonics propagating along y in a z-cut LN crystal, using Maxwell equations in the usual approximation of weak guidance and keeping the second derivatives with respect to y, we get:

$$\begin{aligned} &\frac{\partial^2 E_{TE}^{\omega}}{\partial y^2} + \frac{\partial^2 E_{TE}^{\omega}}{\partial z^2} + k_0^2 (n_o^{\omega}(z))^2 E_{TE}^{\omega} + 2k_0^2 d_{15} E_{TM}^{2\omega} (E_{TE}^{\omega})^{*} = 0 \\ &\frac{\partial^2 E_{TM}^{2\omega}}{\partial y^2} + \frac{(n_{es}^{2\omega})^2}{(n_{os}^{2\omega})^2} \frac{\partial^2 E_{TM}^{2\omega}}{\partial z^2} + 4k_0^2 (n_e^{2\omega}(z))^2 E_{TM}^{2\omega} + 4k_0^2 d_{31} (E_{TE}^{\omega})^2 = 0 \end{aligned} \qquad (2)$$

with n_o^{ω} and $n_e^{2\omega}$ the ordinary and extraordinary graded index distributions at FF and SH, respectively, $n_{os}^{2\omega}$ and $n_{es}^{2\omega}$ the bulk (i. e., substrate) ordinary and extraordinary indices at SH, $d_{15}=d_{31}$ the relevant nonlinear coefficients when Kleinmann symmetry holds. The set (2) can be integrated using the Enhanced Finite Difference Beam Propagation Method (EFDBPM) with transmitting boundary conditions [11].

To evaluate the nonlinear response in a realistic case, we considered typical index profiles for planar RPE waveguides, as prepared and reported by Korkishko *et al.* in z-cut $LiNbO_3$ [8]. The samples were first PE-treated for 14h in an Ammonium Di-Hydrophospate melt at 220°C, then they were thermally annealed for 110h at 330°C; finally, they were RPE-processed in a $LiNO_3$ melt for 100h at 300°C. For a wavelength $\lambda=2\pi c/\omega=1.32\mu m$ such that the top guide supports one mode at FF, i. e., the index distributions can be expressed as:

#30076 - $15.00 US

Received January 02, 2001; Revised January 23, 2001

$$n_{o,e}^{q\omega}(z) = n_{os,es}^{q\omega} + \Delta n_{o,e}^{q\omega} \exp\left[-\left(\frac{z-z_0}{\sigma_{oi,ei}}\right)^2\right] \qquad (3)$$

with q=1 (2) for the FF (SH), i=1 (2) $\forall\, z<z_0$ ($\forall\, z>z_0$), z_0=6μm, σ_{o1}=4μm, σ_{o2}=5μm, σ_{e1}=2μm, σ_{e2}=3μm, Δn_o^{ω}= - 0.028 and $\Delta n_e^{2\omega}$= 0.1.

For the profiles (3) and q=1, we calculated the FF eigenmodes with a Finite Difference Method (FDM). Then, we integrated eqns. (2) launching in the upper guide suitable FF field distributions and studying the y-evolutions of FF and SH waves. In our simulations we employed either an LP01-like (x-invariant) Gaussian beam with a symmetric distribution $u_1(z) = \exp[-(z-z_1)^2/\sigma^2]$ optimally centered at z_1=3μm with σ=0.83z_1; or the zeroth-order TE eigenmode as derived numerically by FDM. Integrating the SH field and its intensity over the output transverse (z) section at a distance L from the input, we evaluated SHG conversion efficiencies (per unit wavefront along x) for various excitation levels, temperatures and device lengths.

3. Results and discussion

Let us first compare the outcomes from standard CMT and EFDBPM with eqns. (2). For a 1cm-long sample at 25°C, it is apparent from Fig. 2 that the computed conversion efficiency with the two approaches (using a Gaussian excitation for the EFDBPM) is markedly different. Examining in more detail the case of a Gaussian excitation, mapping FF and SH intensities

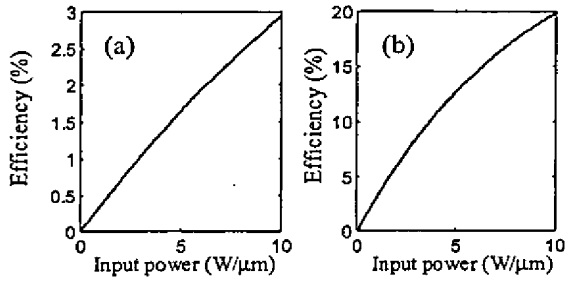

Fig. 2. Computed SHG conversion efficiency versus input power for a 1cm sample at 25°C. (a) CMT and (b) EFDBPM results in case of Gaussian excitation.

versus propagation and depth, we see in Fig. 3 that, for a 10W/μm input power into an RPE waveguide of length L=2cm, nearly 80% of the input beam couples to the TE_0 mode of the upper waveguide, with the remaining 20% exciting a leaky or quasi-mode, as apparent from the lobes visible across the depth coordinate z (Fig. 3a). The parametric nonlinearity generates a TM polarized SH field which, confined in the buried waveguide, grows with propagation. The competition between the two excited modes at FF, however, limits the overall up-conversion efficiency. This insight is supported by Fig. 4, showing the effective index versus modal number at SH at 25°C. The 10^{th} mode is close to phase match the fundamental FF mode, but the FF quasi-mode can interact via higher-order modes, thereby limiting the amount of frequency doubled power through Maker-like interference. Moreover, due to the particular geometry and in contrast to the collinear guided-wave case, the overlap integral with the TE_0 at ω is an increasing function of the modal order at 2ω, as displayed in the inset of Fig. 4. In any case, the EFDBPM clearly provides a more accurate estimate of the up-converted energy at the output.

#30076 - $15.00 US
Received January 02, 2001; Revised January 23, 2001

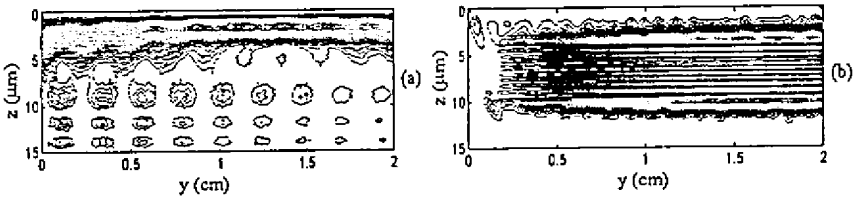

Fig. 3. Contour maps of (a) FF and (b) SH intensity versus z and y for a Gaussian input at 10W/μm in a sample at temperature 25°C.

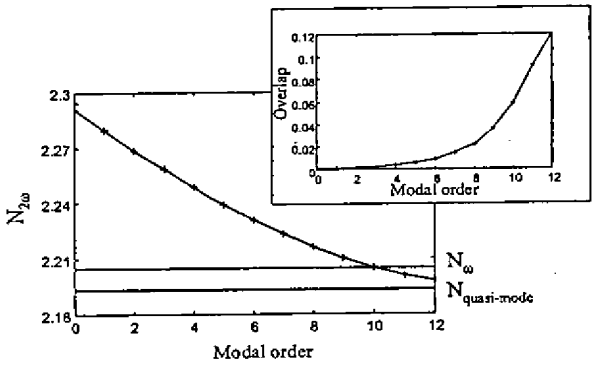

Fig. 4. Phase-matching diagram at 25°C versus modal order m at SH. The horizontal lines refer to the FF modes, TE_0 and leaky (or quasi-mode), respectively. The inset shows the corresponding TM_m-TE_0 overlap integral.

The conversion process can be enhanced by exciting only one FF mode, launching an input beam with transverse profile mapping the TE_0 mode. In this case, at an optimum temperature of 85°C corresponding to phase-matching, the SH grows monotonically along y largely depleting the fundamental, as visible in Fig. 5.

Using this optimum input profile, by a transverse integration in y=L we computed SHG conversion versus input FF power (in W/μm). The results are shown in Fig. 6 for two different sample lengths and temperatures. Due to the nature of the interaction and the substantial pump depletion, the conversion efficiency is sub-linear with both FF excitation and square of the propagation distance. For L=2cm it reaches 90% at 10W/μm, with a maximum normalized value of 14% μm/W cm (Fig. 6b, solid line). The temperature dependence, taken into account at each wavelength and polarization [12], is rather weak. This is clearly visible in Fig. 7, where the SHG efficiency is graphed versus temperature for two different input powers and sample lengths.

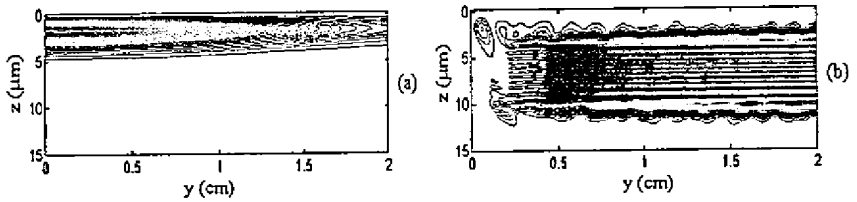

Fig. 5. Contour maps of (a) FF and (b) SH intensity versus z and y for a TE_0 input at 10W/μm.

#30076 - $15.00 US
Received January 02, 2001; Revised January 23, 2001

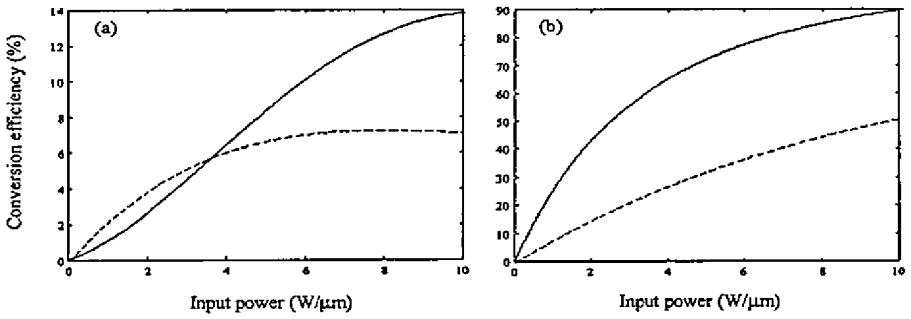

Fig. 6. Conversion efficiency versus input FF power (TE_0 excitation) at (a) 25 and (b) 85°C, for samples 1cm (dashed line) and 2cm (solid line) in length.

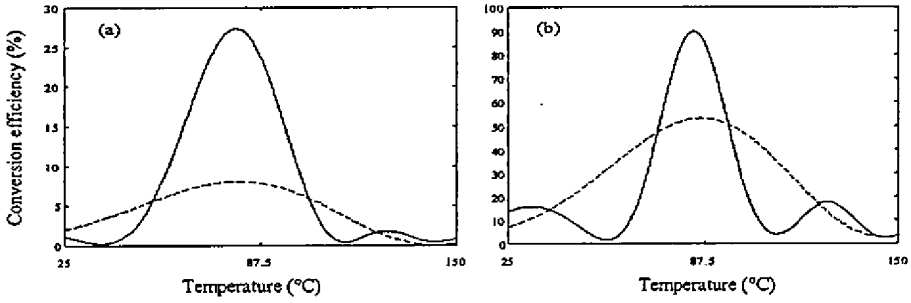

Fig. 7. Conversion efficiency versus temperature (TE_0 excitation) at input powers of (a) 1W/μm and (b) 10W/μm, for samples 1cm (dashed line) and 2cm (solid line) in length.

4. Conclusions

The major drawbacks of Cerenkov and temperature-tuned SHG, i. e. conical emission and critical thickness in PE waveguides [13-14] or critical temperature/modal tuning in Ti:in-diffused channels [15], respectively, can be eliminated in propagation-uniform Reverse Proton Exchanged guides in z-cut Lithium Niobate. The conversion efficiencies, numerically estimated using a propagator based on a robust PDE model, are as high as 90% at a fundamental wavelength of 1.32μm in 2cm-long planar guides optimally excited at 10W/μm. Such values compare well to the best results reported to date in non-periodically-poled LN (i. e., non quasi-phase-matched) waveguides, both in Cerenkov [16-17] and guided-wave interactions [15, 18].

RPE waveguides appear to be promising candidates for robust and low temperature frequency doubling, with the unique advantages of SH confinement, weak temperature sensitivity, polarization selection and physical separation of the harmonics at the output. We are currently investigating channel waveguides for bidimensional confinement and longitudinally tapered transverse profiles for improved coupling/handling of the up-converted output distribution.

Acknowledgements

This work was funded by the Italian Space Agency (ASI-ARS), the Italian Research Council (PF MADESS II) and the Ministry for Scientific Research (Cofin 2000). G. Assanto thanks M. Peccianti and G. Leo for useful suggestions.

#30076 - $15.00 US

Received January 02, 2001; Revised January 23, 2001

Depth profiling of the d_{33} nonlinear coefficient in annealed proton exchanged $LiNbO_3$ waveguides

M. L. Bortz, L. A. Eyres, and M. M. Fejer
E. L. Ginzton Laboratory, Stanford University, Stanford, California 94305

(Received 17 December 1992; accepted for publication 25 February 1993)

We report depth profiling of the d_{33} nonlinear coefficient in annealed proton exchanged $LiNbO_3$ waveguides using reflected second-harmonic generation from angle-lapped samples. At depths greater than the initial proton exchange depth the d_{33} coefficient retains nearly its bulk $LiNbO_3$ value, but within the initial proton exchange region the value of d_{33} varies with annealing time. These results reconcile previous conflicting measurements of the d_{33} coefficient and explain the variation in the efficiency of guided wave frequency conversion devices with annealing.

Quasi-phase matched (QPM) frequency conversion in $LiNbO_3$ waveguides is an efficient method for the generation of short wavelength radiation from infrared laser diodes. While different techniques have been used to form the ferroelectric domain grating necessary for QPM, the annealed proton exchange (APE) process has been used exclusively to provide waveguide confinement. Contradictory measurements of the nonlinear optical properties of proton exchange (PE) and APE-$LiNbO_3$ waveguides have been previously reported.[1-6] The d_{33} coefficient of PE-$LiNbO_3$ has been measured to be between 0 (Refs. 4 and 5) and 0.63 (Ref. 3) of the bulk $LiNbO_3$ value. The effect of annealing is similarly controversial, with measurements of d_{33} in APE-$LiNbO_3$ varying from 0% (Ref. 4) to 90% (Ref. 3) of the bulk value. Recently demonstrated[7,8] guided-wave QPM second-harmonic generation (SHG) devices with normalized conversion efficiencies $> 600\%/W\,cm^2$ indicate that APE-$LiNbO_3$ waveguides must have a large nonlinear coefficient.

In this letter we report measurements of the depth dependence of the d_{33} nonlinear coefficient in APE-$LiNbO_3$ waveguides using reflected SHG from angle-lapped samples. With a 532 nm fundamental wavelength, the 266 nm second-harmonic (SH) wavelength is above the APE-$LiNbO_3$ band edge so that only the SH generated within a 0.05 μm absorption depth[4] of the surface is observed. The samples were angle lapped so that lateral position could be mapped onto depth into the sample, allowing depth profiling via lateral translation. This technique circumvented complications caused by the graded refractive index profile and the unknown spatial variation in the d_{33} coefficient in the APE-$LiNbO_3$. The depth profiles presented here explain the variation in the d_{33} values reported in the literature. Normalized conversion efficiencies calculated with our results are consistent with those observed from guided-wave QPM SHG devices.

APE waveguides were fabricated on x-cut $LiNbO_3$ by proton exchange in pure benzoic acid at 173 °C for 66 min to a depth of 0.42 μm, calculated using the results of Ref. 9, and annealed in air at 333 °C for varying times. The samples were then polished at a wedge angle < 2 mrad, with the actual relationship between lateral position and depth determined using surface profilometry. 532 nm radiation from an injection seeded Q-switched frequency-doubled Nd-YAG laser was focused onto the sample at normal incidence with a 30 μm FWHM spot and a peak intensity of <150 MW/cm^2. The samples were scanned under the focused spot using a motorized translation stage and the reflected 266 nm SH was detected using a dichroic mirror, a solid blind photomultiplier, and a gated integrator. The fundamental and SH fields were polarized parallel to each other and the z axis of $LiNbO_3$ and thus were coupled by the d_{33} nonlinear coefficient. To discriminate against polishing artifacts, each sample had an internal, unexchanged reference portion formed by masking half the sample with Al prior to proton exchange. The mask was removed by etching in NaOH prior to annealing. A portion of the sample remained unwedged, so that reflected SH could be obtained from the original surface. SHG and profilometry measurements were performed over the whole surface to eliminate errors associated with polishing skew. Figure 1 shows the sample orientation and geometry, with the dashed line indicating the beginning of the wedged portion of the sample and the origin for measurements of lateral position; negative values of lateral position represent data from the unwedged portion of the sample, i.e., the original surface.

Figure 2 shows the reflected SH power at 266 nm, normalized to the signal from bulk $LiNbO_3$ versus depth and lateral position for APE-$LiNbO_3$ waveguides annealed for 3, 5, 9, and 63 h. The error bars represent the variation in the depth measurement for 5 different scans. The figure inset shows the spatial step response of the detection system projected onto depth, measured by scanning the focused spot off the end of a bulk $LiNbO_3$ sample. This

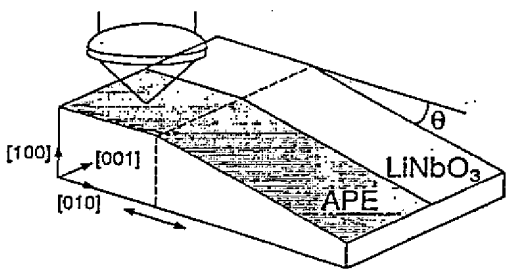

FIG. 1. Geometry of the wedged sample used for reflected SHG measurements.

 0003-6951/93/172012-03$06.00

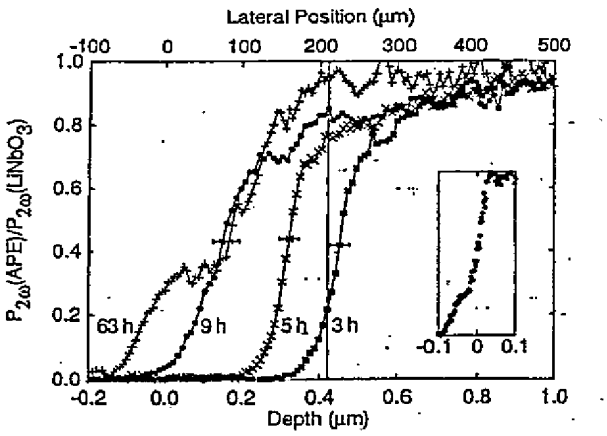

FIG. 2. Reflected 266 nm SH intensity, normalized to that from bulk $LiNbO_3$, vs lateral position (top scale) or depth into the waveguide (bottom scale) for samples proton exchanged to 0.42 μm and annealed for 3, 5, 9, and 63 h. The inset shows the step response of the detection system.

demonstrates a depth resolution of <0.05 μm. The samples displayed constant reflected SH over the entire unexchanged side with intensities equal to that from bulk $LiNbO_3$, with the exception of the sample annealed for 63 h, which had a polishing artifact between lateral positions -75 and $+50$ μm.

For the APE-$LiNbO_3$ sample annealed for 3 h no reflected SH signal was observed from the original surface or from the portion of the wedged surface corresponding to the original PE layer. However, there is an abrupt increase from 0% to 80% of the bulk $LiNbO_3$ value at a position corresponding to the interface between the original PE film and the $LiNbO_3$ substrate. At lateral positions corresponding to depths greater than the initial PE depth, the reflected SH power approaches that measured from bulk $LiNbO_3$. At depths >1 μm the measured reflected SH power is indistinguishable from that of bulk $LiNbO_3$.

With further annealing, the position of the abrupt increase in the reflected SH power moves toward the original surface, and the reflected power approaches that from bulk $LiNbO_3$ at shallower positions. No reflected signal was ever observed from the original surface regardless of annealing time, except from the sample annealed for 63 h at lateral positions where polishing damage was observed. However, no signal was observed over the rest of the unwedged portion of this sample.

The two previous measurements[4,6] of the d_{33} coefficient of APE-$LiNbO_3$ waveguides performed using reflected SHG with a 532 nm fundamental source were made on unwedged samples, only probing a 0.05-μm-thick region at the original surface. Reference 2 reported no reflected SH regardless of annealing time at annealing temperatures of 350 °C, similar to our results when the probe is confined to the unwedged part of the sample. Reference 4 reported that APE-$LiNbO_3$ proton exchanged for 0.5 h and annealed for 1.5 h at 310 °C or for 1 h at 350 °C exhibited reflected SH with an intensity of 1/2 or 1/4 that obtained from bulk $LiNbO_3$. For samples proton exchanged longer than 0.5 h, no reflected SH was observed, regardless of annealing time or temperature.

The absence of any reflected SH from the unannealed PE region could be explained by the formation of a PE-$LiNbO_3$ film with either inversion symmetry or a different $\chi^{(2)}$ tensor that did not result in any reflected SH. Similarly, the progression of the abrupt steplike recovery to the surface region with increasing annealing could be explained by the solid state epitaxial regrowth of the $LiNbO_3$ phase from the original interface between the PE film and the $LiNbO_3$ substrate. After the abrupt increase in the reflected SH from 0% to 80% of the bulk value there is a slower approach to the bulk value occurring over the next 0.5 μm in depth. In this region the measured d_{33} value correlated with concentration, independent of annealing time, so we conclude that for low concentrations the d_{33} coefficient is slightly reduced from its bulk value. While the details of the progression of the d_{33} recovery to the original surface may be dependent on the orientation of the $LiNbO_3$ substrate and annealing temperature, it is unlikely that the d_{33} coefficient of APE-$LiNbO_3$ waveguides fabricated on z- and x-cut substrates differ substantially at depths greater than the initial PE depth. Understanding the absence of reflected SH from the original surface of APE-$LiNbO_3$ may require microstructural and x-ray diffraction experiments to elucidate the crystal structure within the top 0.05 μm of the surface. This is of little practical importance since the modal amplitudes are very small at the surface. To design guided wave frequency conversion devices it is adequate to assume that at depths greater than the initial PE depth the d_{33} coefficient nearly retains its bulk value throughout annealing, while variations occur within the original PE depth.

The measurements of the d_{33} coefficient shown in Fig. 2 can be used to determine the normalized conversion efficiencies (η) for any guided wave nonlinear optical interaction. As an example, we compute η for SHG of $\lambda_\omega=850$ nm radiation in z-cut, x-propagating APE-$LiNbO_3$ waveguides fabricated like those shown in Fig. 2. We assume first-order QPM over an interaction length l with a uniform, depth-independent ferroelectric domain grating, which can be fabricated using an electric-field[7] or electron-beam[8] poling technique. With the output SH power given by $P_{2\omega}=\eta P_\omega^2 l^2$, η is given by

$$\eta=\frac{8\pi^2(d_{\mathrm{QPM}})^2}{n_\omega^2 n_{2\omega} c\epsilon_0 \lambda_\omega^2} \times\left|\int_{-\infty}^{+\infty}\int_0^{+\infty}\bar{d}_{33}^{\mathrm{APE}}(z)E_\omega^2(y,z)E_{2\omega}(y,z)\,dy\,dz\right|^2,$$

where $d_{\mathrm{QPM}}=2d_{33}^{\mathrm{LiNbO_3}}/\pi$, $\bar{d}_{33}^{\mathrm{APE}}(z)=d_{33}^{\mathrm{APE}}(z)/d_{33}^{\mathrm{LiNbO_3}}$, and the fields are normalized to carry unity power. The depth dependence of the refractive index profile was determined using a one-dimensional nonlinear diffusion model for the APE process,[10] and we assume a 4-μm-wide top-hat dependence for the lateral refractive index profile. We assume that the two-dimensional modes are separable, $E(y,z)=E_y(y)E_z(z)$, and compute the mode profiles at

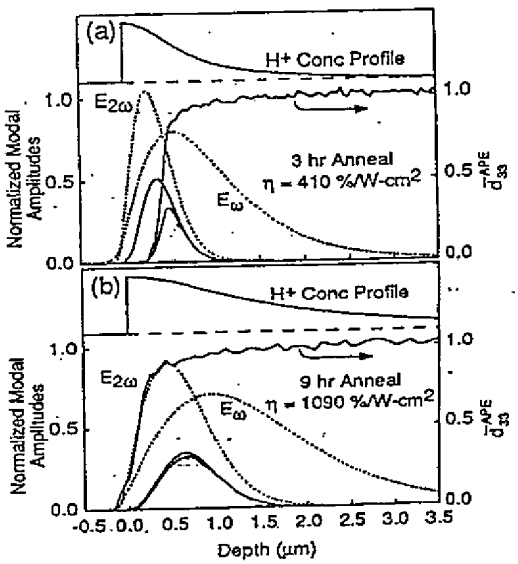

FIG. 3. Fundamental (λ_ω=850 nm) and SH ($\lambda_{2\omega}$=425 nm) modes (dotted lines), modal overlap (solid line), measured normalized nonlinear coefficient $\bar{d}_{33}^{APE}$, the modal overlap with $\bar{d}_{33}^{APE}$ (shaded region), and the H^+ concentration profile vs depth in APE-$LiNbO_3$ waveguides annealed for (a) 3 h and (b) 9 h. The abscissa is the same for (a) and (b).

λ_ω=850 nm and $\lambda_{2\omega}$=425 nm using the effective index method. The depth overlap integral was evaluated using the depth dependence of the d_{33} coefficient derived by taking the square root of the normalized reflected SH power given in Fig. 2. Shown in Fig. 3 versus depth are the optical modes, the measured normalized nonlinear coefficient $\bar{d}_{33}^{APE}(z)$, the modal overlap $E_\omega^2(z)E_{2\omega}(z)$; and as the shaded region, the modal overlap with the measured value of the nonlinear coefficient, $\bar{d}_{33}^{APE}(z)E_\omega^2(z)E_{2\omega}(z)$, for waveguides annealed for 3 and 9 h; the data for a 5 h anneal are not shown for brevity. Also shown is the H^+ concentration profile, proportional to the index profile. At λ_ω the surface index changes are 0.0503, 0.0364, and 0.0230, for 3, 5, and 9 h anneals, respectively. The overlap using the measured value of d_{33} yields η versus annealing of 410, 950, and 1090%/W cm^2. For comparison, the modal overlap assuming the d_3 coefficient to be independent of depth yields η versus annealing of 2010, 1640, and 1280%/W cm^2.[11] For unannealed waveguides η=0 since d_{33}=0 for unannealed PE-$LiNbO_3$. For anneal times longer than 9 h the modal overlap is removed from the region where d_{33}=0 and η decreases because of reduced confinement. Figure 3 shows that the variation in η with annealing is not due to a restoration in the d_{33} coefficient of the APE-$LiNbO_3$ waveguide as much as a variation in the overlap integral due to a spatial redistribution of the modal fields away from the initial PE region.

There are two recent reports of guided-wave QPM SHG using depth-independent ferroelectric domain gratings, with η of 600 (Ref. 7) and 700%/W cm^2 (Ref. 8) for devices with APE waveguides fabricated similarly to the ones modeled above. These values fall within the range modeled, indicating that the general form of the d_{33} depth profile presented here allows reasonably accurate device modeling. However, waveguide loss, laser longitudinal mode structure, QPM grating and waveguide inhomogeneities, and the value of the d_{33} coefficient of bulk $LiNbO_3$ (recently measured to be 23.7 pm/V[12] rather than the accepted value of 34.5 pm/V) render the modeling of the absolute η of real devices difficult and questionable. Measurements of η as a function of waveguide processing are ongoing to refine the models for the linear and nonlinear optical properties of APE-$LiNbO_3$.

The authors acknowledge Joe Vhrel and Chris Remen for excellent sample preparation and Steven Biellak for assistance with profilometry. This work has been supported by DARPA and JSEP.

[1] T. Suhara, H. Tazaki, and H. Nishihara, Electron. Lett. 25, 1326 (1989).
[2] R. W. Keys, A. Loni, and R. M. De La Rue, Electron Lett. 26, 624 (1990).
[3] X. Cao, R. Srivastava, R. V. Ramaswamy, and J. Natour, IEEE Photon. Tech. Lett. 3, 25 (1991).
[4] F. Laurell, M. G. Roelofs, and H. Hsiung, Appl. Phys. Lett. 60, 301 (1992).
[5] M. L. Bortz and M. M. Fejer, Opt. Lett. 17, 704 (1992).
[6] W. Hsu, C. S. Willand, V. Gopalan, and M. C. Gupta, Appl. Phys. Lett. 61, 2263 (1992).
[7] M. Yamada, N. Nada, M. Saitoh, and K. Watanabe, Appl. Phys. Lett. 62, 435 (1993).
[8] M. Fujimura, K. Kintaka, T. Suhara, and H. Nishihara, Electron. Lett. 28, 1868 (1992).
[9] T. Maciak and M. Sokolowski, Opt. Appl. 19, 423 (1989).
[10] M. L. Bortz and M. M. Fejer, Opt. Lett. 16, 1844 (1991).
[11] We assume d_{33}=34.5 pm/V for bulk $LiNbO_3$.
[12] T. Kondo, I. Shoji, K. Yashiki, and R. Ito, in *Quantum Electronics and Laser Science Conference*, 1992 OSA Technical Digest Series Vol. 13 (Optical Society of America, Washington, DC, 1992), pp. 242–244.

ELSEVIER

1 February 1997

Optics Communications 135 (1997) 41–44

OPTICS COMMUNICATIONS

Blue light generation in a periodically poled Ti:$LiNbO_3$ channel waveguide

J. Amin *, V. Pruneri, J. Webjörn [1], P.St.J. Russell, D.C. Hanna, J.S. Wilkinson

Optoelectronics Research Centre, University of Southampton, Southampton, SO17 1BJ, UK

Received 8 May 1996; accepted 23 July 1996

Abstract

We report the first realisation of periodic domain inversion by electric-field poling in Ti:$LiNbO_3$ waveguides, for quasi-phase-matching (QPM) applications. Using a tunable Ti:Al_2O_3 laser we demonstrate guided blue light generation in a third-order QPM interaction.

Keywords: Lithium niobate; Quasi-phase-matching; Blue light generation

1. Introduction

Second harmonic generation (SHG) by quasi-phase-matching (QPM) in $LiNbO_3$, via periodic modulation of the nonlinear coefficient, provides an attractive route for the realisation of blue and green light sources with several mW of output power. Electric-field poling has recently been used extensively for periodic domain reversal in ferroelectric materials, and hence modulation of the nonlinear coefficient. This technique allows the use of the large d_{33} coefficient and provides deep, laminar domain structures with high potential conversion efficiencies. Several devices have been demonstrated using this technique for QPM-SHG from IR wavelengths to the visible, both in bulk geometries [1,2], and in waveguide structures [3,4]. However, as with most other waveguide QPM-SHG devices demonstrated thus far [5], the waveguides in Refs. [3,4] were fabricated using the annealed proton exchange technique. The only demonstration of periodic domain inversion for QPM-SHG in a Ti:$LiNbO_3$ waveguide to date has been that by Webjörn et al. [6], using a periodically segmented waveguide. Domain inversion in this case was achieved through outdiffusion between the patterned Ti segments. However, the conversion efficiency obtained was $0.1\%/W \cdot cm^2$, much smaller than that predicted by theory, possibly due to the domains being too shallow to allow a good overlap with the optical modes. Extension of electric-field poling to Ti-indiffused waveguides would circumvent this problem by providing deep domains, hence allowing better interaction with the guided modes, and would also provide additional design options over those available with proton-exchanged waveguides, such as allowing the use of both the extraordinary and ordinary waves for frequency conversion, and offering opportunities for active guides doped with rare-earths. In this paper we demonstrate, for the first time to our knowledge, blue light generation by QPM in an electric-field poled Ti:$LiNbO_3$ channel waveguide.

2. Fabrication

Channel waveguides were fabricated parallel to the X-axis by diffusing Ti stripes, 95 nm thick and ranging in width from 3 μm to 16 μm in 1 μm steps, into the $-Z$

* Corresponding author. Present address: NIST, Optoelectronics Division (815.04), 325 Broadway, Boulder, CO 80303-3328, USA. Tel: ++1 303 497 3289; Fax: ++1 303 497 3387; Email: jamin@boulder.nist.gov.

[1] Present address: SDL, Inc., 80 Rose Orchard Way, San Jose, CA 95134-1365, USA.

PII S0030-4018(96)00497-X

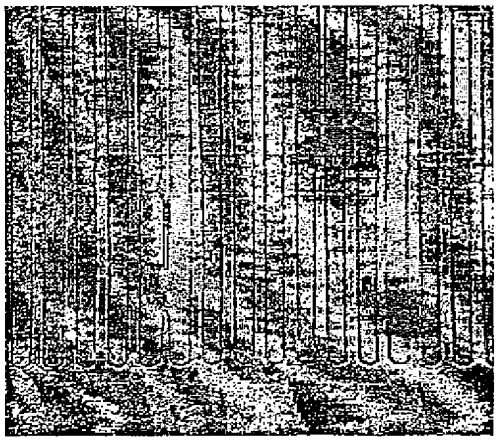

Fig. 1. Etched $-Z$ face of a section of the sample, showing a 10 μm wide waveguide along the X-axis. The non-uniform domains within the waveguide are clearly visible.

face of a 0.2 mm thick piece of $LiNbO_3$ (Z-cut) at 1005°C over a period of 9 hours. Our initial attempts to pole high-temperature-metal-diffused $LiNbO_3$ had been unsuccessful owing to the presence of a thin Li_2O outdiffusion-induced domain-inverted layer on the $+Z$-face, as revealed by wet etching, which blocked the e-field poling. In this case, to facilitate poling we removed the outdiffused layer by polishing off 50 μm of material from the $+Z$ face after the waveguide fabrication, thus ensuring that the crystal domain structure was unidirectional. Next, 1 mm wide rectangular slots of period 9 μm and a duty cycle of 33% (3 μm linewidth), were opened in a photoresist mask on the $-Z$ face of the sample, oriented perpendicular to the waveguides. This period was chosen as suitable for third-order QPM frequency-doubling to the blue from an IR wavelength of approximately 850 nm. Poling was achieved by applying four pulses of ~3 kV and ~300 ms duration via liquid electrodes, as described previously [1]. Fig. 1 shows the $-Z$ face of a small part of the sample, etched in a mixture of HF and HNO_3. The photograph shows a 10 μm wide waveguide, with evidence of non-uniformity of the grating, including random fluctuations in the domain wall positions, within the waveguide. Furthermore, the final grating structure obtained in the waveguides had, on average over the complete interaction length, a duty cycle between 60% and 80%. The occurence of this non-optimal mark/space ratio requires further investigation to allow accurate control of device parameters. A similar grating pattern was observed on the $+Z$ face, the etched regions on this face corresponding to the non-etched regions on the $-Z$ face, hence demonstrating continuous poling through the sample, with the rectangular domain shape generally maintained. The waveguide endfaces were then polished, yielding 5 mm long guides, periodically poled along the entire length.

3. Optical characterisation

A tunable Ti:Al_2O_3 laser was used for the characterisation of SHG from the waveguides. In this initial study we investigated blue light generation from a 6 μm wide guide. Fig. 2 shows the third order SH output, which emerged entirely from the waveguide, as a function of the fundamental wavelength. The fundamental light beam in this case was polarised along the z-direction, i.e. TM polarised, producing an interaction with the d_{33} coefficient. As shown in the figure, conversion was achieved from the TM_{00} mode at the fundamental frequency to the TM_{00} and TM_{10} modes at the SH frequency. It was noticed that, for the same input power, the conversion efficiency to the second order harmonic mode was higher than that to the first order. We believe this to be due to a nonuniformity in the grating across the waveguide over a substantial part of the device length, as revealed through close inspection of the device, so that the second order mode interacts with the fundamental over a QPM structure which has a duty cycle closer to that required for optimum conversion efficiency in third order QPM. Moreover, there may be a reduced nonlinearity near the surface, due to the diffusion process, and variations in the index profile along the length of the waveguide, which would have a strong detrimental effect on the coupling to the TM_{00} mode. Index variation effects are also evident in the difference in shape of the phase matching curves for the first and second order mode interactions. The phase matching curve for the $TM^{\omega}_{00} \rightarrow TM^{2\omega}_{00}$ interaction is centred at ~845 nm, in good agreement with the calculated wavelength using dispersion relations for Ti:$LiNbO_3$ waveguides [7]. The curve however shows a FWHM bandwidth of ~0.25 nm, twice that

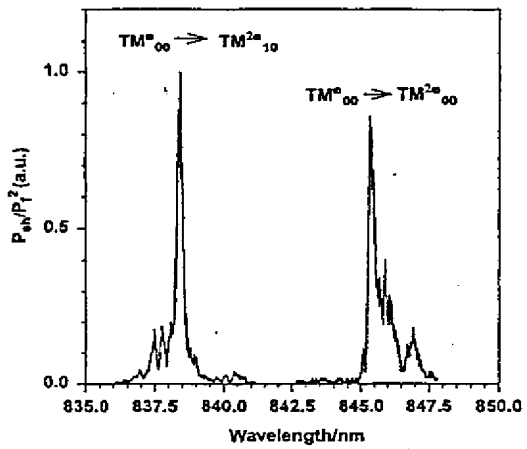

Fig. 2. Guided second harmonic generated power normalised to the launched pump power, as a function of the fundamental wavelength. The phase matching wavelength in the bulk was found to be ~834 nm.

calculated from theory. This could be caused either by the irregular grating period or the above mentioned variation in effective index along the guide, due to inhomogeneities in the waveguide [8,9]. Fig. 3 shows the measured blue power in the fundamental mode of the harmonic frequency as a function of the coupled fundamental power at ~ 845 nm, the line in the figure being the best quadratic fit to the experimental points. The maximum power obtained in the blue was 7.9 μW for a coupled power of 45 mW, giving a conversion efficiency of $1.6\%/\mathrm{W}\cdot\mathrm{cm}^2$. The conversion efficiency in this non-optimised demonstration device is more than one order of magnitude lower than that expected from theory. This, as mentioned above, is believed to be due to the grating mark/space ratio not being ideal, non-perfect axial and transverse uniformity of the grating, non-optimised overlap between the interacting modes and inhomogeneities in the effective index.

The experimental points in Fig. 3 deviate slightly from the expected quadratic dependence, indicating the presence of photorefractive damage. Although periodic poling has been observed to increase the photorefractive damage threshold of $LiNbO_3$ [1], Goldberg et al. have recently observed damage effects at room temperature in their SHG experiments [2]. These were attributed largely to a non-ideal grating structure, which would also apply to our waveguide. At coupled fundamental powers greater than 45 mW, the photorefractive damage was even more evident, with the blue output radiation spreading along the Z-axis. No attempt was made, in this initial experiment, to heat the sample and thereby anneal the damage. However, it is expected that it may be possible to reduce the photorefractive damage in periodically poled Ti:$LiNbO_3$ waveguides by moving to a period smaller than the mode size in the

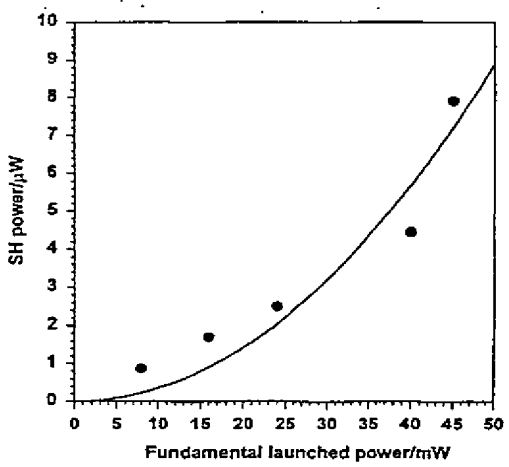

Fig. 3. Second harmonic generated power as a function of the launched pump power. Note that the SHG power is that detected in the fundamental SHG mode at ~ 422.5 nm. The solid line is the best quadratic fit to the measured data points.

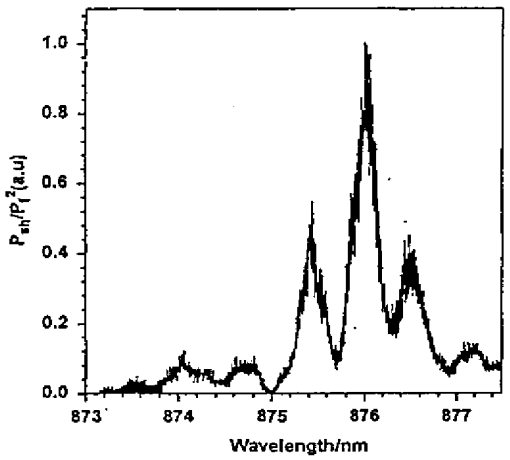

Fig. 4. Phase matching curve for the interaction of the fundamental mode in the TE polarisation to the second order mode of the second harmonic in the TM polarisation ($TE_{00}^{\omega} \rightarrow TM_{01}^{2\omega}$).

waveguide and ensuring that the domain structures are continuous and well defined. Using a period smaller than the mode size would enable a better compensation of the accumulated charges at the top and bottom of the beam profile [10]. These charges have opposite signs in adjacent domains as the photogalvanic current, which produces this charge transport across the beam, follows the direction of the Z-axis. The resulting transverse electric field component, and therefore the induced refractive index change via the electro-optic effect, would thus be reduced.

Finally, the polarisation of the input mode at the fundamental wavelength was rotated by 90°, thus exciting the guides in the TE polarisation, and an interaction was made with the d_{31} coefficient. The phase matching curve for the $TE_{00}^{\omega} \rightarrow TM_{10}^{2\omega}$ interaction, centred at 876 nm, is shown in Fig. 4. The theoretically predicted wavelength for conversion to the first order SH mode is ~ 884 nm, which was outside the tuning range of our laser. The experiment however demonstrates the versatility of poled Ti:$LiNbO_3$ waveguides in terms of accessibility to different wavelengths using the same waveguide. Moreover, using the ordinary polarisation for a given order of QPM-SHG for a given blue wavelength would require a longer period of domain reversal than needed for the extraordinary polarisation, alleviating some of the problems encountered in fabricating short periods. Frequency conversion using the d_{31} coefficient is less efficient ($d_{31} \sim 0.17 d_{33}$) but may be important for interactions which involve very short pulses [11], as the group velocity mismatch between interacting fields at different frequencies is reduced in this polarisation scheme, due to the lower dispersion. This makes the effective pulse interaction length longer, thus maintaining a good $d_{\mathrm{eff}} l_{\mathrm{eff}}$ product. Possibilities for RE-doped waveguide lasers in $LiNbO_3$ can also be extended, as the lasing

signal in these waveguides may be in the ordinary (σ) polarisation.

4. Conclusions

We have demonstrated, for the first time to our knowledge, periodic poling in a Ti:$LiNbO_3$ channel waveguide using electric-field techniques, and generated blue light via third order QPM. Further work is in progress to optimise the domain uniformity and modal overlaps within the waveguide, and achieve control over the resulting mark/space ratio. With these optimisations, and in particular by using a first order QPM interaction, significant increases in conversion efficiencies are expected. Moreover, we have recently demonstrated periodic poling in a Nd-diffused $LiNbO_3$ substrate [12] and also in a Tm-diffused Ti:$LiNbO_3$ waveguide [13], and intend to combine RE-diffusion and poling in Ti-indiffused waveguides for intra-cavity frequency doubling within a waveguide laser.

Acknowledgements

At the time that this work was carried out, J. Amin was with the Optoelectronics Research Centre, Southampton, and acknowledges the support of GEC-Marconi and the EPSRC under a CASE award whilst at Southampton. The Optoelectronics Research Centre is an Interdisciplinary Research Centre, partly supported by a grant from the U.K. EPSRC.

References

[1] V. Pruneri, R. Koch, P.G. Kazansky, W.A. Clarkson, P.ST.J. Russell and D.C. Hanna, Optics Lett. 20 (1995) 2375.
[2] L. Goldberg, R.W. McElhanon and W.K. Burns, Electron. Lett. 31 (1995) 1576.
[3] M. Yamada, N. Nada, M. Saitoh and K. Watanabe, Appl. Phys. Lett. 62 (1993) 435.
[4] K. Kintaka, M. Fujimura, T. Suhara and H. Nishihara, Proc. CLEO/Pacific Rim, 1995, paper FE4, p. 176.
[5] M.L. Bortz, S.J. Field, M.M. Fejer, D.W. Nam, R.G. Waarts and D.F. Welch, IEEE J. Quantum Electron. 30 (1994) 2953.
[6] J. Webjörn, F. Laurell and G. Arvidsson, J. Lightwave Technology LT7 (1989) 1597.
[7] S. Fouchet, A. Carenco, C. Daguet, R. Guglielmi and L. Riviere, J. Lightwave Technology LT5 (1987) 700.
[8] S. Helmfrid, G. Arvidsson and J. Webjörn, J. Opt. Soc. Am. B 10 (1992) 222.
[9] X. Cao, J. Natour, R.V. Ramaswamy and R. Srivastava, Appl. Phys. Lett. 58 (1991) 2331.
[10] V. Pruneri, P.G. Kazansky, J. Webjörn, P.ST.J. Russell and D.C. Hanna, Appl. Phys. Lett. 67 (1995) 1957.
[11] V. Pruneri, S.D. Butterworth and D.C. Hanna, Highly efficient green light generation by quasi-phase-matched frequency doubling of picosecond pulses from an amplified mode-locked Nd:YLF laser, in Optics Lett., to be published.
[12] J. Webjörn, J. Amin, M. Hempstead, P.St.J. Russell and J.S. Wilkinson, Electron. Lett. 30 (1994) 2135.
[13] J.K. Jones, Ph.D. thesis, Diffusively doped thulium and ytterbium lithium niobate waveguide lasers, University of Southampton, 1995.

Appl. Phys. B 73, 501–504 (2001)
DOI: 10.1007/s003400100703

Applied Physics B
Lasers and Optics

G. SCHREIER✉
H. SUCHE
Y.L. LEE
W. GRUNDKÖTTER
V. QUIRING
R. RICKEN
W. SOHLER

Efficient cascaded difference frequency conversion in periodically poled Ti:$LiNbO_3$ waveguides using pulsed and cw pumping

Universität Paderborn, Angewandte Physik, Warburger Str. 100, 33098 Paderborn, Germany

Received: 29 May 2001/Revised version: 10 August 2001
Published online: 2 November 2001 •

ABSTRACT Using an FM-mode-locked Ti:Er:$LiNbO_3$ waveguide laser as the fundamental source, wavelength conversion by cascaded $\chi^{(2)}:\chi^{(2)}$-difference frequency generation with a conversion efficiency of up to +3 (−4.6) dB was demonstrated at a pulse repetition rate of about 2 (10) GHz. In addition, multichannel conversion was demonstrated with a fully packaged wavelength converter using a continuous fundamental source.

PACS 42.65.Ky; 42.65.W; 42.72.Ai; 42.82.Cr

1 Introduction

Wavelength conversion in wavelength-division-multiplexed (WDM) and time-division-multiplexed (TDM) optical networks is a key technology of future high bit-rate transport systems. Wavelength conversion offers a higher flexibility in traffic management and a dynamic reconfiguration of the optical network. In recent years, difference-frequency converters based on periodically poled $LiNbO_3$ (PPLN) waveguides have attracted considerable interest. They fulfill numerous requirements for ideal wavelength converters for telecommunications, such as strict transparency, independence of bit rate and data format, and low cross-talk. They offer a high conversion efficiency without attenuation of the signal, adding only negligible noise from spontaneous fluorescence. In addition, the wavelength conversion bandwidth is broad, and it is possible to cascade many converters. The simultaneous conversion of many wavelength channels, spectral inversion and parametric amplification are also attractive properties of difference-frequency converters. The demonstration of second-harmonic generation (SHG) of unprecedented efficiency in PPLN waveguides [1, 2] allowed the possibility of combining SHG and difference frequency generation (DFG) in a single device or even in the same waveguide or structure [3]. In such a cascaded-DFG (cDFG) device, a strong fundamental wave at λ_f is used to generate a pump wave at $\lambda_p = \lambda_f/2$ by frequency doubling. Simultaneously the pump wave interacts with a signal wave at λ_s to generate an idler wave at λ_i with $\lambda_i^{-1} = \lambda_p^{-1} - \lambda_s^{-1} = 2\lambda_f^{-1} - \lambda_s^{-1}$. In the following we report the first demonstration of cDFG with +3 (−4.6) dB conversion efficiency at a pulse repetition rate of ~2 (~10) GHz.

✉ Fax: +49-5251/2649-11, E-mail: Gerhard.schreier@alcatel.de

2 Fabrication and characterisation

Two different PPLN waveguides (samples Str332 and Pb133z) were fabricated by in-diffusion (7.5 h at 1060 °C) in an argon inert gas atmosphere and 1 h post-diffusion at the same temperature in oxygen to re-oxidize the material of 7-μm-wide and 98-nm-thick Ti-stripes into the −Z-face of a 0.5-mm-thick $LiNbO_3$ substrate (Fig. 1). We found that subsequent electric field poling was not possible due to a shallow domain-inverted layer on the +Z-face. Therefore, we had to remove that layer by careful grinding. As domain inversion always starts on the +Z-face [4], it is advantageous to have the waveguides on that face of the sample. Taking these considerations into account, we performed as the next fabrication step a homogeneous polarisation reversal of the whole sample. Thereafter, the microdomain structure with a $\Lambda = 17$ ($\Lambda = 16.6$) μm period was fabricated by using the electric field poling method with the structured photoresist on the +Z-side. The length of the PPLN waveguides was about 78 (86) mm. After polishing the waveguide end-faces, we characterized its properties by several means. To reveal the domain pattern quality, we selectively etched a part of the sample surface using concentrated HF:HNO_3 acid (see Fig. 2).

A near-infrared camera was used to confirm that the waveguide is single mode in the spectral region of interest (around $\lambda = 1.55$ μm). The waveguide loss was determined to be 0.15 (0.14) dB cm^{-1} at 1.523 μm wavelength. We assume that the loss at about 780 nm wavelength, i.e. at the pump wavelength for DFG, is about 0.3 dB cm^{-1}. To investigate the nonlinear performance of the waveguide we carried out single-pass SHG experiments using a wavelength-tunable external cavity laser (tuning range 1500–1580 nm). As a result, a normalized device efficiency of 570 (500) % W^{-1} was measured, corresponding to a length-normalized efficiency of 9.4 (6.8) % W^{-1} cm^{-2}.

To achieve phase-matching for frequency doubling of the fundamental radiation at a wavelength of 1562 (1556) nm, we had to adjust the device temperature to 100 (188) °C. Figure 3 shows the SHG phase-match curve. From the full width at

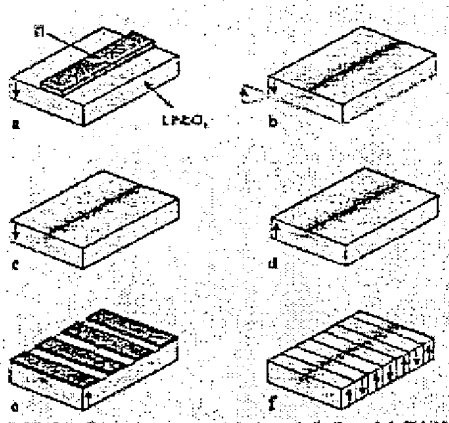

FIGURE 1 Fabrication steps to obtain periodically poled $TiLiNbO_3$ (PPLN) waveguides. **a** Definition of a titanium stripe on the $-Z$-face, **b** in-diffusion of titanium at high temperatures. During in-diffusion a domain-inverted layer merges with the $+Z$-face, **c** Removal of the domain-inverted layer by grinding, **d** Inversion of the spontaneous polarization of the whole sample, **e** Photolithographical definition of a photoresist grating, **f** Periodic electric field poling with Squid electrodes

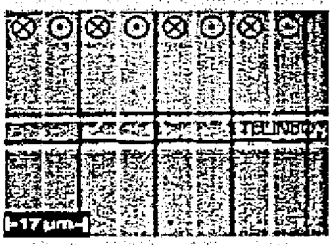

FIGURE 2 Photograph of a selectively etched PPLN sample with a titanium-in-diffused waveguide

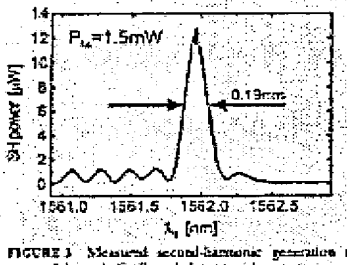

FIGURE 3 Measured second-harmonic generation (SHG) phase-match curve of the periodically poled waveguide

half maximum (Str332: $\Delta\lambda_{1\,\mathrm{dB}} = 0.19$ nm; Pb133z: $\Delta\lambda_{1\,\mathrm{dB}} = 0.2$ nm) an effective interaction length of 62 (59) mm was evaluated. From the device efficiency we conclude that the nonlinear waveguide attains 86 (82) % of the ideal effective nonlinearity ($d_{\mathrm{eff,ideal}} = 2/\pi \cdot d_{33} = 12.1$ pm V^{-1}) [5].

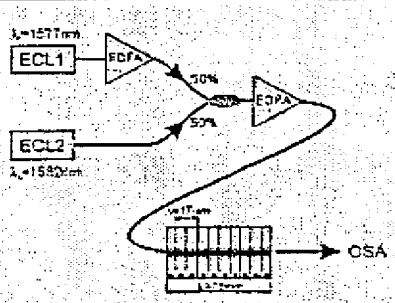

FIGURE 4 Experimental setup used to investigate cw cDFG

3 Experimental setups

3.1 *cDFG with a cw fundamental laser source*

Figure 4 shows the setup used to investigate cDFG. Sample Str332 was used as the nonlinear frequency converter. The fundamental laser source for the frequency-doubling process was a tunable semiconductor laser (external cavity laser: ECL1). We used a second external cavity laser (ECL2) for a signal laser. The pre-amplified fundamental and (unamplified) signal radiation were superimposed in a single fibre using a 50/50 fibre-optic coupler. By using a high-power, erbium-doped fibre amplifier (EDFA) we boosted the total incident power to 320 mW with a fundamental-to-signal power ratio of 16 dB (fundamental power = 213.7 mW; signal power = 5.3 mW; amplified spontaneous emission [ASE] power = 101 mW). Despite the pre-amplification of the fundamental source, a significant amount of ASE was superimposed to the boosted fundamental and signal radiation. To avoid the photorefractive effect (optically induced changes in the index of refraction result in a reduction in the conversion efficiency of the device), we operated the frequency converter at temperatures much higher than 100 °C. The amplification bandwidth of the EDFA limited the maximum operation temperature to 200 °C as the resulting phase-matching wavelength for SHG shifted to 1577 nm.

3.2 *Multichannel conversion with a cw fundamental laser source*

Figure 5 shows the experimental setup used to investigate multichannel conversion in a cDFG scheme (sam-

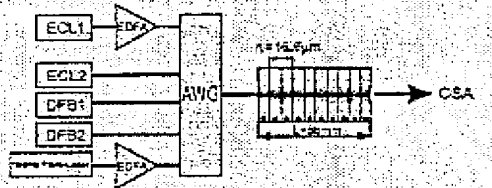

FIGURE 5 Experimental setup used to investigate multichannel conversion. ECL1 is used as the fundamental laser source. The other lasers are tuned to four different ITU wavelengths 200 GHz apart

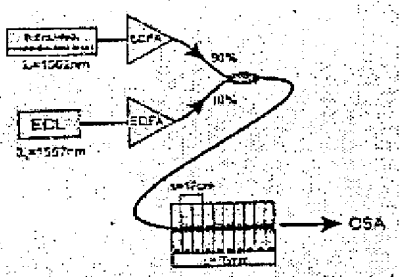

FIGURE 6 Schematic of the cDFG experiment with a pulsed fundamental wave and a cw signal

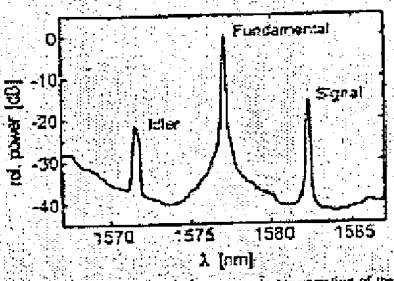

FIGURE 7 Measured optical spectrum in cw operation of the fundamental and signal waves

ple Pb133z). One fundamental source (external cavity laser: ECL1) and four signal laser sources at International Telecommunication Union (ITU) wavelengths were used to perform the experiment. One of the signal lasers was a fibre-amplifier-boosted, mode-locked fibre laser with a 10 GHz repetition rate. A 16-channel arrayed waveguide grating (AWG; channel spacing = 200 GHz) was used to multiplex the different channels. The insertion loss of the AWG is about 3 dB. The single-ended output of the multiplexer was connected to the fibre pigtailed and packaged frequency converter, which was operated at about 190 °C to avoid photorefractive damage. Most of the ASE of the EDFA was blocked by the multiplexer due to its narrow-band spectral transmission characteristic of about 0.7 nm (FWHM) and low cross-talk (< −28 dB).

3.3 *cDFG with a pulsed fundamental laser source*

Figure 6 shows the setup for cDFG in a pulsed mode. We again used the nonlinear waveguide of sample Str332 operated at a sample temperature of 100 °C. The fundamental source was a mode-locked integrated optical Ti:Er:$LiNbO_3$ laser (1562 nm center wavelength) [6] with a repetition rate of 1.8973 GHz (second-harmonic mode-locking) and 9.93 GHz (tenth-harmonic mode-locking). Using an optical autocorrelator, a pulse width of 12.4 (6) ps was measured, leading to a pulse duty cycle of ~16 (~12.3) dB. With an optical spectrum analyzer of 0.1 nm resolution, a spectral width (FWHM) of 0.35 (0.65) nm was determined. This leads to a time-bandwidth product of 0.52 (0.48), slightly exceeding the transform limit for Gaussian pulses. The mode-locked fundamental source was boosted to an average incident power of 88 mW using a 2 W HP-EDFA. Phase-matching was achieved at a temperature of 100 °C. The SHG pulses are about a factor of $\sqrt{2}$ shorter, thus leading to a duty cycle of −17.5 (−13.8) dB for the 12.4 (6)-ps-long fundamental pulses. An external cavity laser operated at 1557 nm was used as the signal source. Fundamental and signal radiation were combined with a 90/10 fibre-optic coupler.

4 Experimental results

4.1 *cDFG with a cw fundamental laser source*

In cw operation of the all-optical wavelength converter, we measured a ratio of −6.1 dB for the output levels of signal and idler power (Fig. 7); this agrees well with a calculated efficiency of −6.2 dB, if we assume a 80% coupling efficiency for the sample. Due to operation at 200 °C the signal and idler output power was very stable as a function of time, without any fluctuations induced by photorefractive effects. Due to the fairly long fundamental wavelength necessary to obtain phase-matching at 200 °C, it was not possible to completely saturate the HP-EDFA, leading to an increased amount of ASE especially towards shorter wavelengths.

4.2 *Multichannel conversion with a cw fundamental laser source*

The result for simultaneous conversion of four different ITU wavelengths is shown in Fig. 8. The incident fundamental power was boosted to 175 mW. A very stable conversion efficiency of −10 dB for each channel was observed for at least 2 h. Instabilities on a longer timescale were mainly due to a slow change in the polarisation state at the output of our EDFA (no polarization-maintaining amplifier). The measured optical signal-to-noise ratio (OSNR) of the converted signal (idler) ranged between 17 and 21 dB for a 0.5 nm resolution bandwidth of the optical spectrum analyzer, depending on the distance of the converted channel from the fundamental line. A further improvement is possible by increasing the signal input power. An increase in the input power of one channel from 0 up to +10 dBm did not cause any measurable degra-

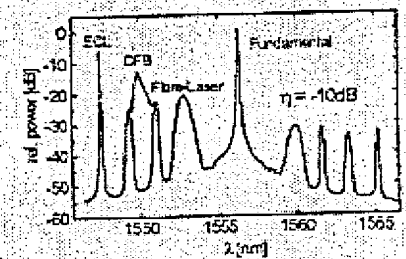

FIGURE 8 Experimental result for multichannel cDFG

dation of the conversion efficiency for all four channels. The observed improvement of the OSNR was also 10 dB. Some residual noise in the spectrum was due to the unblocked ASE from the fibre amplifiers.

4.3 *cDFG with a mode-locked fundamental laser source at a repetition rate of ~ 2 GHz*

Figure 9 shows the measured spectral and power characteristics of our frequency converter, for pulsed pumping an average converted idler power 14.5 dB below the transmitted signal power was measured. Considering the idler pulse duty cycle of −17.5 dB, this leads to a peak conversion efficiency of +3 dB. The estimated peak power of the converted pulses is 1.9 mW. It should be mentioned that the conversion efficiency of +3 dB simultaneously means an optical parametric amplification of the signal of +3 dB.

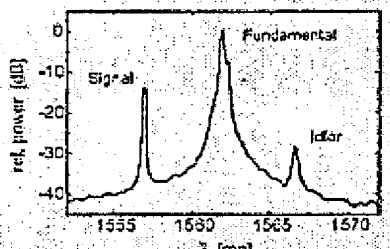

FIGURE 9 Optical spectrum of the pulsed fundamental and idler wave at a repetition rate of 2 GHz and with a cw signal wave

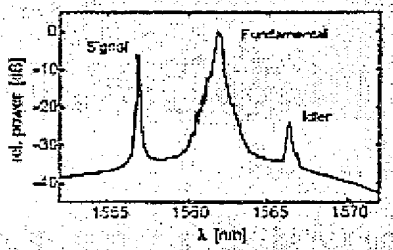

FIGURE 10 Result with a pulsed fundamental laser source at a repetition rate of 10 GHz

4.4 *cDFG with a mode-locked fundamental laser source at a repetition rate of* 10 GHz

Due to the broader fundamental spectrum of about 0.65 nm and some photorefractive damage due to the larger pump duty cycle (−13.8 dB), it was not possible to achieve a conversion efficiency > 0 dB (Fig. 10). On the other hand, the measured efficiency of > −4.6 dB is to our knowledge the best result reported to date at such a high repetition frequency.

5 Summary and conclusions

We demonstrated for the first time nonlinear optical wavelength conversion with an efficiency of +3 (−4.6) dB at a repetition rate of 2 (10) GHz using cascaded difference frequency generation in a periodically poled Ti:$LiNbO_3$ waveguide. We also demonstrated multi-channel wavelength conversion without any reduction of the conversion efficiency by the other wavelength channels. In the future the performance of our frequency converters will be improved. A device with 935 % W^{-1} second-harmonic conversion efficiency has been reported [7, 8] and waveguides of significantly reduced photorefractive sensitivity, such as stoichiometric Mg:$LiNbO_3$ [9] and 5 mol % MgO:$LiNbO_3$, are being investigated. On the modelling side, numerical simulations that take the group velocity dispersion between pump, signal, and idler pulses into account are underway.

ACKNOWLEDGEMENTS This research is supported by the European Union IST project (IST-1999-10626).

REFERENCES

1 M.H. Chou, I. Brener, M.M. Fejer, E.E. Chaban, S.B. Christman: IEEE Photon. Technol. Lett. 11, 653 (1999)
2 W. Sohler, D. Hofmann, G. Schreiber: Contemporary Photonics Technologies (CPT 2000), paper Fa-3, Tokyo, 12–14 January 2000, p. 125
3 X. Gallet, G. Assanto: J. Opt. Soc. Am. B 16, 721 (1999)
4 G.D. Miller: Dissertation (Stanford University 1998)
5 I. Shoji, T. Kondo, A. Kitamoto, M. Shirane, R. Ito: J. Opt. Soc. Am. B 14, 2268 (1997)
6 C. Becker, T. Ossadka, J. Pandavenes, R. Ricken, K. Rochhausen, G. Schreiber, W. Sohler, H. Suche, R. Wessel, S. Balsamo, I. Montrosset, D. Scarcalepore: IEEE J. Sel. Top. Quantum Electron. 6, 101 (2000)
7 G. Schreiber: Dissertation (Universität Paderborn 2001)
8 G. Schreiber, D. Hofmann, W. Grundkötter, Y.L. Lee, H. Suche, V. Quiring, R. Ricken, W. Sohler: Proc. SPIE 4277, 144 (2001)
9 Y. Furukawa, K. Kitamura, S. Takekawa, K. Niwa, H. Hatano: Opt. Lett. 23, 1892 (1998)

Fabrication, Characterization and Index Profile Modeling of High-Damage Resistance Zn-Diffused Waveguides in Congruent and MgO: Lithium Niobate

W. M. Young, M. M. Fejer, M. J. F. Digonnet, A. F. Marshall, and R. S. Feigelson

Abstract— **A study of the fabrication and optical properties of planar waveguides fabricated in MgO:$LiNbO_3$ and $LiNbO_3$ substrates by diffusion of a ZnO film is presented. Transmission electron microscopy was used to show that using ZnO instead of metallic zinc as a source, and maintaining the ZnO film thickness below a prescribed value, greatly reduces second phase precipitation and produces usable waveguides. Dopant and refractive index profiles were characterized by electron microprobe analysis and interference microscopy, respectively. The dependence of the Zn diffusion coefficient on temperature and the dependence of the refractive-index change on Zn concentration are inferred from these measurements. A simple model is also reported which predicts the index profile of the waveguide given the film thickness, diffusion time and temperature. The validity of the model is demonstrated by comparison between calculated profiles and profiles measured by prism coupling and IWKB analysis.**

I. Introduction

OPTICAL waveguides in lithium niobate ($LiNbO_3$) have been widely studied for applications including telecommunication systems, nonlinear optics and fiber sensors. To date the two most widely used waveguide fabrication processes are titanium diffusion and proton-exchange (PE) [1], [2]. Both processes yield waveguides with low propagation loss, typically lower than 0.5 dB/cm [2], [3]. However, neither method produces waveguides with ideal performance for all applications. Ti-diffused waveguides in both $LiNbO_3$ and MgO:$LiNbO_3$ guide both polarizations but suffer from photorefractive damage even at wavelengths as long as 0.85 μm [4], [5]. On the other hand, PE waveguides are much more resistant to photorefractive damage but guide only the extraordinary polarization.

The objective of this work was to develop a new type of waveguide in $LiNbO_3$ which can guide both polarizations and exhibit high resistance to photorefractive damage. The current model for the photorefractive effect involves a refractive-index perturbation due to an interaction between the electrooptic effect and the local electric field created by charge separation under visible laser illumination [6]. Since the charge generation and trapping centers are strongly related to dopant valence state, we speculated that cation dopants with a single valence state less than or equal to 2, such as Mg^{+2} and H^+, will have similar effects on photorefractive damage. This hypothesis was based on the experimental observations that both Mg^{+2} and H^+ reduce the photorefractive damage [7], [8], while cation dopants with multivalent states or a valence state greater than or equal to 3, such as Fe^{+3}/Fe^{+2}, Nd^{+3} and Ti^{+4}, increase the photorefractive damage [9], [10].

In this work, Zn was chosen as a dopant because it matches the requirements predicted from the above arguments. In a recent article, we reported the fabrication and optical properties of planar waveguides made by the diffusion of ZnO into both $LiNbO_3$ and MgO:$LiNbO_3$. Waveguides made in the latter material guide both polarizations, although with a substantial difference in index profile, and have propagation losses in the range of 0.3 to 1.2 dB/cm. They also exhibit no photorefractive in-plane scattering up to 90 kW/cm^2 at 514.5 nm, which is one of the highest values reported in the literature [11].

In this paper we present detailed material and optical studies of Zn-diffused waveguides in both MgO:$LiNbO_3$ and $LiNbO_3$. Fabrication conditions required to obtain low loss waveguides are identified, in particular to avoid the formation of second phase precipitation of $LiZnNbO_4$ and surface degradation. We report measurements by electron microprobe analysis of the dopant distribution in Zn-diffused lithium niobate waveguides, as well as optical characterization of their index profiles. This data is used to obtain values of the diffusion coefficient of Zn in congruent and MgO-doped $LiNbO_3$, their dependence on temperature, and the relationship between the refractive-index change and the Zn concentration. We also introduce a simple model, employing the diffusion and fabrication parameters, to calculate the dopant concentration profile, and from it the index profile of the waveguide. Comparison between the predictions of this model and the measured waveguide index profiles establishes the validity of this model.

II. Fabrication

A. Experimental Procedures

To prepare the Zn-diffused samples, a ZnO film was first sputtered onto the $LiNbO_3$ substrates. The dimensions of the substrates used to produce waveguides were 20 × 6 × 2 mm for MgO:$LiNbO_3$ and 20 × 6 × 1 mm for $LiNbO_3$. Diffusion studies for both materials were carried out on 6 × 4 × 1

Manuscript received November 25, 1991; revised March 27, 1992.

W. M. Young and R. S. Feigelson are with the Department of Materials Science and Engineering, Stanford University, Stanford, CA 94305.

M. M. Fejer and M. J. F. Digonnet are with the Edward L. Ginzton Laboratory, Stanford University, Stanford, CA 94305.

A. F. Marshall is with the Center for Materials Research, Stanford University, Stanford, CA 94305.

IEEE Log Number 9201292.

mm substrates. During diffusion, the samples were placed on platinum foil stands in the center of a covered alumina boat filled with congruent lithium niobate powder. The purpose of the powder is to suppress the net transport of Li ions in or out of the lithium niobate crystal [12]. To control the Li_2O vapor pressure in the vicinity of the $LiNbO_3$, we used a mass of powder substantially larger than that of the sample (about 13 g versus less than 0.6 g). The alumina boat was placed in the center of an alumina process tube, closed at both ends with alumina caps, which, in turn, was placed in a tube furnace for diffusion at elevated temperatures in dry air [13]. The temperature difference between the control thermocouple and a monitor thermocouple at the sample location was less than 0.5°C. In the text the quoted temperatures are provided by the control thermocouple. The thermal cycle, carried out in dry air, typically involved heating at about 8°C/min up to the diffusion temperature of 1000–1100°C, diffusion for typically less than 1 hour, and cooling at an initial rate of 10°C/min.

B. Surface Roughness

To produce low scatter loss waveguides it is crucial that the surface quality be not degraded by the diffusion process. In our initial diffusion experiments the surfaces of all the samples were translucent after diffusion. Similar observations of surface degradation resulting from the diffusion of metallic Zn into $LiNbO_3$ were previously reported by Yoon *et al.* [14]. Based on the ZnO-Li_2O-Nb_2O_5 pseudo-ternary phase diagram [15], we speculated that the surface roughening originated from the formation of a new phase on the substrate surface. The phase diagram suggests that $LiZnNbO_4$ is a stable compound, which could therefore form near the sample surface and degrade its quality. For comparison, in the case of the diffusion of Ti in lithium niobate, the TiO_2-Li_2O-Nb_2O_5 pseudo-ternary phase diagram indicates that TiO_2 and $LiNbO_3$ can coexist in equilibrium at temperatures up to 1100°C [16]. Consequently, during the diffusion of Ti some metastable phases may form at elevated temperature but they will dissolve into lithium niobate over the course of the fabrication process [17], [18].

Transmission electron microscopy (TEM) confirmed the presence of $LiZnNbO_4$ precipitates near the diffusion surface. Fig. 1 shows a bright field TEM picture of the substrate surface after diffusion of a 400 nm-thick film of ZnO at 1000°C for 1 h. Isolated second phases, on the order of a few microns in size, were observed across the surface of the substrate. Energy-dispersive spectrometry confirmed that these precipitates contained high Zn concentration. The electron diffraction pattern of the precipitate has been identified as $LiZnNbO_4$. Fig. 2 shows the electron diffraction pattern of the substrate (Fig. 2(a)) and of the precipitate (Fig. 2(b)). The lattice constants measured in Fig. 2(b) are consistent with documented values for $LiZnNbO_4$. The precipitates are always in a {201} orientation and have a specific in-plane alignment with respect to the {001} $LiNbO_3$ substrate. The {100} and {112} planes of the precipitates are parallel to the {10.0} planes of the substrate. For the $LiZnNbO_4$ structure, the angle between the two sets of planes is 59.2°, whereas the in-plane angles for <001> $LiNbO_3$ are 60°. The reflections from the precipitate (Fig. 2(b)) can be superimposed on the substrate (Fig. 2(a)) which indicates that the precipitates are slightly strained to give better alignment with the substrate. The orientation relationship between precipitates and substrate also gives three variants for the orientation of the precipitates and all of these can be observed within a given precipitate region. These results strongly suggest that a $LiZnNbO_4$ precipitate formed epitaxially on the top surface of the waveguide during Zn diffusion. These isolated precipitates were probably responsible for the prohibitively high loss observed in early waveguides.

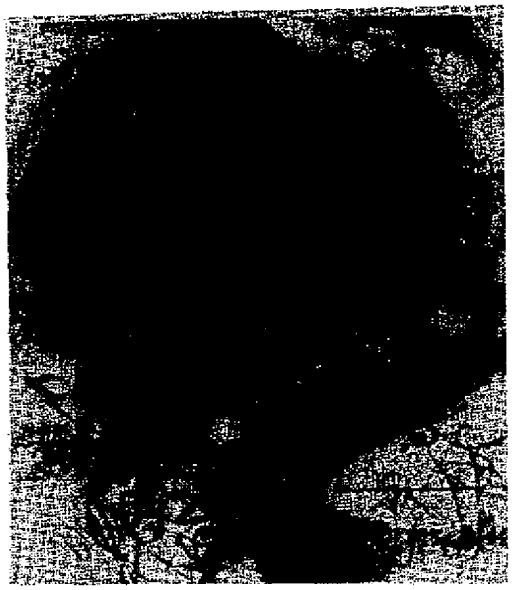

Fig. 1. Bright-field TEM photograph of a Zn-diffused congruent $LiNbO_3$ surface showing a precipitate (400-nm ZnO diffused at 1000°C for 1 hour).

There are at least two approaches to eliminate these second phase precipitates: 1) synthesize the dopant source from a composition within the $LiNbO_3$-$ZnNb_2O_6$-$ZnLiNbO_4$ tie triangle where $LiNbO_3$ is in equilibrium with quaternary Zn containing compounds or 2) find a set of parameters for ZnO diffusion which avoids the precipitation. The first approach would involve an in-depth study of dopant synthesis techniques and

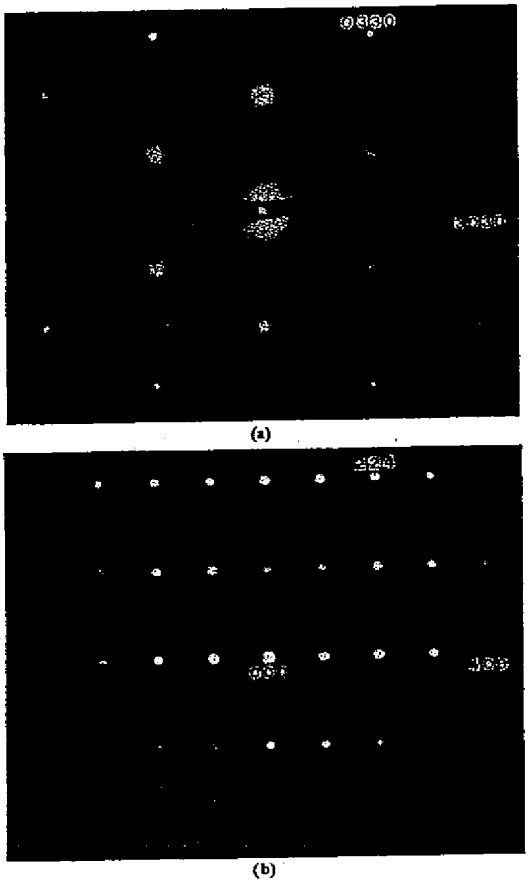

Fig. 2. Electron diffraction patterns from the $LiNbO_3$ substrate (a) and precipitate (b) measured from the sample shown in Fig. 1. The reflections indexed {30.0} planes from the substrate $LiNbO_3$ in Fig. 2(a) matches the {400} and {224} planes from the precipitate in Fig. 2b, indicating epitaxial relationship between the substrate and the precipitate.

compositional control during deposition of the source on the substrate. As a result the second alternative appeared to be a more desirable approach for establishing the usefulness of Zn-diffused $LiNbO_3$ waveguides.

The key point in the second approach is to avoid any kinetic paths leading to compound formation. To this end ZnO was chosen instead of metallic zinc to avoid unnecessary metal oxidation which may enhance the formation of the intermediate phase [19]. We also found that an important parameter controlling the formation of the precipitate is ZnO film thickness. We established experimentally that compound formation is greatly reduced, if not completely eliminated, when the film thickness is kept below some critical value. This critical thickness is approximately 160 nm for MgO:$LiNbO_3$ and 100 nm for $LiNbO_3$. No precipitate was observed in these materials with thicknesses of ZnO smaller than these values and for diffusion temperatures anywhere between 1000 and 1100°C. Satisfying the thickness condition was found to be essential to maintaining a good surface quality and producing low loss waveguides. By appropriate selection of the diffusion time and temperature (between 1000 and 1100°C for MgO:$LiNbO_3$ and around 1000°C for congruent $LiNbO_3$), the Zn concentration in the diffused region is high enough (typically 2–3 mol%) to provide good optical confinement, and yet low enough to maintain a good surface quality.

III. Dopant and Diffusion Characterization

Electron microprobe analysis (EMPA) to measure the dopant profiles in the Zn-diffused region required longer diffusion times (1–10h) and thicker ZnO films (0.4–1.0 m) than those used for the fabrication of waveguides. This was necessary so that high enough Zn concentrations would be present over greater depths to permit accurate EMPA measurement. Prior to characterization, a Zn-diffused sample was first sandwiched between two glass slides, then cut into two pieces. Each piece was polished at both ends, perpendicular to the diffusion surface. One piece was used for EMPA measurements, the other for Mach–Zehnder interference microscope measurements, as described in Section IV. The glass slides were used to prevent rounding of the edges of the diffused region during polishing, which would otherwise upset EMPA and microscopy measurements.

An example of dopant profile is shown in Fig. 3 for an x-cut MgO:$LiNbO_3$ substrate after diffusion of a 200-nm ZnO film at 1000°C for 10 h. For all diffused samples studied here the ZnO film was not completely depleted at the end of the diffusion process. This assumption was checked by integrating the measured dopant profile along the depth of the diffused region to obtain the total amount of Zn present in the sample, and comparing it to the amount of Zn initially contained in the film. It is well known from diffusion theory that when the film is undepleted (and the diffusion coefficient is independent of concentration) the profile is a complementary error function (erfc). This is in agreement with measured profiles, as illustrated by theoretical fit of the experimental profile to an erfc plot in Fig. 3. Consequently, the diffusion coefficient D was obtained by fitting each measured dopant profile with an erfc function.

Table I lists the values of D obtained from a total of 10 samples in 3 different types of substrates (z- and x-cut MgO:$LiNbO_3$ and z-cut congruent $LiNbO_3$) processed at temperatures between 900 and 1100°C. For short diffusion times, typically 1 hour or less, a nonnegligible amount of diffusion takes place during both the heating and cooling parts of the cycle. This was taken into account in correcting the measured diffusion coefficients by first estimating $D(T)$, without applying any corrections, for samples diffused at different temperatures. From these values the amount of diffusion occurring during heating and cooling was evaluated, assuming an exponential dependence $D(T)$, which provided a second, more accurate value of $D(T)$. This process was iterated 2 or 3 times until it converged to constant values. Table I lists both the uncorrected and the corrected values of D. Error bars were obtained from the average of several EMPA scans, typically

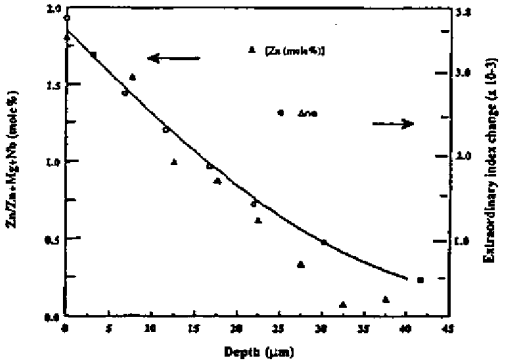

Fig. 3. Extraordinary refractive index (open circles) and Zn dopant (triangles) profiles of an x-cut MgO:$LiNbO_3$ substrate after diffusion of a 200-nm ZnO film at 1000°C for 10h. The solid line is a complementary error function fitted to the experimental concentration profile.

TABLE I
ZN DIFFUSION COEFFICIENTS FOR DIFFERENT TEMPERATURES AND SUBSTRATES. THE CORRECTED D ACCOUNTS FOR THE CONTRIBUTION OF FINITE DIFFUSION DURING WARMING AND COOLING.

Samples	Temp.	Time	ZnO thickness	$D(\mu m^2/h)$	D(corrected, $\mu m^2/h$)
MgO:$LiNbO_3$ z-cut	1100°C	1.4 h	160 nm	140±10	119±8
"	1100°C	10 h	160 nm	24.8±2	24.3±2
"	950°C	10 h	1 μm	8.7±2	8.5±2
"	900°C	100 h	1 μm	1.9±0.3	1.9±0.3
MgO:$LiNbO_3$ x-cut	1100°C	1 h	200 nm	138±12	110.8±10
"	1000°C	10 h	200 nm	27±6	26.4±6
"	900°C	10 h	200 nm	2.4±0.2	2.4±0.2
$LiNbO_3$ z-cut	1100°C	1 h	1 μm	280±26	230±21
"	1000°C	4 h	1 μm	35.5±4	34±4
"	950°C	10 h	1 μm	9.6±1.4	9.4±1.4

2 to 4, taken at different positions on the same sample. They reflect some compositional nonuniformity across the samples as well as measurement uncertainties. Comparing the error bars of samples fabricated under similar conditions, it appeared that the dopant profile was more uniform for thinner ZnO films. This may be an important consideration in the preparation of waveguides with uniform index profiles.

The samples used for D(T) measurements, which were fabricated with thick ZnO films, exhibit erfc profiles with a depth that varies as the square root of the diffusion time. This is an indication that, while second phase precipitation was present in these samples, the formation of this phase is clearly not a significant limiting step in the Zn transport process, at least within the accuracy of our measurements. Instead, the rate limiting step is diffusion of Zn in lithium niobate. The values of the diffusion coefficients $D(T)$ measured from the diffusion of thick films should be applicable to the analysis of the diffusion of thin films necessary for waveguide fabrication.

Fig. 4 shows the Arrhenius plot ($\ln D$ versus $1/T$) for x-cut and z-cut MgO:$LiNbO_3$. The dependence is linear between 900°C to 1100°C, as expected. The activation energy inferred from the slope of the curve is $E_0 = 2.72 \pm 0.2$ eV. Within our measurement accuracy, we did not detect diffusion anisotropy in MgO:$LiNbO_3$, as shown by the results of Fig. 4. Fig. 5 shows a similar curve for z-cut $LiNbO_3$. The points falls on a straight line between the 950 and 1100°C, with an activation energy of $E_0 = 3.02 \pm 0.3$ eV. This measurement was not carried out for x-cut $LiNbO_3$. These high activation energies suggest that the diffusion mechanism of Zn in $LiNbO_3$ favors substitutional over interstitial mechanisms, as the latter type is usually characterized by a smaller activation energy [20]. The diffusion of Zn is much faster than that of Ti, and fabrication times are correspondingly shorter.

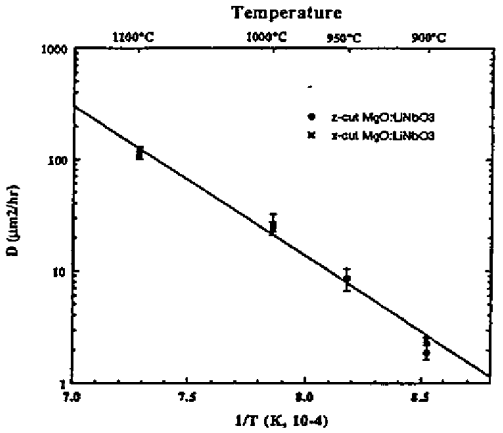

Fig. 4. The Arrhenius ($\ln D$ versus $1/T$) plot for the diffusion of ZnO, under conditions specified in the text, in z-cut and x-cut MgO:$LiNbO_3$ between 900 and 1100°C.

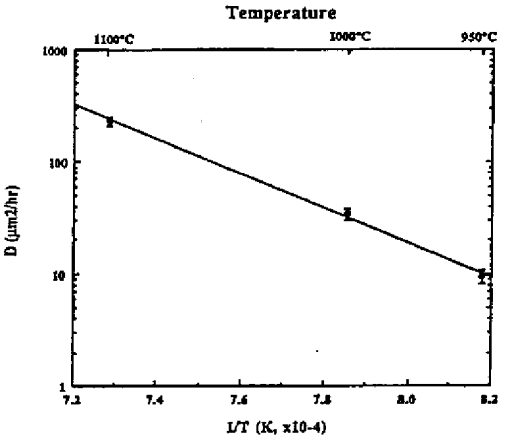

Fig. 5. Same as Fig. 4, for Zn diffused z-cut $LiNbO_3$ between 950 and 1100°C.

IV. Index Characterization and Index-Dopant Relationship

The index profiles, later used to establish the relationship between the refractive-index change and the dopant concentration, were obtained by interference microscopy. For this purpose, the samples were sliced and polished as described in Section III. The samples, typically 1-mm thick, were placed in one of the arms of a Mach–Zehnder interference microscope operated with a 632.8 nm He–Ne laser, such that the light traveled through the length of the diffused region. The microscope produced a magnified image of the diffused region on which refractive index changes were mapped as distortions of the interference fringe pattern. Index profiles were inferred from the number of fringes of distortion at different positions along the depth of the diffused region. This method was generally preferred over prism coupling and IWKB analysis [21] because it is more easily applied to small samples with rough surfaces. In cases where the two methods were compared, the profiles agreed within 20%.

Since the refractive-index change was typically small (less than 0.005), potential changes in the index from sources other than the Zn dopant had to be carefully evaluated. These sources include impurities in the ZnO film or in the furnace, departure from parallelism in the sample end faces, and Li in-or-out diffusion, which is known to change the extraordinary refractive index of lithium niobate [22]. To make sure that no other process was affecting the index, a monitor sample of congruent $LiNbO_3$ (with no ZnO film) was routinely placed in the furnace and checked for contaminants by X-ray photoelectron spectrometry (XPS) and for index change by Mach–Zehnder interference microscopy. Within the resolution of both methods, we observed no detectable furnace contamination or Li in-or-out diffusion in the monitor sample. A slight wedge between the sample end faces and residual rounding of the edges can also be a source of error when interpreting the fringe pattern obtained from Mach–Zehnder interference microscopy. Michelson interference microscopy indicated that effects of rounding were negligible and that the contribution of any wedge to the measured refractive-index change was less than 1×10^{-4}.

Studies of index profiles were carried out on samples diffused at 1100 and 1000°C for both x- and z-cut $MgO:LiNbO_3$, and at 1000°C for z-cut $LiNbO_3$. A typical index profile is shown in Fig. 3 for the extraordinary index of x-cut $MgO:LiNbO_3$. We estimate the error on the index measurement to be about 5×10^{-4}, and the spatial resolution to be 2–3 μm. The index change is maximum at the surface and equal to 3.7×10^{-3}. The half-maximum depth of the index profile is about 16 μm. The measured refractive-index profile resembles the Zn concentration profile measured in the same sample (see Fig. 3). Fig. 6 shows the dependence of the index change on the Zn concentration taken from the data of Fig. 3. The slope of a linear fit to the data is about $1.90 \pm 0.1 \times 10^{-3}$ per Zn mol%. Fig. 7 shows a similar curve for another sample, also fabricated in x-cut $MgO:LiNbO_3$ but at 1100°C. For this particular sample, the index change appears to vary somewhat nonlinearly with Zn concentration. A linear fit to the data gives

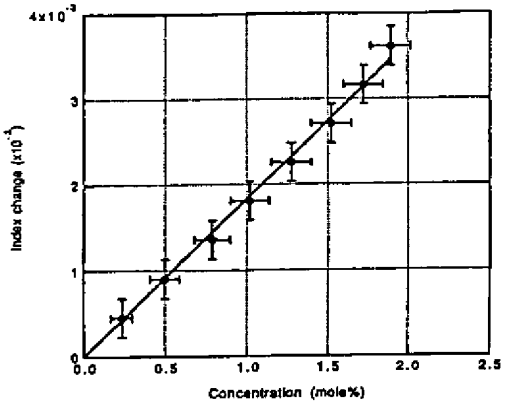

Fig. 6. The extraordinary index change as a function of Zn concentration measured in an x-cut $MgO:LiNbO_3$ sample after diffusion of a 200-nm ZnO film at 1000°C for 10h.

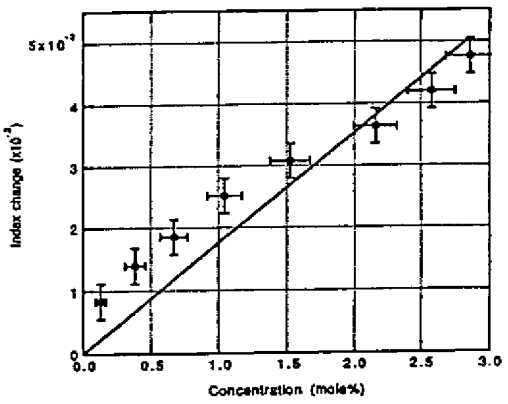

Fig. 7. Same as Fig. 6, but for diffusion at 1100°C for 1 h.

a slope of about $1.77 \pm 0.12 \times 10^{-3}$ per Zn mol%. More study needs to be done to define this dependence more precisely.

Table II summarizes the index change per Zn mol% measured on several samples representing a variety of materials, orientations and fabrication conditions. In both x- and z-cut $MgO:LiNbO_3$, the extraordinary index change is greater for diffusion at 1000°C than at 1100°C. For a given material the index change appears to depend only slightly on the substrate orientation and diffusion temperature. These conclusions are based on a limited number of samples, and should be considered as tentative.

For $MgO:LiNbO_3$ only the extraordinary index Δn_e was studied, as the ordinary index change Δn_o is generally too small to be measured accurately by interference microscopy, but was estimated to be on the order of 1/4 to 1/5 the value of Δn_e. The ordinary modes were successfully excited by end-firing [11] but not by prism coupling, at least in x-cut samples, so that n_o could not be measured by this method either.

TABLE II
THE INDEX CHANGE PER ZN CONCENTRATION FOR DIFFERENT MATERIALS, ORIENTATIONS AND TEMPERATURES.

Samples	Temp.	Time	ZnO thickness	Index change/[Zn mol%]
1.MgO:$LiNbO_3$,z-cut	1100°C	1 h	200 nm	$1.77\pm0.12\times10^{-3}$ (Δn_e)
2. "	1000°C	10 h	"	$1.83\pm0.02\times10^{-3}$ (Δn_e)
3.MgO:$LiNbO_3$,z-cut	1100°C	1.4 h	160 nm	$1.22\pm0.04\times10^{-3}$ (Δn_e)
4. "	1000°C	10 h	"	$1.90\pm0.10\times10^{-3}$ (Δn_e)
5. $LiNbO_3$,z-cut	1000°C	4 h	200 nm	$0.72\pm0.03\times10^{-3}$ (Δn_o)

For congruent $LiNbO_3$ the ordinary modes were easily excited by prism coupling. On the other hand the extraordinary modes were successfully excited by end firing but not by prism coupling. We also observed that the extraordinary index change is a nonmonotonic function which presents one or more extrema depending on the processing conditions. This behavior, which we believe may be related to local variations in lithium concentration, could be at the origin of the difficulty in prism coupling into this polarization. More studies are needed to elucidate this effect, which could be of interest to produce buried waveguides. This situation should be kept in mind when dealing with congruent $LiNbO_3$.

V. COMPARING CALCULATED AND MEASURED INDEX PROFILES

For the purpose of waveguide design, it would be useful to be able to predict the index profile of a waveguide from the fabrication conditions, i.e., from the film thickness, diffusion temperature, diffusion time, and the substrate material and orientation. To address this issue, we computed the concentration profile from diffusion theory, then multiplied this profile by the factor $\Delta n/[Zn]$ (the measured ratio of index change Δn to zinc concentration [Zn] listed in Table II). We present results for Zn:$LiNbO_3$ in this section. The index profiles predicted are shown to agree within 30% error with the profiles measured from prism coupling and IWKB analysis.

We considered the problem of one-dimensional diffusion of species A into solid B, with the assumption that (1) the solid solubility of A in B exists and is equal to C_o, and (2) the diffusion coefficient of A into B is independent of concentration. We also assume that as long as the film is not depleted, the dopant concentration at the surface of solid B is pinned at the value of the solid solubility C_o. This approximation for diffusion of thin ZnO films neglects the initial kinetics associated with dissolving Zn into $LiNbO_3$, but predicts results for waveguide samples with reasonable accuracy. Detailed modeling of the kinetic process is beyond the scope of this work. As discussed in Section II-B, in the present study this last assumption only applies when the ZnO film does not exceed a prescribed thickness. In this case it is well known that the solution of the diffusion equation is a complementary error function (erfc) [23], which can be written as:

$$c(x,t) = C_0\mathrm{erfc}\left[\frac{x}{4Dt}\right] \qquad (t \le t_1) \tag{1}$$

where t is the total diffusion time and x is the depth measured from the diffusion surface (i.e., the original interface between species A and B). This solution applies only until the film is completely depleted, which first occurs at time $t = t_1$. The time t_1 is given by mass conservation, i.e., at $t = t_1$ the amount of material diffused into the solid per unit area is equal to the amount of material per unit area present in the film at time $t = 0$. Integration in x of (1) yields:

$$t_1 = \left(\frac{\kappa d}{1.128C_0}\right)^2\left(\frac{1}{D}\right) \tag{2}$$

where C_0 is expressed in mole%, d is the initial film thickness, and κ is given by:

$$\kappa = \frac{\rho_A}{\rho_B}\frac{M_B}{M_A}N \tag{3}$$

ρ_A and ρ_B are the density of species A and B, respectively, M_A and M_B are their respective molecular weight, and N is the number of ions per molecule. For the case under study N=1 and $\kappa = 2.23$.

For $t > t_1$, the solution of the diffusion equation is known to be:

$$c(x,t_2) = \frac{C_0}{\sqrt{4\pi Dt_2}}\int_0^\infty\left(\frac{x'}{\sqrt{4Dt_1}}\right)\left[e^{-\frac{(x-x')^2}{4Dt_2}} + e^{-\frac{(x+x')^2}{4Dt_2}}\right]dx' \qquad (t \ge t_1) \tag{4}$$

where $t_2 = t - t_1$. In general, this solution can not be cast in a simple closed form expression and the integral has to be calculated numerically. As is well known, for $t_2 \gg t_1$ this solution approaches a Gaussian given by:

$$c(x,t_2) = \frac{\kappa d}{\sqrt{\pi D(t_1+t_2)}}e^{-\frac{x^2}{4D(t_1+t_2)}} \qquad (t_2 \ge t_1) \tag{5}$$

The 1/e width in (5) is $w_G = 4D\sqrt{(t_1+t_2)}$. The exact solution (4) converges toward the approximate solution fairly rapidly. For $t_2 = t_1$ the exact width differs from the approximate width w_G by only 11%, and for $t_2 = 4t_1$ by less than 4%. In practical diffusion runs, t_2 is usually longer than t_1, so that (5) provides a convenient and accurate approximation of the dopant profile.

The solid solubilities of Zn in $LiNbO_3$ and MgO:$LiNbO_3$ are necessary inputs for this calculation. In an ideal system, we would expect the solid solubility to depend on temperature, but at a given temperature the Zn concentration at the surface should be pinned at that value as long as the film is undepleted. In the Zn:$LiNbO_3$ system, in which the ZnO is not in thermodynamic equilibrium with the substrate materials, we obtained an effective solid solubility by measuring the Zn surface concentration with EMPA in several waveguides (with no detectable second phase precipitation, i.e., starting from ZnO film thicknesses smaller than the bounds specified in Section II-B). For a given temperature and substrate material,

the highest measured value provided a lower bound value of the solid solubility. For example, in a waveguide fabricated at 1100°C in x-cut MgO:$LiNbO_3$ the highest Zn surface concentration was equal to 3.5 ± 0.6 mole%. We assume C_o takes this value for all temperatures between 1000 to 1100°C, as no data was available for 1000°C. For $LiNbO_3$, the highest surface concentration observed and the value of C_o used was 5.4 ± 0.5 mole%. These two values were consistent with mass conservation, assuming that the film was just depleted at the end of these runs.

The diffusion temperature profile $T(t)$ is not rectangular in practice, as assumed in the model. Instead, the furnace is gradually heated to the diffusion temperature T_0, the temperature is then maintained at T_0 for a duration t, and finally the furnace is gradually cooled down. As mentioned earlier, a finite amount of diffusion takes place during heating and cooling cycles. The real cycle can be replaced by an equivalent rectangular cycle (i.e., with infinitely fast heating and cooling) producing the same amount of diffusion, provided time t is replaced by an equivalent diffusion time t_{eff} which can be shown to be given by:

$$t = t + \frac{kT_0^2}{E_0}\left(\frac{1}{\beta_+} + \frac{1}{\beta_-}\right) \tag{6}$$

where k is the Boltzman constant, E_0 is the activation energy of the dopant diffusion in the substrate, and β_+ and β_- are the heating and cooling rates, respectively. The correction term in (6) becomes negligible when t is large. For the heating and cooling rates used in this study, in the case of ZnO diffusion in lithium niobate the correction is negligible when t exceeds about 10 h.

To verify the applicability of this model to Zn-diffused waveguides, we compared the measured index profiles of six waveguides with profiles calculated as follows: 1) calculate the corrected diffusion coefficient D at the diffusion temperature from Table I, 2) calculate both the effective diffusion time t_{eff} (6) and t_1 (2), 3) calculate the dopant profile, using (1) if $t_{eff} < t_1$ or (4) if $t_{eff} > t_1$ (or (5) if $t_{eff} \geq 2t_1$), and 4) multiply the dopant profile by the $\Delta n/[Zn]$ factor (Table II) to obtain the index profile.

The waveguide mode effective indices and mode turning points were measured by prism coupling and IWKB analysis. In the IWKB analysis a curve fitting routine was used to fit the experimental index profile to either a erfc or a Gaussian (depending on whether t was smaller or larger than t_1) and determine the index at the surface. Error in the effective index measurement was ± 0.0003. For a typical three mode waveguide fabricated in this research, the uncertainty in the assignment of the surface index in IWKB analysis calculation and the mode turning points are about ± 0.0006 and ± 0.6 m, respectively.

Fig. 8 shows the measured index profile and the calculated index profiles for the extraordinary polarization of a waveguide in MgO:$LiNbO_3$. The fabrication conditions were 80-nm ZnO film diffused at 1000°C for 1 h in a x-cut sample. Including the finite ramping time, the effective diffusion time was calculated to be 72 min. The calculated value of t_1 (2) was 45 min. In this case, $t_2 = 72 - 45 = 27$ min. The solid and dashed lines in Fig. 8 represent the profiles calculated according to the exact solution (4) and the approximate solution (5), respectively. The agreement between the exact profile and the measured profile is reasonable. The measured index value at the surface is somewhat higher than predicted, which could be due to uncertainties in the measured value of $\Delta n/[Zn]$, as discussed in Section IV.

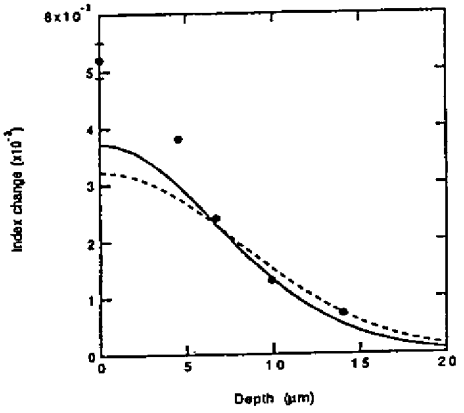

Fig. 8. Extraordinary index data measured by IWKB analysis on a waveguide fabricated in x-cut MgO:$LiNbO_3$ by diffusion of a 80-nm ZnO film at 1000°C for 1 h. The solid curve is the exact calculated profile (4) and the dotted line the approximate calculated profile (5).

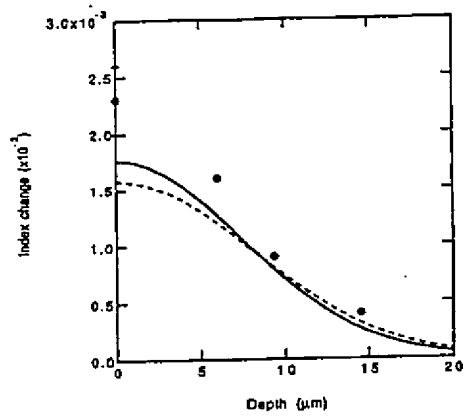

Fig. 9. Similar as Fig. 8, for z-cut $LiNbO_3$ (ordinary index data) after diffusion of a 100-nm ZnO film at 1000°C for 45 min.

Similar results are presented in Fig. 9 for a waveguide in $LiNbO_3$ (100-nm thick ZnO film, z-cut sample, 1000°C, 45 min). Including the finite ramping time, this corresponds to an effective diffusion time of 56.6 min. The calculated value of t_1 (2) was 23 min. In this case, $t_2 = 33$ min, the ratio $t_2/t_1 = 1.4$ is large enough that the exact profile resembles a Gaussian. Again the theoretical profiles are in reasonable agreement with the measured index profile.

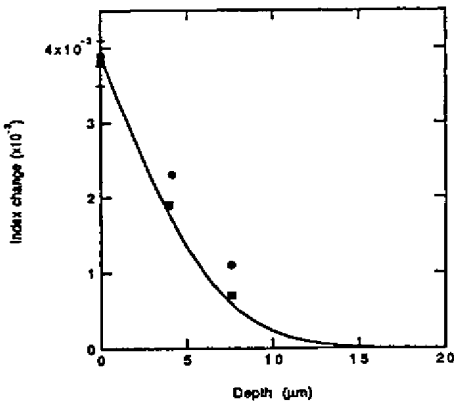

Fig. 10. Same as Fig. 9, with a diffusion time of 12 min. for two waveguides. Both waveguides were fabricated under the same conditions but in different runs. The solid curve is the calculated index profile calculated from (1).

Fig. 10 shows similar results for two waveguides as in Fig. 9 except that the diffusion time was decreased to 12 min. These two waveguides were fabricated under the same conditions but in different runs. Including the finite ramping time, the effective diffusion time was calculated to be 23.6 min. In this case $t_1 = 23$ min. so that the film was just depleted at the end of the diffusion process and (1) was used to generate the theoretical profile of Fig. 10. The surface index for the IWKB fit was determined by fitting to an erfc. For one of the waveguides the measured and calculated profiles agreed very well, to better than a few percent. For the second waveguide the agreement was fair; the actual profile depth was approximately 20% larger than the calculated depth.

The difference between the two data sets obtained from two different waveguides illustrates the limits of the reproducibility of our fabrication process. We believe this sample-to-sample variation is largely due to variations in film thickness. These variations change the total amount of Zn diffused into the sample, and therefore the total area under the index profile (see Fig. 10). Also, we speculate that film thickness variations may influence the total rate of Zn transport through the following process. While diffusion rate in single phase $LiNbO_3$ is similar for both thin and thick ZnO film samples, the initial kinetics associated with Zn dissolution into $LiNbO_3$ might require a period of time t_{sp}. In this ZnO-$LiNbO_3$ nonequilibrium system, t_{sp} may differ for films of different thickness. As discussed earlier, for typical diffusion times (30–60 min) this initial transient is not a significant rate limiting step and has a negligible effect on the final waveguide depth. However, in the case of the two waveguides of Fig. 10 the diffusion time was unusually short ($t = 12$ min), and the initial transient may influence the final waveguide depths. If t_{sp} depends on the film thickness, in this regime of very short diffusion times sample-to-sample variations in film thickness may lead to variations in waveguide depth (see Fig. 10)

The index profile is fairly sensitive to the fabrication conditions, so that the accuracy of our model in predicting a given waveguide profile is limited by the accuracy of the input parameters. For example, in the case of Fig. 9, a nearly perfect fit to the experimental profile is obtained when increasing the ZnO film thickness by 15% and decreasing the value of D by 15%. These variations are within the experimental errors in our measurements of these two quantities. The predictions of the model presented here should become more accurate when the process is better characterized.

Similar agreement was obtained for three other waveguides. Together with the examples illustrated in Figs. 8–10, these comparisons indicate that our model provides reasonable predictions of the index profile, generally within 40% for the surface index change and 20% for the 1/e depth. More detailed measurements are needed to refine the values of the model parameters, i.e., the diffusion coefficients and the $\Delta n/[Zn]$ coefficients.

VI. Conclusions

ZnO diffusion in MgO:$LiNbO_3$ and congruent $LiNbO_3$, and the index profile of waveguides fabricated by this process have been characterized. Earlier reports established the usefulness of this new type of waveguide, which guides both polarizations with low propagation losses and, in the case of MgO:$LiNbO_3$, exhibits high resistance to photorefractive damage. In the present study it was found that using ZnO instead of metallic zinc as a source and maintaining the ZnO film thickness below a prescribed value were important steps in avoiding second phase precipitation and maintaining the surface quality required for low loss waveguides. The refractive-index change produced by the Zn dopant varies approximately linearly with Zn concentration, with only a slight dependence on substrate orientation and diffusion temperature. Simple expressions from linear diffusion theory predict the waveguide index profile from the fabrication conditions. Comparison between calculated and measured profiles for a variety of waveguides showed that these model predictions are fairly accurate. Further studies of the dependence of the index change on Zn concentration and of the extraordinary index change in congruent $LiNbO_3$ are needed to improve the understanding of these waveguides. Diffusion studies using suitable dopant sources within the tie triangles containing $LiNbO_3$ can potentially provide useful information about the Zn transport. ZnO diffusion in lithium niobate appears to be an interesting process which has the potential to extend the spectrum of available waveguide devices.

Acknowledgment

The authors would like to thank Dr. Mei-Fan Sung Tang for helpful discussions, Crystal Technology for providing the crystals, and Lance Goddard for sputtering ZnO films. This work was supported by the NSF-MRL program through the Center for Materials Research at Stanford, and by Litton Systems, Inc.

References

[1] R. V. Schmidt and I. P. Kaminow, "Metal diffused optical waveguides," *Appl. Phys. Lett.*, vol. 25, pp. 458–460, 1974.

[2] J. L. Jackel, C. E. Rice, and J. J. Veselka, "Proton exchange for high-index waveguides in $LiNbO_3$," *Appl. Phys. Lett.*, vol. 41, pp. 607–608, 1982.
[3] S. K. Korotky and R. C. Alferness, in *Integrated Optical Circuits and Components*, L. D. Hutcheson, Ed. New York: Marcel Dekker, 1987, ch. 6, p. 215.
[4] R. A. Becker, "Thermal fixing of Ti-diffused $LiNbO_3$ channel waveguides for reduced photorefractive susceptibility," *Appl. Phys. Lett.*, vol. 45, pp. 121–123, 1984.
[5] M. M. Fejer, M. J. F. Digonnet, and R. L. Byer, "Generation of 22 mW of 532-nm radiation by frequency doubling in Ti:MgO:$LiNbO_3$ waveguides," *Opt. Lett.*, vol. 11, pp. 230–232, 1986.
[6] A. M. Glass, "The photorefractive effect," *Opt. Eng.*, vol. 17, pp. 470–479, 1978.
[7] G. Zhong, J. Jian, and Z. Wu, "Measurements of optically induced refractive damage of lithium niobate doped with different concentrations of MgO," in *Proc. 11th Int. Quantum Electron. Conf.* (Optical Society of America, Washington, D.C.), 1980, p. 631.
[8] J. Jackel *et al.*, "Damage-resistant $LiNbO_3$ waveguides," *J. Appl. Phys.*, vol. 55, pp. 269–270, 1984.
[9] G. E. Peterson, A. M. Glass, and T. J., Negran, "Control of the susceptibility of lithium niobate to laser-induced refractive index changes," *Appl. Phys. Lett.*, vol. 19, pp. 130–132, 1971.
[10] I. P. Kaminow and L. W. Stulz, "Nd:$LiNbO_3$ laser," *IEEE J. Quantum Electron.*, vol. QE-11, pp. 306–308, 1975.
[11] W. M. Young, R. S. Feigelson, M. M. Fejer, M. J. F. Digonnet, and H. J. Shaw, "Photorefractive damage resistant Zn-diffused waveguides in MgO:$LiNbO_3$," *Opt. Lett.*, vol. 16, 995–997, 1991.
[12] R. L. Holman, P. J. Cressman, and J. F. Revelli, "Chemical control of optical damage in lithium niobate," *Appl. Phys. Lett.*, vol. 32, pp. 280–283, 1978, Lindberg Furnace Company, Watertown, Wisconsin.
[13] D. W. Yoon and O. Eknoyan, "Characterization of vapor diffused Zn:LiTaO3 optical waveguides," *J. Lightwave Technol.*, vol. 6, pp. 877–880, 1988.
[14] V. B. Nalbandyan, B. S. Medvedev, V. I. Nalbandyan, and A. V. Chinenova, "Ternary system of niobium, zinc, and lithium niobate," *Inorganic Materials*, pp. 830–833, 1988.
[15] M. E. Villafuerte-Castrejon, A. Aragon-Pina, R. Valenzuela, and A. R. West, "Compound and solid-solution formation in the system Li_2O-Nb_2O_5-TiO_2," *J. Solid State Chem.*, vol. 71, pp. 103–108, 1987.
[16] M. N. Armenise *et al.*, "Characterization of TiO_2, LiNb3O8, and $(Ti0.65Nb0.35)O_2$ compound growth observed during Ti:$LiNbO_3$ optical waveguide fabrication," *J. Appl. Phys.*, vol. 54, pp. 6223–6231, 1983.
[17] C. E. Rice and R. J. Holmes, "A new rutile structure solid-solution phase in the LiNb3O8-TiO_2 system, and its role in Ti diffusion into $LiNbO_3$," *J. Appl. Phys.*, vol. 60, pp. 3836–3839, 1986.
[18] D. W. Yoon and O. Eknoyan, "Characterization of vapor diffused Zn:LiTaO3 optical waveguides," *J. Lightwave Technol.*, vol. 6, pp. 877–880, 1988.
[19] R. E. Hill, *Physical Metallurgy Principles, 2nd ed.* New York: Van Nostrand, 1973, ch. 6, 10, 11.
[20] J. M. White and P. F. Heidtich, "Optical waveguide refractive index profiles determined from measurement of mode indices: A simple analysis," *Appl. Opt.*, vol. 15, pp. 151–155, 1976.
[21] J. R. Carruthers, I. P. Kaminow, and L. W. Stulz, "Diffusion kinetics and optical waveguiding properties of outdiffused layers in lithium niobate and lithium tantalate," *Appl. Opt.*, vol. 13, pp. 2333–2342, 1974.
[22] C. R. Barrett, W. D. Nix, and A. S. Tetelman, *The Principles of Engineering Materials.* New Jersey: Prentice-Hall, 1973, p. 158, ch. 5.
[23] B. I. Boltaks, *Diffusion in Semiconductors.* New York: Academic, 1963, ch. 4, p. 102.
[24] See, for example, W. M. Young, Compositional Control by Diffusion in Lithium Niobate ($LiNbO_3$) for Optical Applications, Ph. D. dissertation, Stanford Univ., 1992.

W. M Young, photograph and biography not available at the time of publication.

M. M Fejer, photograph and biography not available at the time of publication.

M. J. F. Digonnet, photograph and biography not available at the time of publication.

A. F. Marshall, photograph and biography not available at the time of publication.

R. S. Feilgelson, photograph and biography not available at the time of publication.

Zn Indiffusion Waveguide Polarizer on a Y-Cut $LiNbO_3$ at 1.32-μm Wavelength

Ruey-Ching Twu, Chia-Chih Huang, and Way-Seen Wang, *Member, IEEE*

***Abstract*—A polarization-dependent loss measurement of Zn indiffusion (ZI) waveguide on a Y-cut $LiNbO_3$ substrate is firstly reported. The measured results show that the waveguides support either a single extraordinary polarization or both extraordinary and ordinary polarizations depending on the fabrication process parameters. For the single extraordinary polarization waveguide, the measured propagation loss at 1.32-μm wavelength is 0.9 dB/cm and the best measured polarization extinction ratio is 44 dB at a distance of 1.5 cm from the input end, which are quite good for being a waveguide polarizer. Moreover, the voltage-length product measured for the ZI Mach–Zehnder modulator shows that the substrate electrooptic coefficient is not degraded.**

***Index Terms*—Lithium niobate, polarization-dependent loss measurement, polarizer, Zn indiffusion.**

I. Introduction

SINGLE polarization waveguides are widely used for the fabrication of integrated optical sensors because a single polarization wave is essential to increase the optical sensitivity [1]. Moreover, a combination of a single and both polarization waveguides can be a polarization splitter with large splitting extinction ratio and fabrication tolerance [2]–[4]. To date, metal-clad Ti indiffusion (TI) and proton-exchange (PE) are two well-known methods for making single polarization waveguides on $LiNbO_3$ [5], [6]. In the metal-clad waveguide, the TM-wave propagation attenuation, depending on the buffer layer thickness and chosen metal-clad, is much larger than that of the TE-wave. After propagating a certain distance, only the TE-wave is left in the waveguide and it will be slightly affected by the cladding layers. As to the PE waveguide, the change in the extraordinary index Δn_e is positive while the change in the ordinary index Δn_o is negative. Thus, it supports only an extraordinary polarization wave. An annealing process is often used to reduce the propagation loss and restore the electrooptic coefficients. Therefore, good-performance devices have been successfully demonstrated on the z- and x-cut substrates [6], [7]. However, proton-exchanged waveguides suffer from surface damages and the guiding properties are consequently degraded on y-cut substrates [8]. This may cause serious problems in surface-wave acoustic-optical applications, since surface acoustic wave devices frequently require y-cut substrates. Although a tunable PE directional coupler with a SiO_2 cladding and thermal annealing has been demonstrated on a y-cut substrate at 0.6328-μm wavelength by Lee *et al.* [9], it is still difficult to fabricate a well confined waveguide at the near-IR-wavelength region due to the PE depth and concentration limitations for avoiding surface damage.

Recently, Zn indiffusion (ZI) waveguides have been studied extensively to make optical devices in $LiNbO_3$ due to less susceptibility to photorefractive damage in comparison to TI waveguides [10]. Also, the Zn atoms have larger diffusion coefficients than those of the Ti atoms. Therefore, ZI diffusion needs no additional out-diffusion suppression and saves the time for diffusion, which provides flexibility for the fabrication of optical waveguides. The guiding characteristic at 0.6328-μm wavelength of a planar waveguide have been discussed [10], [11]. However, the variations of guided mode profiles and the polarization-dependent losses of a channel waveguide fabricated with different process parameters have never been addressed at the 1.32-μm wavelength.

In this paper, the polarization-dependent loss measurement of ZI waveguides on a y-cut, x-propagation $LiNbO_3$ substrate are demonstrated. The results show that the ZI waveguide supports a single extraordinary or both extraordinary and ordinary polarizations depending on process parameters. In such single extraordinary polarization waveguide, the propagation loss is 0.9 dB/cm and the best polarization extinction ratio measured at a distance of about 1.5 cm away from the input end of the waveguide is 44 dB. Therefore, it is quite suitable for using as a waveguide polarizer. Moreover, the fabricated ZI Mach–Zehnder modulator shows that it has a nondegraded electrooptic coefficient r_{33}. On the y-cut substrate, a ZI waveguide polarizer has the advantage of better performance and simpler fabrication process than that of a PE or a metal-clad waveguide polarizer.

II. Experiments

First, a Zn thin film is deposited on the substrate by thermal evaporation. As Zn atoms are difficult to be leeched directly on the surface of $LiNbO_3$ substrate, a 50-Å Ni film is predeposited onto the $LiNbO_3$ substrate in order to increase the adhesion. The channel waveguide and a Mach–Zehnder modulator patterns are then formed by the lift- off technique. The waveguide width is 8 μm, the Y-branch angle is 2°, and the gap between two arms of the Mach–Zehnder modulator is 16 μm. The samples were placed on a covered alumina crucible, which was then placed in a high-temperature oven. The thermal cycle, which is carried out in dry air, typically involves heating at a rate of about 10 °C/min up to the diffusion temperature, maintaining at that temperature

Manuscript received August 4, 1999; revised October 28, 1999. This work was supported by the National Science Council, Taipei, Republic of China under Contract NSC 89-2215-E-002-007.

The authors are with the Department of Electrical Engineering and Graduate Institute of Electro-Optical Engineering, National Taiwan University, Taipei 10617, Taiwan, R.O.C.

Publisher Item Identifier S 1041-1135(00)01121-6.

for a certain time, and cooling at a rate of 10 °C/min down to the room temperature.

After the thermal diffusion, the substrate end faces are cut and polished to allow end butt coupling. A schematic diagram of the polarization-dependent loss measurement setup is shown in Fig. 1. A He-Ne laser of wavelength 0.6328 μm is used for optical alignment. The polarization of an incident Nd:YAG laser light of wavelength 1.32 μm is controlled by rotating the polarizer. The angle is varied from 0° to 360° relative to the y-axis with a step of 10°. The incident light is in the TM polarization when the angle is set at 0° or 180°, and in the TE polarization, when the angle is set at 90° or 270°. For comparison, an attenuator is used to keep the incident power constant at different polarizations. The light is divided into a reference and a measurement light after passing through the beam splitter. The measurement light is coupled into the front end face of the waveguide with a 40× lens and the output beam is imaged onto an InGaAs photodetector (or a charge-coupled device camera) also with a 40× lens. Both reference and measurement lights are detected by a dual-channel power meter at the same time. The measured output mode profile is displayed on a video monitor.

For the fabrication of a Mach–Zehnder modulator, a pair of aluminum electrodes of thickness 3000 Å, length 6 mm, and gap 14 μm is formed for electrooptic modulation. The switching voltage measurement setup is also shown in Fig. 1. A triangular voltage signal from the function generator is applied across the electrodes. The input and measured signals were both shown on an oscilloscope which were further used to calculate the switching voltage.

III. Results and Discussion

The mode profiles are dependent on the strip film thickness τ, waveguide width W, diffusion temperature T, diffusion time t, and operation wavelength λ. As single-mode waveguides are essential for most device applications, only the single-mode waveguides are further discussed latter on. The TE (extraordinary polarization) and TM (ordinary polarization) mode profiles versus different process parameters are shown in Fig. 2. Consider case A as illustrated in Fig. 2. The TE and TM modes show that they have similar guiding profiles. In case B, the TE mode size is slightly larger than that of the TM mode. In case C, the TM mode is not well-confined in the waveguide and most of the power is radiated into the substrate. However, only the TE mode is guided in case D. The above experimental results show that the ZI waveguide supports a single extraordinary or both extraordinary and ordinary polarizations depending on fabrication process parameters. Besides, the single extraordinary polarization waveguide is easier achieved than the single ordinary polarization waveguide due to $\Delta n_e > \Delta n_o$, particularly when fabricated at a lower diffusion temperature [11]. Also, well-confined TE and TM waveguides are more difficult to be obtained when the diffusion temperature is below 900 °C.

In order to further study the polarization-dependent loss, the normalized output power versus different polarizations with some process parameters is shown in Fig. 3. As the incident power is kept constant for any polarizations, the polarization

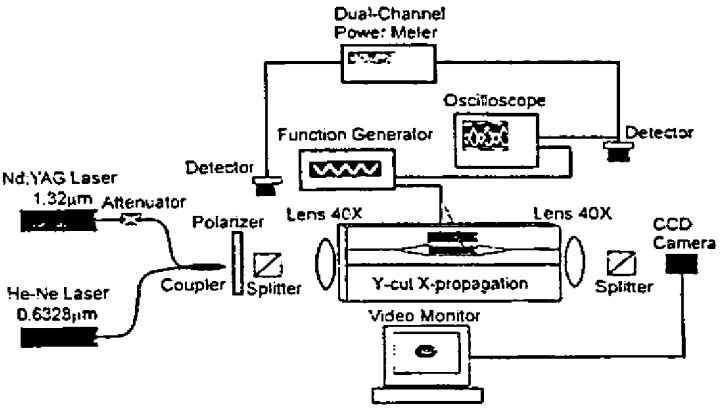

Fig. 1. A schematic diagram of the polarization-dependent loss and switching voltage measurement setup.

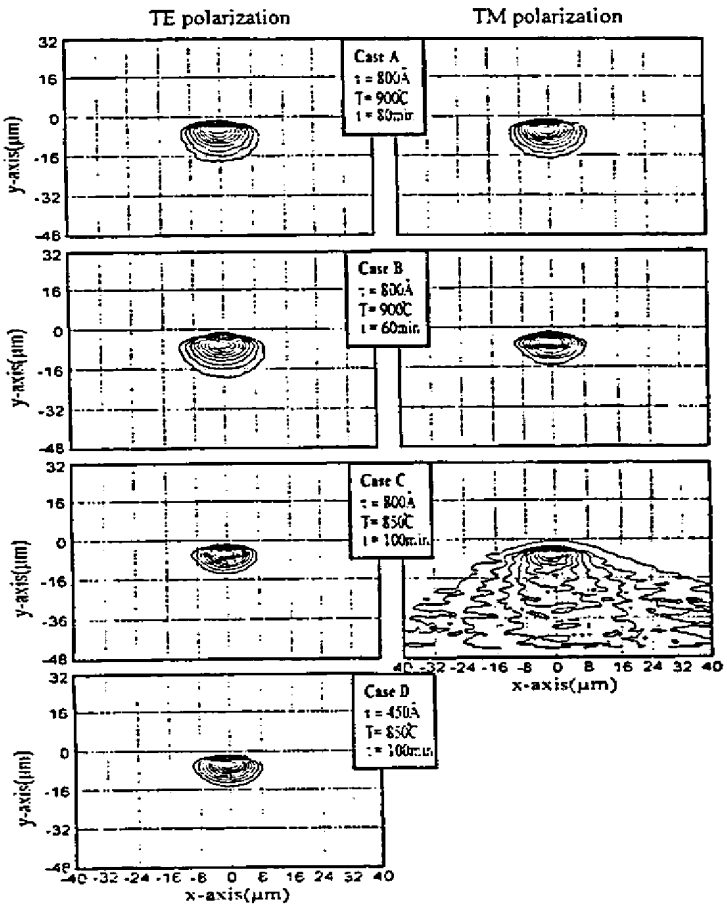

Fig. 2. TE (left) and TM (right) mode profiles versus different process parameters (unguided).

extinction ratio λ is simply defined as $\gamma = 10\log(P_{TE}/P_{TM})$, where P_{TE} and P_{TM} are the output powers of TE and TM modes, respectively. In case D, the best γ obtained is 44 dB at a distance of about 1.5 cm away from the input end of the waveguide and the propagation loss measured by a cut-back method is 0.9 dB/cm. Fig. 4 gives the modulation characteristics curve of a Mach–Zehnder modulator with its waveguides fabricated as those of case D. The measured switching voltage is 17.5 V, the corresponding voltage-length product is 10.5 V-cm, the calculated overlap integral factor by the reported method [12]

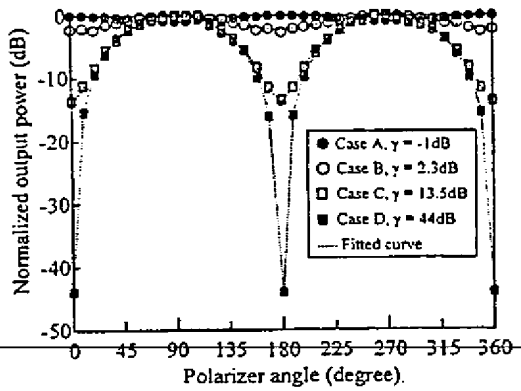

Fig. 3. The normalized output power versus polarization for waveguides fabricated with different process parameters.

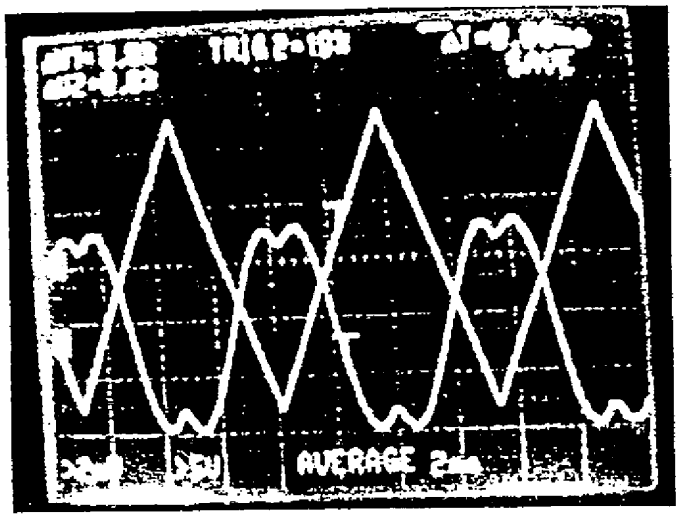

Fig. 4. Measured sinusoidal output signal (2 mV/div) of a zinc indiffusion Mach–Zehnder interferometer with an input saw-tooth wave (5 V/div).

is 0.45. From the above data, the derived r_{33} coefficient is about 30.8 pm/V, which shows that the r_{33} coefficient of a ZI waveguide is not degraded under the specific process condition presented in this work.

IV. Conclusion

A polarization-dependent loss measurement of ZI waveguides on a y-cut, x-propagation $LiNbO_3$ substrate for the 1.32-μm wavelength fabricated with different process parameters is firstly and successfully reported. The results show that the ZI waveguide supports a single extraordinary or both extraordinary and ordinary polarizations depending on the process parameters. For the single extraordinary polarization waveguide, the best γ measured is 44 dB and the propagation loss is 0.9 dB/cm. These are all good enough for making a waveguide polarizer. The fabricated ZI Mach–Zehnder modulator also shows that it has a nondegraded electrooptic coefficient r_{33}. With the excellent properties of process-dependent polarization, more flexibility on waveguide device fabrication is of great interest in the near future.

References

[1] T. Saida and K. Hotate, "General formula describing drift of interferometer fiber-optic gyro due to Faraday effect: Reduction of the drift in twin-depo-I-FOG," *J. Lightwave Technol.*, vol. 17, no. 2, pp. 222–228, 1999.

[2] O. Miami, "$LiNbO_3$ coupled-waveguided TE/TM mode splitter," *Appl. Phys. Lett.*, vol. 36, no. 7, pp. 491–493, 1980.

[3] H. Maruyama, M. Haruna, and H. Nishihara, "TE-TM mode splitter using directional coupling between heterogeneous waveguides in $LiNbO_3$," *J. Lightwave Technol.*, vol. 13, no. 7, pp. 1550–1554, 1995.

[4] P. K. Wei and W. S. Wang, "A TE-TM mode splitter on lithium niobate using Ti, Ni, and MgO diffusions," *IEEE Photon. Technol. Lett.*, vol. 6, pp. 245–248, Feb. 1994.

[5] L. Sun and G. L. Yip, "Analysis of metal-clad optical waveguide polarizers by the vector beam propagation method," *Appl. Opt.*, vol. 33, no. 6, pp. 1047–1050, 1994.

[6] P. G. Suchoski, T. K. Findakly, and F. J. Leonberger, "Low-loss high-extinction polarizers fabricated in $LiNbO_3$ by proton exchange," *Opt. Lett.*, vol. 13, no. 2, pp. 172–174, 1988.

[7] P. G. Suchoski, T. K. Findakly, and F. J. Leonberger, "Stable low-loss proton exchanged $LiNbO_3$ waveguide devices with no electro-optic degradation," *Opt. Lett.*, vol. 13, no. 11, pp. 1050–1052, 1988.

[8] A. Campari, C. Ferrari, G. Mazzi, C. Summonte, S. M. Al-Shukri, A. Dawar, R. M. De La Rue, and A. C. G. Nutt, "Strain and surface damage induced by proton exchange in Y-cut $LiNbO_3$," *J. Appl. Phys.*, vol. 58, pp. 4521–4524, 1985.

[9] S. S. Lee, M. C. Oh, Y. K. Jhee, and S. Y. Shin, "Y-cut $LiNbO_3$ directional coupler with a self-aligned electrode," *J. Lightwave Technol.*, vol 12, no. 5, pp. 872–875, 1994.

[10] W. M. Young, M. M. Fejer, M. J. F. Digonnet, A. F. Marshall, and R S. Feigelson, "Fabrication, characterization and index profile modeling of high-damage resistance Zn-diffused waveguides in congruen MgO:$LiNbO_3$," *J. Lightwave Technol.*, vol. 10, no. 9, pp. 1238–1246 1992.

[11] F. Schiller, B. Herreros, and G. Lifante, "Optical characterization o vapor Zn-diffused waveguides in lithium niobate," *J. Opt. Soc. Amer A*, vol. 14, no. 2, pp. 425–429, 1997.

[12] C. M. Kim and R. V. Ramaswamy, "Overlap integral factors in integrate optic modulators and switches," *J. Lightwave Technol.*, vol. 7, no. 7, pp 1063–1070, 1989.

Jpn. J. Appl. Phys. Vol. 39 (2000) pp. L 864–L 865
Part 2, No. 8B, 15 August 2000

Fabrication of Zn:$LiNbO_3$ Waveguides by Diffusing ZnO in Low-Pressure Atmosphere

Toshiaki SUHARA, Tasuku FUJIEDA, Masatoshi FUJIMURA and Hiroshi NISHIHARA

Department of Electronic Engineering, Graduate School of Engineering, Osaka University, 2-1 Yamada-Oka, Suita, Osaka 565-0871, Japan

(Received June 5, 2000; accepted for publication July 5, 2000)

Fabrication of Zn:$LiNbO_3$ planer and channel waveguides by diffusing ZnO in low-pressure air is presented. The process is simple and does not require special apparatus. Pressure control is crucial to ensure modest indiffusion with suppressed outdiffusion. The waveguides support both ordinary and extraordinary polarization modes, and are expected to be photorefractive-damage resistant. The diffusion temperature considerably lower than that for Ti-indiffusion is advantageous for applications to quasi-phase matched nonlinear optic devices. Single-mode guides of ~1 dB/cm propagation loss for 1.5 μm wavelength band were obtained.

KEYWORDS: optical waveguide, lithium niobate, quasi phase matching, nonlinear optics, diffused waveguide

1. Introduction

There has been much research and development interest in quasi-phase-matched (QPM) nonlinear-optic (NLO) devices and rare-earth doped lasers in $LiNbO_3$ waveguides. Annealed-proton-exchanged (APE) waveguides[1,2] are widely used for such applications. The APE waveguides, however, have a drawback that they support only extraordinary guided modes, and it may pose limitations in implementation of polarization-independent NLO wavelength converters and integration of NLO, laser and electrooptic devices. Ti-indiffused guides,[3] which support both ordinary and extraordinary modes, involve the photorefractive damage problem.[4] Fabrication of periodically-domain-inverted grating for QPM in Ti:$LiNbO_3$ guide requires a complicated process[5] to solve the problem caused by unwanted domain inversion during the high-temperature Ti diffusion process.

An alternative waveguide is Zn-indiffused waveguides, which support both polarization modes and are considered to be photorefractive-damage resistant.[6–9] Planar guides were fabricated by diffusing ZnO at 1000–1100°C into z-cut undoped and MgO-doped $LiNbO_3$ crystals in Li-rich atmosphere, and were characterized at 0.63 μm wavelength.[6] Er-doped lasers have been demonstrated using channel guides fabricated by diffusing ZnO into z-cut Er:MgO:$LiNbO_3$ at 930°C for 0.5 h in air, although the detail of the atmosphere was not presented.[7] Another feature of Zn:$LiNbO_3$ guides is that they can possibly be fabricated by diffusion at temperatures lower than that for Ti-indiffusion. In fact, planar guides were fabricated by metallic Zn diffusion from vapor-phase at 600–700°C in low-pressure nitrogen atmosphere using a specially designed apparatus, and were characterized at 0.44–0.63 μm wavelengths.[8] Channel guides for 1.3 μm wavelength were fabricated by diffusing Zn film into y-cut $LiNbO_3$.[9] However, techniques for fabrication of Zn:$LiNbO_3$ guides have not been fully established.

In this letter, we present fabrication of Zn-indiffused planer and channel waveguides for up to 1.5 μm wavelength band in z-cut $LiNbO_3$ by diffusing ZnO in low-pressure atmosphere.

2. Planar Waveguides

As a preliminary experiment, diffusion of ZnO was tried with various atmosphere. Congruent optical-grade z-cut $LiNbO_3$ crystals were used, and thin film of ZnO of 280 nm thickness was deposited on the +z surface by RF magnetron sputtering in Ar/O_2 (1 : 1) atmosphere using a ZnO target. An ordinary quartz-tube electric furnace was used for heat treatment at 930°C for 0.5–24 h. The surfaces of crystals heated in (dry and wet) O_2 and air at 1 atm were rough and were covered with nonuniform residual which seemed to have been yielded by ZnO–$LiNbO_3$ reaction, and therefore waveguide was not obtained with such samples. This result is in contrast with the successful waveguide fabrication in Er:MgO:$LiNbO_3$ by similar process.[7] The surface of crystals heated in quartz tube evacuated by a rotary pump, on the other hand, was clear, and planar guides were obtained. Waveguides obtained by diffusing 175 nm thick ZnO at 930°C for 0.5 h, for example, supported transverse electric (TE) and transverse magnetic (TM) modes at 0.46, 0.63, 1.06 and 1.54 μm wavelengths. The refractive-index increment at the surface estimated from m-line measurement at 0.46 μm wavelength was 0.006 for both ordinary and extraordinary waves. Almost same results were obtained using an IR-heating rapid thermal annealing (RTA) furnace.

3. Channel Waveguides

To examine further the dependence of the diffusion on the process parameters and find conditions for fabrication of waveguides for device applications, channel guides were fabricated. The ZnO film of 220 nm thickness was patterned into 7 μm wide stripes by lift-off technique. The air pressure in the quartz tube was monitored with a Pirani gauge and was controlled by a throttle valve. The crystals were slightly darkened due to reducing by heating in oxygen-poor atmosphere, depending upon the temperature, time and pressure. The crystals heated at lower pressure were darker. The original transparency was recovered by annealing in O_2 (1 atm) at 650°C for 5 h. Examination of the crystal surface after etching in $HF–HNO_3$ showed no evidence of unwanted ferroelectric-domain inversion. The both ends of the waveguides were polished for end-fire coupling. The waveguide length was approximately 10 mm. The waveguiding characteristics were examined at a few wavelengths. The results are summarized in Table I.

It was found that the diffusion depends significantly on the pressure. For guides diffused at 930°C in pressures at or lower than 1 Torr, channel guiding was weak or not observed, and evidence of planar guiding of TM mode only was observed as a result of increase of extraordinary index due to Li_2O outdiffusion enhanced in low pressure. For guides diffused at 10 Torr, on the other hand, only channel guiding was observed. The fact that no channel guiding was observed for

Table 1. Result of the optical waveguiding test of the fabricated channel guides.

Sample	Diffusion Temprature, Time, Pressure	Evalution wavelength, polarization	
		0.63 μm TM/TE	1.54 μm TM/TE
#1	930°C, 0.5 h, 1 Torr	p/n	p/n
#2	930°C, 0.5 h, 10 Torr	s/s	s/n
#3	890°C, 0.5 h, 0.6 Torr	m/m	s/s
#4	890°C, 0.5 h, 10 Torr	m/m	s/s
#5	890°C, 1.0 h, 10 Torr	m/m	m/s
#6	890°C, 2.0 h, 10 Torr	m/m	m/s

p: planar guiding s: single-mode guiding m: multimode guiding n: no guiding.

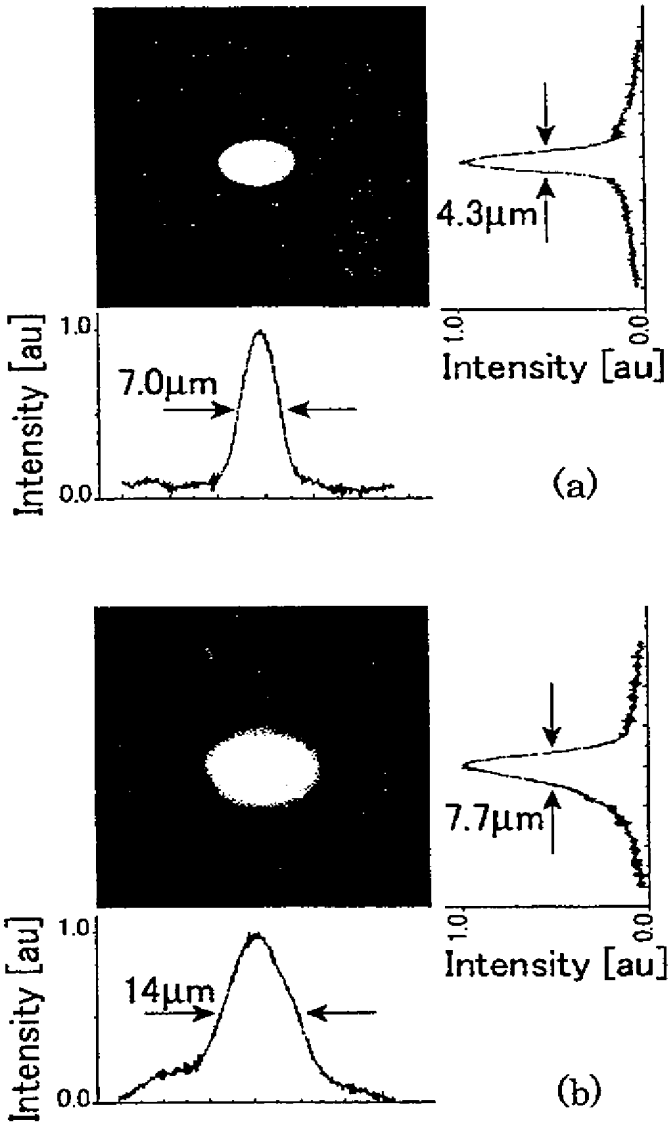

Fig. 1. Near field patterns of the guided modes at 1.54 μm wavelength observed in channnel guide #4. (a) TM-like mode, (b) TE-like mode.

samples diffused at higher temperature and in lower pressure may be explained by insufficient index increment due to fast (too deep) diffusion, although further experimental study is required to clarify the reason. These results indicate that for fabrication of device-quality cannel waveguides pressure control is crucial to ensure modest indiffusion with suppression of outdiffusion, support the observation that the diffusion of Zn is enhanced by oxygen vacancies,[8] and also suggest the possibility of fabrication at even lower temperature.

The guides #3 and #4 supported single mode at 1.54 μm wavelength. The mode confinement was stronger in #4 than in #3. Figure 1 shows the mode patterns of guide #4 diffused at 930°C and 10 Torr. The full width at half-maximum (FWHM) mode size was 4.3 μm (depth) × 7.0 μm (width), and 7.7 μm × 14 μm for TM-like and TE-like modes, respectively. The propagation loss was measured as approximately 1 dB/cm for both modes by the waveguide Fabry-Perot interference method using a temperature-tuned distributed feedback (DFB) laser.

4. Conclusion

We demonstrated successful fabrication of Zn-indiffused $LiNbO_3$ waveguides by diffusing ZnO in low-pressure air. Control of the pressure is crucial for obtaining device-quality guides with good reproducibility. The process is simple and does not require a special apparatus. The guides support both polarization modes, and are expected to be photorefractive-damage resistant. Further experimental study is required to optimize the diffusion conditions and clarify the photorefractive characteristics. The diffusion temperature considerably lower than that for Ti-indiffusion is advantageous for application to QPM-NLO devices. Most recently, we actually fabricated QPM second harmonic generation devices and difference frequency generation devices, and obtained encouraging results. The results will be published elsewhere.

Acknowledgement

This work was supported by Grant-in-Aid from the Ministry of Education, Science and Culture.

1) P. G. Suchoski, T. K. Findakly and F. J. Leonberger: Opt. Lett. 13 (1988) 1050.
2) A. Loni and R. M. De La Rue: Electron. Lett. 14 (1991) 1245.
3) J. L. Jackel, V. Ramaswamy and S. P. Lyman: Appl. Phys. Lett. 38 (1981) 509.
4) R. A. Becker: Appl. Phys. Lett. 45 (1984) 121.
5) D. Hofmann, G. Schreiber, C. Haase, H. Herrmann, W. Grundkotter, R. Ricken and W. Sohler: Opt. Lett. 24 (1999) 896.
6) W. M. Young, R. S. Feigelson, M. M. Fejer, M. J. F. Digonnet and H. J. Shaw: Opt. Lett. 16 (1991) 995.
7) C. Huang and L. McCaughan: Electron. Lett. 33 (1997) 1639.
8) B. Herreros and G. Lifante: Appl. Phys. Lett. 66 (1995) 1449.
9) R. Twu, C. Huang and W. Wang: IEEE Photon. Technol. Lett. 12 (2000) 161.

$LiNbO_3$ optical waveguides by Zn diffusion from vapor phase

B. Herreros and G. Lifante
Departamento de Física de Materials, C-IV, Universidad Autónoma de Madrid, 28049 Madrid, Spain

(Received 28 July 1994; accepted for publication 3 January 1995)

Fabrication of optical waveguides on $LiNbO_3$ by Zn diffusion from the vapor phase has been demonstrated, using a specially designed diffusion apparatus. The planar waveguides on z-cut samples support both TE and TM propagations, indicating an increase of refractive indices for n_0 and n_e. Energy dispersive x-ray analysis measurements confirm the diffusion of Zn into the crystal, and analysis of the content of Zn as a function of diffusion depth for samples treated at different temperatures indicates much higher diffusion coefficients than those obtained for Ti diffusion in $LiNbO_3$. The technique is versatile, easy to operate, and allows fabrication of waveguides at temperatures as low as 600–700 °C, thus preventing Li outdiffusion. © *1995 American Institute of Physics.*

$LiNbO_3$ is an important inorganic key material for optoelectronics, which combines high optical nonlinearities with the capability of incorporating high concentrations of laser active ions. Several methods are now widely used for fabricating waveguides in this material,[1–3] the most popular being Ti diffusion, proton exchange, and ion implantation. Each one of the developed techniques has some limits of applicability: proton exchange only increases in the extraordinary refractive index; ion implantation requires the use of ion accelerators. Even though, Ti diffusion does not have these drawbacks but the process is performed at temperatures ranging from 950 to 1200 °C,[4] and at such high temperatures the Li-outdiffusion problem (which could form undesirable surface waveguides competing with channel waveguides[5]), must be addressed. Several methods for suppressing outdiffusion have been proposed,[6] which add complexity to the technique.

To overcome such difficulties, low temperature diffusion is desirable; this requires the use of elements that have high diffusivity and low activation energy, and that, upon diffusion, could cause an index increase and do not introduce excessive absorption at the operating wavelength.

Under these requirements, metallic Zn appears to be a potential candidate. In fact, Zn diffusion from the vapor phase has been demonstrated to produce low loss optical waveguides in $LiTaO_3$.[7] The procedure consists of loading a bare, cleaned substrate together with Zn wire or granules in a quartz ampoule, which is evacuated with a diffusion pump and sealed. The diffusion is then performed by heating the ampoule in a tube furnace. Nevertheless these authors reported no success in waveguide formation in $LiNbO_3$ due to severe pitting and surface damage on the substrates.[8]

In the present work we report a successful method to produce monomode and multimode optical waveguides in $LiNbO_3$ by metal Zn diffusion in a controlled way at temperatures as low as 600 °C. This has been achieved by diffusing the metal Zn from the vapor phase in a specially designed diffusion apparatus. We also report measurements by energy dispersive x-ray analysis (EDAX) of the dopant distribution in Zn-diffused $LiNbO_3$ waveguides, as well as the optical characterization of their index profiles. These data are used to obtain values of the diffusion coefficient of Zn in $LiNbO_3$, their temperature dependence and the relationship between the refractive index change and the Zn concentration. Comparison between diffusion coefficients of Zn, ZnO, and Ti establishes the potential advantage of this method for fabricating waveguides in $LiNbO_3$.

Single crystals of congruent $LiNbO_3$ were grown in our laboratory by the Czochralski method from grade I Johnson–Mathey powder. The initial preparation of the samples involved cutting slices from the boule and polishing the crystals to optical quality. The finished samples were all of the same cut (z cut) and had final dimensions of $2\times6\times8$ mm^3. The diffusion apparatus used in this work is based in a Van Doorn heatpipe, traditionally used in the additive coloration of alkali halides. The setup is described in the literature,[9] and consists basically of a stainless steel tube previously cleaned at high temperature, where the metal is deposited on the bottom, and the sample is placed on a basket. Stablizied 347-type stainless steel was used to prevent corrosion in the bottom (welded zone) of the tube. Water cooling in the upper part and a conic condenser were used to confine the metal vapor. The upper part of the tube is a standard NW-20 KF flange connection through which the tube is either evacuated or filled with nitrogen at the desired pressure, also providing space for the thermocouple feedthrough and the crystal container fixing. The tube is finally introduced in an oven, the heating and cooling rates being 10 °C/min, to avoid thermal shock to the crystals.

Zn diffusion profiles were determined by EDAX measurements. Prior to EDAX characterization, Zn-diffused samples were first sandwiched between two glass slides, and the end perpendicular to the diffusion surface was polished. Glass slides were used to prevent rounding of the edge of the diffused region during polishing, which would otherwise upset EDAX measurements. Optical characterization of the samples includes determination of the refractive index profiles of the planar waveguides, computed by fitting the mode spectra measured at $\lambda=442$, 488, 514, and 633 nm with appropriate Gaussian index profiles.

Z-cut samples of $LiNbO_3$ were treated at 500, 600, and 700 °C during 0.5, 4, and 4 h respectively (hereafter labeled as Nos. 1, 2, and 3), using a nitrogen buffer pressure of 10 Torr, with ~2 g of metallic Zn. This pressure is adequate in this range of temperature to provide high enough Zn vapor

 0003-6951/95/66(12)/1449/3/$6.00

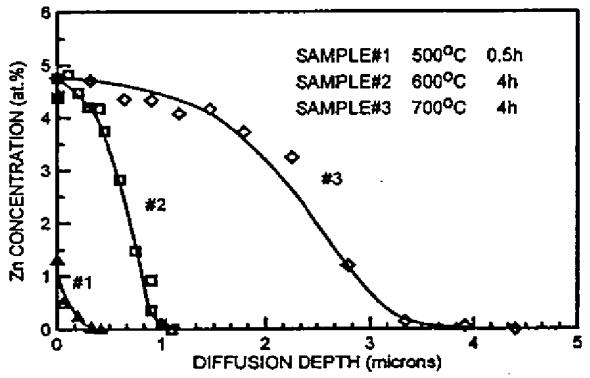

FIG. 1. Zn concentration in atomic percentage, measured by EDAX technique, as a function of depth normal to the diffused surface for $LiNbO_3$ crystals treated at different temperatures in Zn metallic vapor atmosphere (lines are only a guide for the eyes).

surrounding the sample, thus allowing the diffusion. After the diffusion, the samples showed a dark gray color coming from color center formation during this process. Subsequent annealing in air removed these color centers and the samples became transparent.

We have followed the metal diffusion through the crystals by means of the EDAX technique. After diffusion, one end of the samples was repolished, and EDAX scannings of the edges were performed. Figure 1 shows the Zn concentration (at. %) plotted as a function of diffusion depth for the three samples. As can be observed, sample No. 1 has a peak value in %Zn of ~1.2%, with a penetration depth (computed at $1/e^2$ of its maximum value) of ~0.2 μm. Samples Nos. 2 and 3 have similar values for a Zn concentration near the surface of ~4.7%, and diffusion depths of ~0.9 and ~3.0 μm, respectively. This concentration at the surface for sample Nos. 2 and 3 is close to the highest surface concentration observed in $LiNbO_3$:Zn waveguides formed from ZnO at higher temperature[10] (5.4%), indicating similar values of the effective solid solubility for both fabrication procedures.

The calculated values for the diffusion coefficients are $D(600\ °C) \approx 0.06\ \mu m^2/h$ and $D(700\ °C) \approx 0.6\ \mu m^2/h$. These coefficients are about two orders of magnitude higher than the diffusion coefficients of Zn from ZnO source at these temperatures, calculated by extrapolating data given by Young *et al.*,[10] using $D_0 = 4.2 \times 10^{13}\ \mu m^2/h$, $E_0 = 3.0$ eV. Although the origin of this discrepancy is uncertain, a possible origin could be connected with the rate of oxygen vacancies annhilation depending on the atmosphere, as suggested by Burns[11] for Ti indiffusion in $LiNbO_3$. Moreover, the value of D at 700 °C is comparable to the reported diffusion coefficient for Ti at 1100 °C,[11] indicating that at a given temperature, the diffusion of Zn from the vapor phase is much faster than that of Ti. This behavior is similar to that found in Zn vapor diffused Zn into $LiTaO_3$, where the authors[8] report a value of $D(800\ °C) = 0.7\ \mu m^2/h$, which may be compared with $D(1200\ °C) = 0.29\ \mu m^2/h$ for Ti diffusion.[11]

Optical waveguiding properties of the samples were then examined by dark mode experiments after removing the color centers. Sample No. 1, treated at 500 °C, did not show any dark mode either for TE or TM polarizations. The fact that this sample did not reveal optical waveguiding behavior could be due to the small amount of diffused Zn and a too short diffusion depth, as shown in Fig. 1. By contrast, the other two samples Nos. 2 and 3, treated at 600 and 700 °C, showed several dark modes in both TE and TM propagation, indicating optical waveguide formation was taking place.

TABLE I. Number of observed dark modes for sample Nos. 2 and 3 at different wavelengths.

	600 °C		700 °C	
λ (nm)	n_0	n_e	n_0	n_e
442	0	2	5	2
488	0	1	5	2
514	0	1	4	2
633	0	1	3	1

Table I shows a summary of the number of observed dark modes for samples Nos. 2 and 3, at the wavelengths provided by several laser lines. As can be seen, while sample No. 2 supports only TM propagation, and is monomode at λ=488, 514, and 633 nm, sample No. 3, fabricated at 700 °C, reveals several modes on all the wavelengths checked for both TE and TM propagation, indicating that both the ordinary and extraordinary refractive indices of the diffused layer have increased. The fact that the sample treated at 700 °C reveals less number of modes for n_e than for n_0, in contrast with the observed modes in sample No. 2, is somewhat unexpected, taking into account that both samples have the same surface Zn concentration, and sample No. 3 is three times deeper. This behavior could be related to the difficulty of exciting all the propagating modes by prism-coupling, as Young *et al.* found[10] in waveguides fabricated by ZnO diffusion in congruent $LiNbO_3$, and may be related to local variations in Li concentrations.[10]

Although the number of observed modes for TE propagation in sample Nos. 2 and 3 are too low to determine the exact index profile of the waveguides, this determination can be achieved for the ordinary index on samples treated at 700 °C. Figure 2 presents these results, where we have plotted the increase in ordinary refractive index (as % to the unmodified substrate value) as a function of the penetration depth, obtained by fitting the dark mode spectra at λ=488 nm to a Gaussian profile $\Delta n_0 = \Delta n_{0,max} \exp(-x^2/d^2)$. In order to show the goodness of this profile, we have also plotted in this figure (upper x axis) the calculated mode curve for this profile (dotted line) and the measured effective refractive indices (triangles). This fit gives a depth of $d \sim 2.7$ μm, in agreement with the diffusion depth extracted from EDAX data, and a value of $\Delta n_{0,max} \approx 1.4\%$. Combining this value with the Zn concentration near the surface, a value of $\Delta n_0(\%)/[Zn] \approx 0.30$ is obtained. This ratio is about twice the value earlier obtained for ZnO:$LiNbO_3$ waveguides,[10] the reason for this difference could be due to the different wavelength used for measuring the refractive indices (λ=633 nm in referenced work, λ=488 nm in this

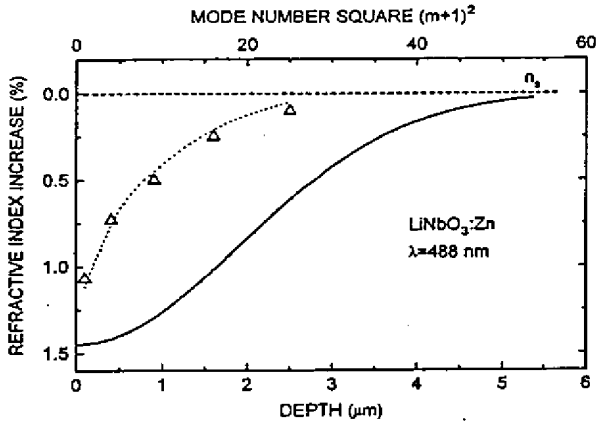

FIG. 2. Gaussian refractive index profile at 488 nm for n_0 (continuous line) of a Zn-diffused $LiNbO_3$ waveguide fabricated at 700 °C during 4 h. Dotted line represents the mode curve calculated for this profile, and triangles are the measured effective refractive indices (upper x axis).

work) and the uncertainties for measuring the refractive index profile and the dopant concentration.

The satisfactory results reported here are clearly at variance with previous unsuccessful reports of waveguides produced by vapor Zn diffusion in $LiNbO_3$,[8] where the authors did not find evidence of waveguide formation by means of the dark mode characterization technique. To explain this failure one can possibly mention the use of too high a temperature for the diffusion, or the different method used to carry out the diffusion.

It is worth noting that at the relatively low temperature at which waveguide formation was observed (600–700 °C) that any outdiffusion of Li ions is precluded. Thus, one of the drawbacks pointed out in Ti-diffused $LiNbO_3$ waveguides, where the diffusion is performed at 950–1200 °C, is overcome. Also, the low temperature diffusion is desirable to fabricate waveguide lasers in doped $LiNbO_3$, thus avoiding the possibility of outdiffusion of the dopants.

It has been established that addition of ~6% of Zn to the melt dramatically reduces the photorefractive effect in bulk $LiNbO_3$.[12] Therefore, the use of Zn as an element to carry out the diffusion could help to avoid the photorefractive damage on these waveguides, as it has already been shown in Zn waveguides.[13] This element is an even better choice than Mg, because it does not modify the spectroscopic properties of doubly doped $LiNbO_3$:RE:Zn.[14]

In conclusion, we have shown an alternative method to fabricate optical waveguides in $LiNbO_3$ by diffusing Zn from the vapor phase. Using metallic Zn for diffusion has the advantage of the low vapor pressure of the Zn and the possibility of eliminating photorefractive damage. Good results have been obtained with diffusion carried out at temperatures as low as 600–700 °C, and the diffusion coefficient for Zn at 700 °C is comparable to that obtained from Ti diffusion at 1100 °C. This low temperature processing is significant in that it slows down outdiffusion of Li and other elements in doped $LiNbO_3$, and avoids perturbation of ferroelectric domain distributions. These advantages may counteract the use of an experimental apparatus somewhat more complex than the traditional ZnO diffusion. Let us finally indicate that it has been recently demonstrated the fabrication of channel waveguides in $LiNbO_3$ by Zn diffusion from vapor phase,[15] and the same method could be used for $LiNbO_3$. The method here reported offers a versatile way to tailor the parameters of the guide by independently controlling temperature, time, and vapor pressure, although a precise prediction of the relationship between processing and waveguide parameters for engineering applications needs further characterization.

Future work includes measurements of the photorefractive damage threshold and losses of the produced waveguides, and investigating the possibility of using the method here described to extend the fabrication of optical waveguides to other insulator materials.

The authors are grateful to Professors F. Cussó, C. Zaldo, and J. M. Cabrera for encouragement and helpful discussions, and Professor P. D. Townsend for critical reading of the manuscript. They also acknowledge the assistance of J. M. Cabrera and J. Olivares for the dark mode measurements, M. Voda for providing the crystals, and the SIDI facilities at the Universidad Autónoma de Madrid for EDAX measurements. This work was supported by Ministerio de Educación y Ciencia of Spain (CICYT, Project No. MAT92-0250) and the European Community (HCM, Project No. ERB4050PL921612), and B. Herreros was supported by a CICYT grant.

[1] R. V. Schmidt and I. P. Kaminov, Appl. Phys. Lett. 25, 458 (1974).
[2] M. Digonnet, M. Fejer, and R. Byer, Opt. Lett. 10, 235 (1985).
[3] L. Zhang, P. J. Chandler, and P. D. Townsend, Nucl. Instrum. Methods Phys. Res. B 59/60, 1147 (1991).
[4] G. J. Griffiths and R. J. Esdaile, IEEE J. Quantum Electron. QE-20, 149 (1984).
[5] I. P. Kaminov and J. R. Carruthers, Appl. Phys. Lett. 22, 326 (1973).
[6] J. L. Jackel, V. Ramaswamy, and S. P. Lyman, Appl. Phys. Lett. 38, 509 (1981).
[7] O. Eknoyan, D. W. Yoon, and H. F. Taylor, Appl. Phys. Lett. 51, 384 (1987).
[8] D. W. Yoon and O. Eknoyan, J. Lightwave Technol. 6, 877 (1988).
[9] P. Silfsten, G. Lifante, F. Cussó, and J. A. Medina, J. Mater. Sci. 26, 1937 (1991).
[10] W. M. Young, M. M. Fejer, M. J. F. Digonnet, A. F. Marshall, and R. S. Feigelson, J. Lightwave Technol. 10, 1238 (1992).
[11] W. K. Burns, P. H. Klein, and E. J. West, J. Appl. Phys. 50, 6175 (1979).
[12] T. R. Volk, V. I. Pryalkin, and N. M. Rubinina, Opt. Lett. 15, 996 (1990).
[13] W. M. Young, R. S. Feigelson, M. M. Fejer, M. J. F. Digonnet, and H. J. Shaw, Opt. Lett. 16, 995 (1991).
[14] L. Nuñez, R. Duchowicz, M. Voda, and F. Cussó, J. Phys. C 4, 443 (1994).
[15] T. Suzuki, O. Eknoyan, and H. F. Taylor, J. Lightwave Technol. 11, 285 (1993).

Jpn. J. Appl. Phys. Vol. 39 (2000) pp. L 488–L 489
Part 2, No. 6A, 1 June 2000

Express Letter

Preservation of Periodically Poled Structures in Zn-Diffused $LiNbO_3$ Waveguides

Rubén NEVADO, Eugenio CANTELAR, Ginés LIFANTE and Fernando CUSSÓ
Departamento de Física de Materiales, C-IV Universidad Autónoma de Madrid, 28049-Madrid, Spain

(Received April 24, 2000; accepted for publication May 9, 2000)

In this work, the formation of optical waveguides in periodically poled lithium niobate (PPLN) substrates by Zn-diffusion from vapour phase is studied. It has been found that the diffusion of the Zn ions is homogeneous in the PPLN substrates and the optical waveguides can be fabricated with the same parameters used in single-domain lithium niobate. The periodic ferroelectric domain pattern initially present in the substrate is preserved in the waveguides.

KEYWORDS: lithium niobate, PPLN, waveguide, Zn-diffusion, microdomain

1. Introduction

Periodically poled (PP) non-linear crystals offer the possibility of obtaining compact coherent light sources via optical frequency conversion by quasi-phase matching (QPM).[1,2] This procedure has been demonstrated using ferroelectric crystals such as $KTiOPO_4$ (KTP), LiB_3O_5 (LBO)[1,3] and particularly in $LiNbO_3$ (LN) thanks to the large effective non-linear coefficient of periodically poled lithium niobate (PPLN).[3]

Taking advantage of the high power density available in wave-guiding structures, several nonlinear waveguide devices have been recently reported,[4–7] in which the periodic modulation of the effective non-linear coefficient is combined with guided-wave geometries.

$LiNbO_3$ nonlinear waveguides incorporating periodic domains have been fabricated using different techniques,[8–12] but these studies have identified difficulties associated with domain switching caused by the waveguide fabrication process[4,13] at high temperatures.

An alternative method to fabricate $LiNbO_3$ waveguides at relatively low temperatures has been recently demonstrated.[14] In this technique, Zn ions from a vapour bath are exchanged and then diffused using temperatures (700–900°C) substantially lower than the Curie temperature and therefore offers the prospect of preserving periodically poled structures previously defined, with potential advantages in integrated optics technology.

In this work it is demonstrated: (i) the feasibility of fabrication of waveguides in periodically poled lithium niobate substrates by Zn diffusion, and (ii) the initial periodic ferroelectric domain pattern present in the substrate is preserved in the waveguides.

2. Experimental Results and Discussion

Figure 1 shows an optical microscopy image of the lithium niobate substrate used in this work. The substrate has been cut (z-cut) from a crystal boule grown in our laboratory by the Czochralski method using automatic diameter control system by weighing crucible system.[15]

The periodically poled pattern observed in the figure corresponds to an area of around $2 \times 2\,mm^2$ with a modulation period of 35 μm approximately. This periodic structure was induced during the crystal growth by using the appropriate growth conditions.[16] The ferroelectic domain pattern was revealed by etching using a diluted solution of $HF:HNO_3$ (1:2 by vol) at room temperature.[4] This is subsequently polished to a flat surface with optical quality and then the planar waveguide was fabricated by Zn diffusion from the vapour phase[17] at a temperature of 800°C.

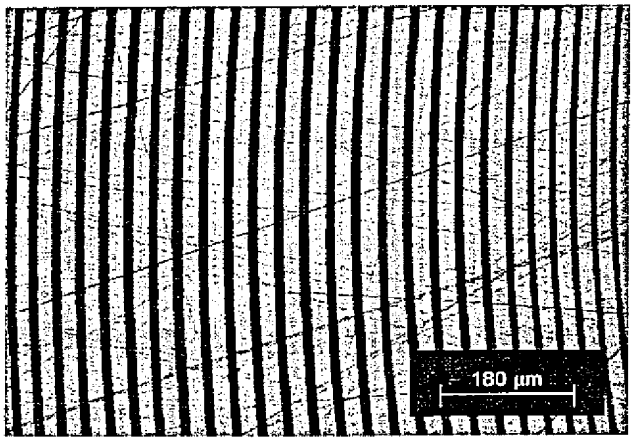

Fig. 1. Optical microscopy photograph showing the periodic ferroelectric domain pattern in a z-cut lithium niobate substrate.

After diffusion the sample surface appeared clean and free of damage, allowing the optical characterisation by the prism coupling technique.[17] This has been performed using a linearly polarised He-Ne laser ($\lambda = 632.8\,nm$) and a rutile prism. The assembly is mounted in a rotatory stage linked to a PC which allows the automatic determination of the sample reflectivity, with an angular resolution of 0.001°. This procedure gives a precision of 1×10^{-5} in the determination of the effective refractive indices of the modes.[17,18]

Figure 2 (continuous line) shows the reflectivity spectra of the waveguide taken at 632.8 nm after the Zn-diffusion process. As it can be observed, Zn-diffusion increases both the ordinary and extraordinary indices allowing TM and TE propagation (Figs. 2(a) and 2(b), respectively). The reflectivity curves indicate that the waveguide has a monomode character for both propagations, in accordance with previous results in single-domain LN substrates.[17] These results indicate that waveguide fabrication in PPLN is similar that in monodomain LN substrates.

After the initial optical characterisation stage, the waveguide has been carefully etched by immersion in a diluted $HF:HNO_3$ solution (1:2 by vol) at room temperature, and inspected regularly at short time intervals (15 min.) in order to stop the etching immediately that the domain structure was observed. It was found that after 4 hours the ferroelectric domain pattern is revealed sufficiently to identify the positive and negative domains.

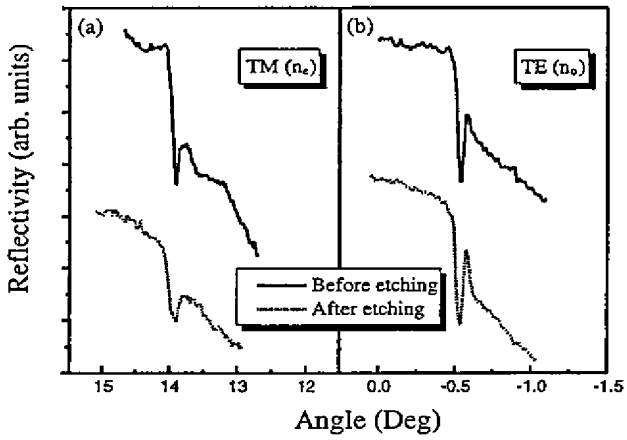

Fig. 2. Reflectivity spectra of the optical waveguide taken at 632.8 nm (HeNe laser) for: (a) TM and (b) TE propagation. Continuous and dotted lines represent the spectra before and after the etching process, respectively.

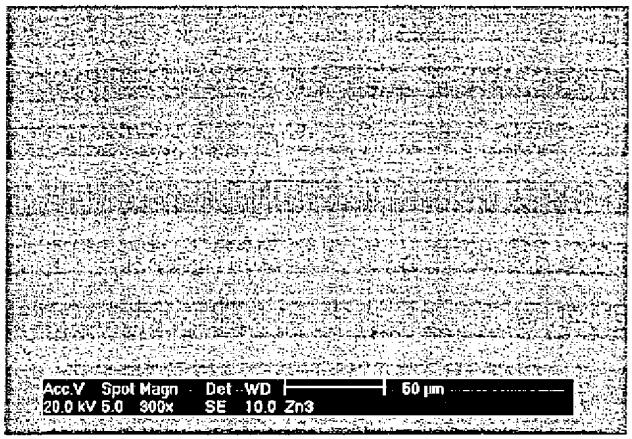

Fig. 3. SEM micrograph of the PPLN structure after waveguide formation by Zn-diffusion.

The waveguide was observed in a Scanning Electron Microscope (SEM) to asses the quality of the ferroelectric domain structures. Figure 3 shows a SEM micrograph corresponding to the Zn-diffused PPLN where it is possible to recognise the alternate ferroelectric domains, which have been preserved with no changes in comparison with the structure before waveguide preparation (Fig. 1).

Nevertheless, it would be necessary to confirm that this structure corresponds to the waveguide and that this has not been removed by the etching process (otherwise the observed PP structure could correspond to the underlying undiffused region). This fact is confirmed by two procedures: First, Energy Dispersive X-Ray Analysis (EDX) measurements have been performed after the etching process in order to confirm the presence of Zn ions. This analysis indicates a concentration of Zn ions close to 5.0 mol% related to Nb ions, which is similar to the concentration in the waveguide prior to etching. This concentration is the same in the positive and in the negative domains, indicating that the metal diffusion is homogeneous in the PPLN substrate.

Further information is obtained again by optical characterisation of the sample after the etching process. In fact the final confirmation of the waveguide presence after the etching process is obtained by coupling the light to the sample using again the prism coupling technique. Figure 2 (dotted line) shows the reflectivity spectra after the etching process. It can be observed that the waveguide remains practically similar than before the etching process, which confirms that the waveguide parameters (depth and index change) are the same than prior to the etching and therefore the observed periodic structure corresponds to the waveguide region.

So, in conclusion, it has been demonstrated that it is possible the fabrication of optical waveguides in PPLN substrates by Zn-diffusion from the vapour phase, using the same diffusion parameters than in mono-domain LN substrates. Zn ions are incorporated homegeneously to the positive and negative domains of the PP structure. The initial PP ferroelectric doimain pattern has been preserved in the waveguide by the Zn-diffusion process. These results are promissing for the fabrication of integrated OPO's and other frequency conversion devices based on lithium niobate.

Acknowledgement

Work partially supported by Dirección General de Enseñanza Superior del Ministerio de Educación y Cultura (PB97-0019) and Comunidad de Madrid (07T/0026/1998).

1) L. E. Myers and W. R. Bosenberg: IEEE J. Quantum Electron. 33 (1997) 1663.
2) F. Laurell: Opt. Mat. **11** (1999) 235.
3) V. Pruneri, S. Butterworth and D. C. Hanna: Appl. Phys. Lett. 69 (1996) 1029.
4) M. Houé and P. D. Townsend: J. Phys. D 28 (1995) 1747.
5) J. Webjörn, S. Siala, D. K. Nam, R. G. Waarts and R. J. Lang: IEEE J. Quantum Electron. 33 (1999) 1673.
6) M. Fujimura, A. Shiratsuki, T. Suhara and H. Nishihara: Jpn. J. Appl. Phys. 37 (1998) L659.
7) H. Ohta, S. Nogiwa, Y. Kawaguchi and Y. Endo: Jpn. J. Appl. Phys. **38** (1999) 5905.
8) M. H. Chou, I. Brener, K. Paeameswaran and M. M. Fejer: *Proc. 9th European Conf. Integrated Optics (ECIO'99), Torino, Italy, 1999*, p. 497.
9) D. Hofmann, G. Schreiber, C. Haase, H. Herrmann, R. Ricken and W. Sohler: *Proc. 9th European Conf. Integrated Optics (ECIO'99), Torino, Italy, 1999*, p. 505.
10) P. Baldi, L. Chanvillard, P. Aschieri, J. Pruvot, M. P. De Micheli and D. B. Ostrowsky: *Proc. 9th European Conf. Integrated Optics (ECIO'99), Torino, Italy, 1999*, p. 99.
11) J. Aimin, V. Pruneri, J. Webjn, P. St. J. Russell, D. C. Hanna and J. S. Wilkinson: Opt. Commun. 135 (1997) 41.
12) M. L. Bortz, M. A. Arbore and M. M. Fejer: Opt. Lett. 20 (1995) 49.
13) T. Nozawa and S. Miyazawa: Jpn. J. Appl. Phys. 35 (1996) 107.
14) W. M. Young, M. M. Fejer, M. J. F. Digonnet, A. F. Marshall and R. S. Feigelson: J. Lightwave Technol. 10 (1992) 1238.
15) E. Cantelar, J. A. Sanz-García and F. Cussó: J. Cryst. Growth 205 (1999) 196.
16) N. Ming, J. Hong and D. Feng: J. Mater. Sci. **17** (1982) 1663.
17) R. Nevado and G. Lifante: J. Opt. Soc. Am. A 16 (1999) 2574.
18) G. Lifante, E. Cantelar, J. A. Muñoz, R. Nevado, J. A. Sanz-García and F. Cussó: Opt. Mater. 13 (1999) 181.

phys. stat. sol. (a) 192, No. 1, 135–138 (2002)

Blue Light by SHG in Diode Pumped $LiNbO_3$ Waveguides

M. Domenech[1]), R. E. Di Paolo, G. Lifante, and F. Cussó

Departamento de Física de Materiales C-IV, Universidad Autónoma de Madrid, 28049, Madrid, Spain

(Received February 26, 2002; in revised form April 16, 2002; accepted April 20, 2002)

PACS: 42.65.Ky; 42.82.Et; 77.84.Dy

In this work, second harmonic generation (SHG) in nonlinear channel waveguides by quasi phase matching is reported. The photorefractive damage resistant waveguides were fabricated by Zn-diffusion technique using periodic poled lithium niobate wafers (PPLN). The SH wave, at 397.8 nm, was generated by using a CW diode laser with emission wavelength at 795.6 nm and 1 W peak power was used as fundamental wave. The nonlinear waveguides exhibit a stable conversion even at room temperature with no sign of deterioration induced by the optical damage.

Introduction Due to the large effective nonlinear coefficient of periodically poled lithium niobate (PPLN) this crystal provides an attractive route for the realisation of compact coherent light sources via optical frequency conversion by quasi-phase matching (QPM) [1, 2]. Combining the periodic modulation of the effective nonlinear coefficient with the high power density in wave-guiding structures, several nonlinear waveguide devices have been reported [4–7].

The method we have used to fabricate $LiNbO_3$ waveguides is a two-step Zn-diffusion [8]. This technique permits to use PPLN substrates in which the periodic modulation is induced during the crystal-growth process. It is also important to consider that Zn-diffusion from the vapour phase at low temperatures produces low-loss optical waveguides with high photorefractive damage resistance [9–10].

In this work SHG, at room temperature, in the blue spectral region has been detected for fundamental wave in the near-infrared range using a CW diode laser to investigate the optical frequency conversion by QPM in Zn-diffused $LiNbO_3$ waveguides.

Experimental Procedure Congruent lithium niobate crystals ([Li]/[Nb] = 0.945) periodically structured were grown along the x-axis by the Czochralski method with automatic diameter control by weighting the crucible. This technique allows to induce the formation of periodic domain structures during the crystal growth using the appropriate growth conditions as reported elsewhere [11].

The crystal boule was X-ray orientated and then wafers with the selected crystal orientation were cut. These wafers were polished to a flat surface with optical quality prior to perform the channel waveguide fabrication.

Ultraviolet photolitographic techniques, adapted from microelectronic technology, have been used to define the channels in which the metal diffusion takes place [12]. Once the channels are defined, the waveguides were fabricated by a two-step Zn diffu-

[1]) Corresponding author; Tel.: +34 91 397 52 86; Fax: +34 91 397 85 79; e-mail: manuela.domenech@uam.es

 0031-8965/02/19207-0135 $ 17.50+.50/0

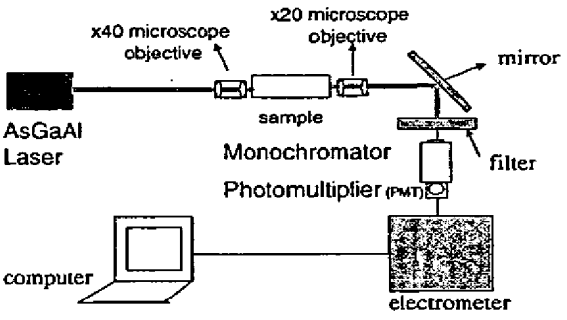

Fig. 1. Experimental setup to obtain the second harmonic generation

sion technique [8]. In the first step the sample was placed in a Zn atmosphere, with pressure controlled by an Ar buffer, and heated during 2 h at 550 °C. As a consequence of this process a Zn-rich layer is formed in the surface of the sample. In the second step, this layer is diffused by annealing the sample in open air during 4 h at 850 °C. This method produces low-loss optical waveguides preserving the periodic structures induced during the crystal growth [12].

In order to obtain the second harmonic signal the following experimental setup (Fig. 1) was arranged. A pig-tailed AlGaAs CW diode laser, with emission peaking at 795.6 nm, was coupled to the channel waveguides by using a 40× microscope objective. The output light from the waveguide was collected using a 20× microscope objective and directed to the entrance slit of a monochromator (ARC SpectraPro 500-I) where both signals, excitation and SHG, were discriminated and recorded by online computer-controlled detection system using an EMI-9558QB photomultiplier tube. To avoid contamination of the SHG signal from the intense laser excitation a cut filter (LS-450-S-1075-CORION) was placed just in front of the monochromator slit.

Results and Discussion Figure 2 shows an image of the waveguides by reflective light optical microscopy. Two different waveguides, 10 and 20 μm wide, can be observed. The microscope has been focused onto the crystal surface in order to show the periodic

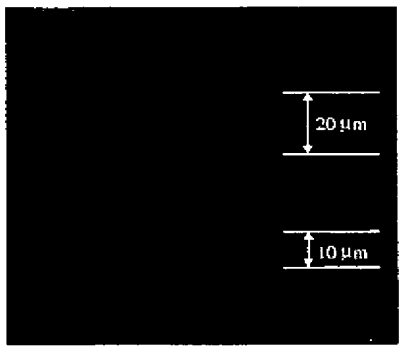

Fig. 2

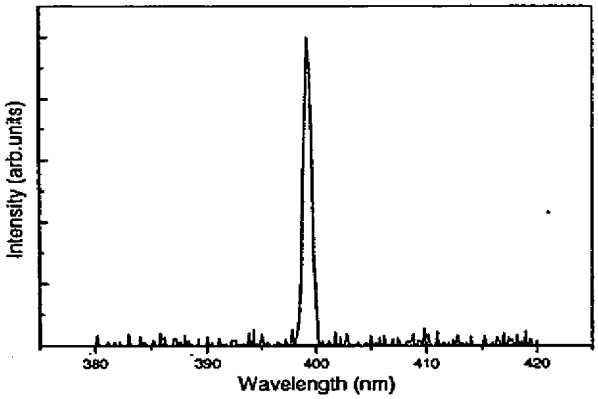

Fig. 3

Fig. 2. Image of a PPLN crystal observed by an optical microscope with reflective light

Fig. 3. Blue emission band corresponding to the SH wave generated in the Zn-diffused nonlinear waveguides for a fundamental wave centered at 795.6 nm

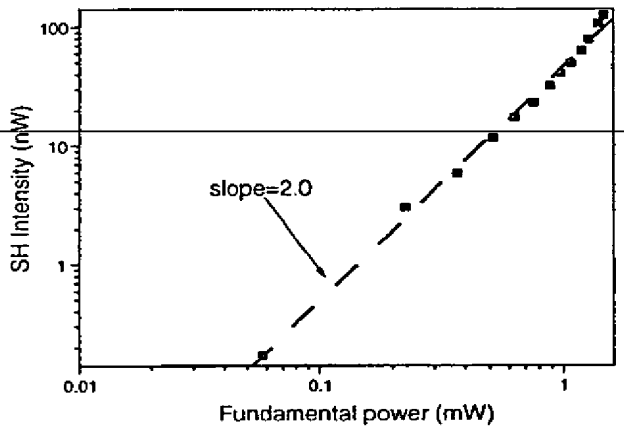

Fig. 4 (online colour). Quadratic dependence of the SH intensity versus the power of the fundamental beam

domains perpendicular to the channel waveguides, whose walls appear then diffused/unfocused. The periodicity of the domains is 5 μm, which corresponds to a high efficiency of the SHG at a wavelength $\lambda = 397.8$ nm [13].

In Fig. 3 the second harmonic signal can be observed. The emission of the blue light has been associated to TM → TE conversion by QPM, in accordance with the phase-matching condition [13] taking into account the periodicity of the substrates. The fundamental wave was polarised along the ordinary direction, in order to produce an interaction with the d_{32} coefficient, giving a strong polarised character along the extraordinary direction for the second harmonic wave.

Figure 4 shows the dependence of the blue light intensity on that of the fundamental beam. The least square fitting shows that it follows a quadratic dependence, as expected for the nonlinear conversion mechanism.

For a coupled pump power of 1.28 mW, which corresponds to a value slightly lower than the maximum coupled power attained within the waveguide, the power obtained in the blue was 78 nW representing a conversion efficiency of $\sim 10^{-4}$. This value is similar to that previously reported for Ti-diffused $LiNbO_3$ waveguides [3], and lower than theoretical estimations, which could be attributed to a non-uniform periodicity of the domain that implies that the effective interaction length is reduced [13].

At variance with Ti-diffused waveguides [3] the infrared to blue light conversion obtained in this work using Zn-diffused waveguides, was operated at room temperature with a stable output and no sign of deterioration in the SHG. Also, as it has been already mentioned, the power dependence was quadratic during the whole range of excitation power used in these experiments, and no sign of photorefractive damage. These results confirm the potential advantages of the fabrication of channel waveguides by Zn diffusion, although the efficiency should be increased by improving homogeneity and a matching period of the domains.

Conclusions It has been demonstrated that the periodic structures induced during the crystal growth in $LiNbO_3$ allow SHG under AlGaAs pumping at $\lambda = 795.6$ nm, using Zn-diffused channel waveguides. These experimental results prove that the nonlinear characteristics are preserved by Zn diffusion and simultaneously the photorefractive damage is reduced.

References

[1] L. E. Myers and R. Bosenberg, IEEE J. Quantum Electron. **33**, 1663 (1997).
[2] F. Laurell, Opt. Mater. **11**, 235 (1999).
[3] J. Amin, V. Pruneri, J. Webjorn, P. S. J. Russell, D. C. Hanna, and J. S. Wilkinson, Opt. Commun. **135**, 41 (1997).
[4] P. Baldi, L. Chanvillard, P. Aschieri, J. Pruvot, M. P. De Micheli, and D. B. Ostrowsky, Proc. 9th Europ. Conf. Integr. Opt. (ECIO '99), Torino, Italy 1999 (p. 99).
[5] G. Schreiber, H. Suche, Y. L. Lee, W. Grundkötter, V. Quiring, R. Ricken, and W. Sohler, Proc. 10th Europ. Conf. Integr. Opt. (ECIO '01), Paderborn, Germany, April 4–6 2001 (p. 209).
[6] I. Cristiani, C. Liberale, V. Degiorgio, G. Tartarini, and P. Bassi, Proc. 10th Europ. Conf. Integr. Opt. (ECIO '01), Paderborn, Germany, April 4–6, 2001 (p. 213).
[7] Yu. Avestisyan, Y. Sasaki, and H. Ito, Proc. 10th Europ. Conf. Integr. Opt. (ECIO '01), Paderborn, Germany, April 4–6, 2001 (p. 217).
[8] R. Nevado and G. Lifante, J. Opt. Soc. Am. **16**, 2574 (1999).
[9] R. Nevado, E. Cantelar, G. Lifante, and F. Cussó, Jpn. J. Appl. Phys. **39**, L489 (2000).
[10] R. E. Di Paolo, E. Cantelar, R. Nevado, J. A. Sanz-García, M. Domenech, P. L. Pernas, G. Lifante, and F. Cussó, Ferroelectrics, in press.
[11] E. Cantelar, J. A. Sanz-García, and F. Cussó, J. Cryst. Growth **205**, 196 (1999).
[12] P. L. Pernas, M. J. Hernández, E. Ruíz, E. Cantelar, R. Nevado, C. Morant, G. Lifante, and F. Cussó, Appl. Surf. Sci. **161**, 123 (2000).
[13] E. Cantelar, R. E. Di Paolo, J. A. Sanz-García, P. L. Pernas, R. Nevado, G. Lifante, and F. Cussó, Appl. Phys. B **73**, 515 (2001).

Appl. Phys. B 73, 515–517 (2001)
DOI: 10.1007/s003400100716

Applied Physics B
Lasers and Optics

E. CANTELAR[1]
R.E. DI PAOLO[1,2]
J.A. SANZ-GARCÍA[1]
P.L. PERNAS[3]
R. NEVADO[1]
G. LIFANTE[1,✉]
F. CUSSÓ[1]

Second-harmonic generation in Zn-diffused periodically poled $LiNbO_3$ channel waveguides

[1] Departamento de Física de Materiales, C-IV, Universidad Autónoma de Madrid, 28 049 Madrid, Spain
[2] Centro de Investigaciones Ópticas (CIOp), Casilla de Correo 124, 1900 La Plata, Argentina
[3] Departamento de Física Aplicada, C-XII, Universidad Autónoma de Madrid, 28 049 Madrid, Spain

Received: 16 May 2001/Revised version: 7 September 2001
Published online: 30 October 2001 •

ABSTRACT In this work second-harmonic generation by quasi-phase matching (QPM) in Zn-diffused periodically poled lithium niobate channel waveguides is presented. A stable TM→TE conversion by QPM has been found. The results are in good accordance with theoretical estimations obtained by the phase-matching condition, either for the polarisation character of the second-harmonic wave as well as for the spectral range, taking into account the periodicity of the domains.

PACS 42.82.-m; 42.65.Ky; 77.84.-s

1 Introduction

Optical frequency conversion by quasi-phase matching (QPM) has been demonstrated using different ferroelectric crystals [1–3]. Particularly interesting is lithium niobate ($LiNbO_3$) due to the large effective non-linear coefficients of periodically poled lithium niobate (PPLN) [1]. Several non-linear devices based on this material, in which the periodic modulation is combined with the high power densities available in waveguiding structures, have been reported [4–7].

The potential advantages of Zn diffusion have been previously reported [8, 9] as a fabrication technique to obtain $LiNbO_3$ waveguides. It has also been recently reported that Zn diffusion from the vapour phase at low temperatures produces low-loss waveguides in this material, and preserves the initial domain pattern of the substrate [10, 11]. Therefore, with this technique it is possible to use PPLN substrates in which the periodic modulation is induced during the crystal-growth process.

In this work the non-linear character of Zn-diffused periodically poled $LiNbO_3$ channel waveguides is explored. A CW Ti:sapphire laser has been used to investigate the optical frequency conversion by QPM. Second-harmonic generation (SHG), at room temperature, in the blue spectral region has been detected for fundamental waves in the near-infrared range. A good accordance between experimental data and theoretical estimations has been found.

✉ Fax: +34-91/397-8579, E-mail: gines.lifante@uam.es

2 Experimental procedure

Periodically poled lithium niobate crystals have been grown along the x-axis in an air atmosphere with automatic diameter control by a crucible weighing system [12]. The initial melts, containing the congruent $LiNbO_3$ ([Li]/[Nb] = 0.945), have been doped with erbium and ytterbium oxides with a purity grade of 99.99%. The concentration of both dopants in the initial melts was 0.5 mol%. This technique allows us to induce the formation of periodic domain structures during the crystal growth by using the appropriate growth conditions [13–15].

After cutting and polishing to optical grade, the ferroelectric domain pattern of a Y-cut substrate from one of the PPLN crystals has been revealed by chemical etching in a diluted solution of $HF:HNO_3$ (1:2 by volume) at room temperature for 1 h. Scanning electron microscope (SEM) measurements have been done to characterise the ferroelectric domains.

The wafer was again polished to a flat surface with optical quality in order to perform the channel-waveguide fabrication. Ultraviolet photolithographic techniques, adapted from microelectronic technology, have been used to define the channels in which the metal diffusion takes place [16]. The Zn diffusion was performed following the two-step procedure reported in [10]. In the first step the sample was placed in a Zn atmosphere at 550 °C for 2 h, and a second step of diffusion at 850 °C for 4 h was selected in order to produce low-loss waveguides.

A CW Ti:sapphire laser, with a tunability range from 720 nm to 870 nm, was used to perform the characterisation of the SHG in the Zn-diffused PPLN channel waveguides. The intensity of the second-harmonic wave was detected by using an EMI-9558QB photomultiplier tube.

3 Results and discussion

The ferroelectric domain pattern of the substrate was revealed by chemical etching and then analysed by using a scanning electron microscope. The SEM measurements confirm that different periodically poled (PP) regions, about 1 mm in length and of different periods, were generated during the crystal-growth process. Figure 1a and b show the micrographs corresponding to two regions with periods of 5 μm and 10 μm respectively. Although there are different

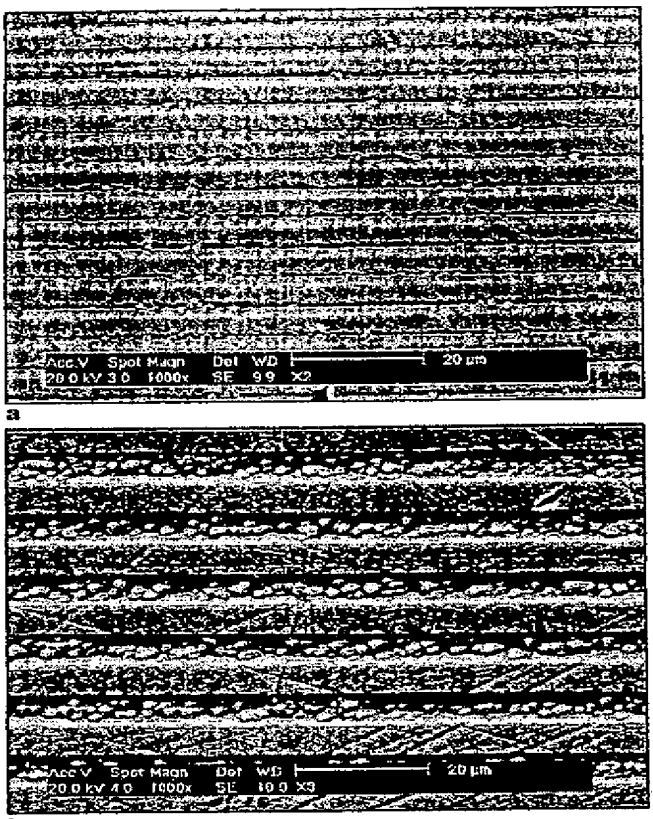

a

b

FIGURE 1 SEM micrographs of PP regions with a 5-µm and b 10-µm periods

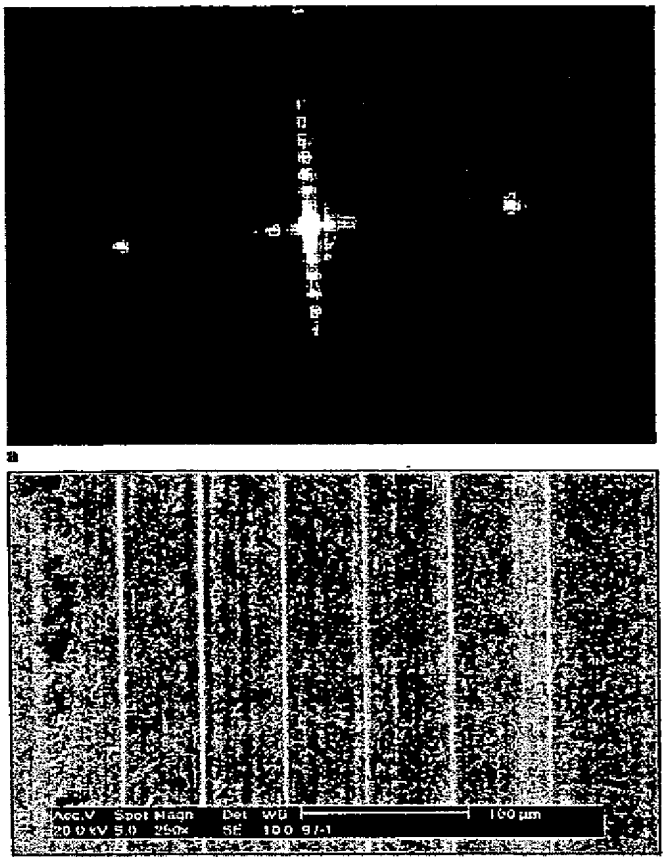

a

b

FIGURE 2 a Diffraction pattern at 632.8 nm showing the perpendicularity achieved between the channels in the SiO_2 stopping mask and the PP domains; *vertical* and *horizontal patterns* respectively. b SEM micrograph of Zn-diffused waveguides (1-, 2-, 4-, 6-, 10-and 20-µm widths)

regions with periods ranging from 5 µm to 16 µm, most of these periodically poled regions have a period value around 6–8 µm.

The initial stage in the fabrication of the channel waveguides is the definition of the mask that stops the Zn diffusion. The motifs of a Cr_2O_3 commercial mask have been transferred to a SiO_2 film, previously deposited over the substrate, by UV photolithographic techniques [16].

The perpendicularity between the channels in the SiO_2 stopping mask and the PP domains in the $LiNbO_3$ substrate has been checked, prior to the Zn diffusion, by diffraction techniques. A helium–neon laser (632.8 nm) was used to illuminate the sample surface that contains the channels; Fig. 2a shows one of the diffraction patterns obtained. The diffraction in the vertical line corresponds to the periodic series of channels in the SiO_2 film, while the pattern in the horizontal line is induced by the presence of a periodic modulation in the ferroelectric domains, showing that a good perpendicularity between channels and PP domains has been achieved.

In Fig. 2b a SEM micrograph of the Zn-diffused channels (with dimensions 1-cm long and 1-, 2-, 4-, 6-, 10-and 20-µm wide), before removing the SiO_2 stopping mask, is presented. The channel waveguides are parallel to the x-axis (the c-axis perpendicular to the channels).

The non-linear character of the Zn-diffused channel waveguides has been explored in continuous-wave mode at room temperature by using a CW Ti:sapphire laser. The fundamental wave (ω), polarised along the ordinary direction (in order to produce an interaction with the d_{32} coefficient), was coupled into the waveguides by using a microscope objective. A second objective, at the other end, was used to collect the second-harmonic wave (2ω). A strong polarised character (higher than 90%) has been found along the extraordinary direction for the 2ω wave, indicating that the QPM involves a TM→TE conversion.

Figure 3 shows the phase-matching curve for the TM→TE conversion measured in the 2-µm channel waveguide with 1-cm length (containing non-uniform PP regions, as has been mentioned previously). As can be seen, the phase-matching condition is satisfied for fundamental wavelengths higher than 770 nm, the 2ω wave having its maximum intensity for excitation at around 822 nm. The inset in this figure shows the expected quadratic dependence of the SH intensity on the intensity of the fundamental wave.

Figure 4 shows the calculated relationship between the ferroelectric domain period (Λ) and the fundamental wavelength

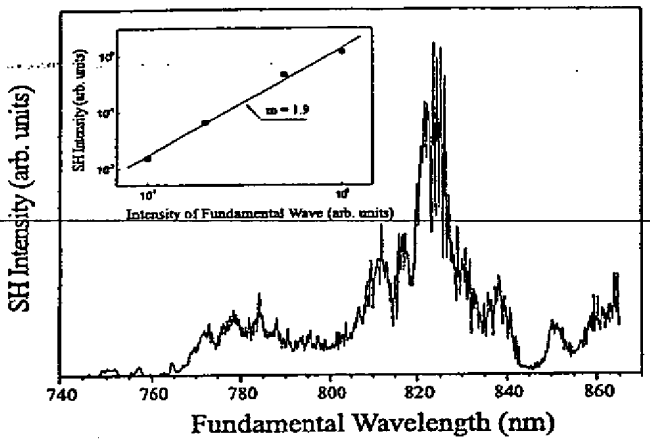

FIGURE 3 Phase-matching curve at room temperature measured in the 2-μm channel waveguide. The *inset* shows the dependence of the SH wave on the intensity of the fundamental wave

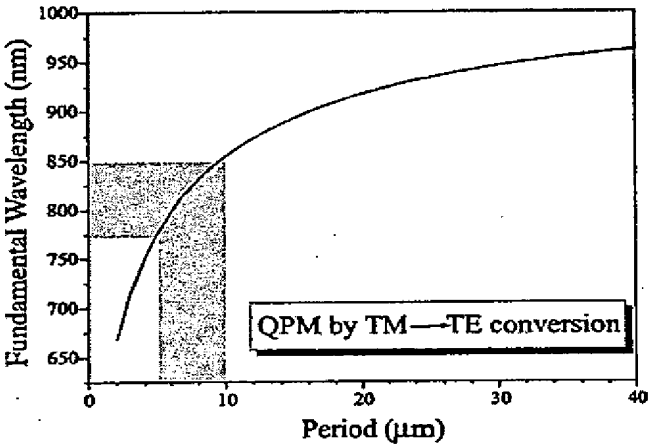

FIGURE 4 Calculated relationship, in the case of QPM by TM→TE conversion, between the ferroelectric domain period and the fundamental wavelength

(λ_ω) at first order for QPM by TM→TE conversion, which is given by [3]:

$$\Lambda = \frac{\lambda_\omega}{2\,[n_e(2\omega) - n_o(\omega)]} \qquad (1)$$

where $n_o(\omega)$ and $n_e(2\omega)$ are the ordinary and extraordinary refractive indices at the corresponding wavelengths.

This theoretical calculation proves that by taking into account the different periods in the ferroelectric pattern of the substrate, which has been indicated in Fig. 4 by a shadowed region, it should be possible to obtain SHG for a wide range of fundamental wavelengths. The QPM relationship is satisfied from 770 nm to 850 nm, being in perfect agreement with the experimental phase-matching curve. The maximum conversion in the generation of blue light is reached for fundamental wavelengths close to 820 nm. From (1), it can be deduced that the periods needed for this conversion should be close to 7 μm. This value is also in good accordance with the initial SEM analysis of the substrate (mentioned above), which reveals the dominant period value (around 6–8 μm) in the periodically poled regions.

Preliminary measurements related to the photorefractive damage indicate that, at the incident power level used in these experiments (around 0.1 W), the fundamental mode pattern and the SH intensity remain stable, although a quantitative estimation of the optical damage threshold has not been obtained. Detailed evaluation of this figure is currently in progress.

4 Conclusions

The feasibility of Zn diffusion from the vapour phase to produce non-linear waveguides in lithium niobate has been demonstrated. Optical frequency conversion by quasi-phase matching has been obtained in Zn-diffused $LiNbO_3$ channel waveguides via TM→TE conversion. The SH wave exhibits a broad phase-matching curve in consequence of variations in the period associated with the PP ferroelectric domains.

Further investigations in order to precisely control the domain period during crystal growth are needed in order to obtain a higher efficiency in blue-light generation.

ACKNOWLEDGEMENTS This work was partially supported by DGES (PB97-0019) and Comunidad de Madrid (07T/0026/1998). R.E. Di Paolo is supported by a grant from Ministerio de Educación y Cultura (Spain).

REFERENCES

1 M. Houé, P.D. Townsend: J. Phys. D **28**, 1747 (1995)
2 L.E. Myers, W.R. Bosenberg: IEEE J. Quantum Electron. QE-33, 1663 (1997)
3 F. Laurell: Opt. Mater. **11**, 235 (1999)
4 J. Amin, V. Pruneri, J. Webjorn, P.St.J. Russell, D.C. Hanna, J.S. Wilkinson: Opt. Commun. **135**, 41 (1997)
5 P. Baldi, L. Chanvillard, P. Aschieri, J. Pruvot, M.P. De Micheli, D.B. Ostrowsky: Proc. 9th Eur. Conf. Integr. Opt. (ECIO'99), Torino, Italy (1999) p. 99
6 M.H. Chou, I. Brener, K. Paeameswaran, M.M. Fejer: Proc. 9th Eur. Conf. Integr. Opt. (ECIO'99), Torino, Italy (1999) p. 497
7 D. Hofmann, G. Schreiber, C. Haase, H. Hermann, R. Ricken, W. Sohler: Proc. 9th Eur. Conf. Integr. Opt. (ECIO'99), Torino, Italy (1999) p. 505
8 W.M. Young, M.M. Fejer, M.J.F. Digonnet, A.F. Marshall, R.S. Feigelson: J. Lightwave Technol. **10**, 1238 (1992)
9 C. Huang, L. MacCaughan: IEEE Photon. Technol. Lett. **9**, 599 (1997)
10 R. Nevado, G. Lifante: J. Opt. Soc. Am. A **16**, 2574 (1999)
11 R. Nevado, E. Cantelar, G. Lifante, F. Cussó: Jpn. J. Appl. Phys. **39**, L489 (2000)
12 E. Cantelar, J.A. Sanz-García, F. Cussó: J. Cryst. Growth **205**, 196 (1999)
13 N. Ming, J. Hong, D. Feng: J. Mater. Sci. **17**, 1663 (1982)
14 V. Bermúdez, M.D. Serrano, P.S. Dutta, E. Diéguez: Solid State Commun. **109**, 605 (1999)
15 D. Callejo, V. Bermúdez, E. Diéguez: J. Phys.: Condens. Matter **13**, 1337 (2001)
16 P.L. Pernas, M.J. Hernández, E. Ruíz, E. Cantelar, R. Nevado, C. Morant, G. Lifante, F. Cussó: Appl. Surf. Sci. **161**, 123 (2000)

November 1998

ELSEVIER

Materials Letters 37 (1998) 246–254

MATERIALS LETTERS

Microstructuring of lithium niobate using differential etch-rate between inverted and non-inverted ferroelectric domains

Ian E. Barry [a,*], Graeme W. Ross [a], Peter G.R. Smith [a], Robert W. Eason [a], Gary Cook [b]

[a] *Optoelectronics Research Centre, University of Southampton, Southampton SO17 1BJ, UK*
[b] *Defence Evaluation Research Agency, Malvern, WR14 3PS, UK*

Received 5 January 1998; revised 30 April 1998; accepted 30 April 1998

Abstract

Single crystal samples of lithium niobate have been spatially patterned with photoresist, and subsequently domain inverted using electric field poling, to produce a range of two dimensional spatial domain structures. Differential etching has subsequently been carried out using mixtures of hydrofluoric and nitric acids, at a range of temperatures between room temperature and the boiling point. The structures produced show very smooth, well defined, deep features, which have a range of applications in optical ridge waveguides, alignment structures, V-grooves, and micro-tips. Details are given of the fabrication procedures, and examples of structures are shown.

Keywords: Lithium niobate; Differential etching; Ferroelectric domains

1. Introduction

Lithium niobate is a material of considerable interest to the optical, laser and communications industry, due to the large values of nonlinear optical, electro-optic, piezoelectric and acousto-optical coefficients and figures of merit that are available [1]. Current uses span the laser area, where fabrication of periodically poled material has achieved record efficiencies in quasi-phased matched nonlinear interactions [2], to the microwave communications sector for use in surface acoustic wave delay lines and filters [3]. In the telecommunications field, it is widely used for integrated optical modulators where switching rates of 10 GHz and above are currently required for wavelength division multiplexed fibre optical networks. Finally, although regarded as a problem in many areas, it continues to maintain interest in the photorefractive community for optical storage, holographic and phase conjugate applications.

A number of techniques have been reported for machining and microstructuring in lithium niobate. These include reactive ion etching (RIE) [4], reactive ion beam etching (RIBE) [5], laser ablation, both above and below bandgap [6], and laser assisted chemical etching using chlorine [7] and KF [8]. Wet etching has also been used for many years to reveal domain and defect structures in lithium niobate [9], but not so far to our knowledge for intentionally producing ordered microstructures subsequent to lithographically defined, spatially patterned, domain inversion. Such microstructuring has obvious appli-

* Corresponding author.

00167-577X/98/$ - see front matter
PII: S0167-577X(98)00100-1

cations for the fields of optics and optoelectronics: the ability to spatially define very smooth and precise structures for lateral guidance (waveguides), and multiple arrays (photonic bandgap devices) will have immediate impact.

The most common wet etchant reported has been a mixture of hydrofluoric (HF) and nitric acids (HNO_3), which attacks the negative z face ($-z$) at a rate that is appreciably higher than the positive z face ($+z$). Additionally, defect sites in the crystal lattice may also experience higher etching rates. This last property has been utilised recently to produce ridge waveguides for improved electrical-to-optical coupling in integrated optical interferometer devices [10]. Many such techniques require the use of a prior lithographic spatial defining step, which has implications in the ultimate quality of structures obtainable due to mask fabrication limitations. In our technique, although domain inversion still requires a lithographic procedure, involving photoresist inhibition of the electric field required for domain inversion, the latter process is inherently a manipulation of the crystal local structure at the atomic, or unit cell level. Subsequent differential etching can therefore produce structures that reflect this level of perfection, and extremely smooth features are therefore generic to this technique.

We report here the combination of spatially selective poling of lithium niobate, and subsequent differential etching, to produce structures up to 150 μm deep with very smooth walls, as imaged using scanning electron microscopy. The results obtained suggest that this technique may be very suitable for production of high quality ridge waveguides, V-grooves and other alignment aids, electro-optically active tips for atomic force microscopy applications, and arrays of highly uniform holes, for filtration and sensing purposes, and columns for photonic band gap structures.

2. Materials and methods

The samples of lithium niobate had dimensions of 15 mm × 15 mm and were either 300 or 500 μm thick. All material was supplied by Koto Electric (Japan) in the form of z cut, 76 mm diameter wafers, which were cut to size in house. The $-z$ face was marked to show the y direction. (Nomenclature of the coordinate system is as described in Ref. [11]). All samples were subjected to a sequential multiple solvent cleaning process using ultrasonic agitation at 50°C. The samples were then dried with compressed air. Photoresist was spin coated onto the $-z$ face, producing a 1.1 μm thick film. The samples were finally baked at 90°C for 30 min.

The photoresist was patterned using a Karl Suss MA4 mask aligner and chrome on quartz masks. The patterns used to measure the temperature dependant etch rate consisted of gratings with periods between 3 and 27 μm, channels of width between 3 and 14 μm, and arrays of square, triangular and round points with feature sizes of 5, 10 and 20 μm. The channels and gratings were aligned with their grating vector parallel with the crystallographic x direction,

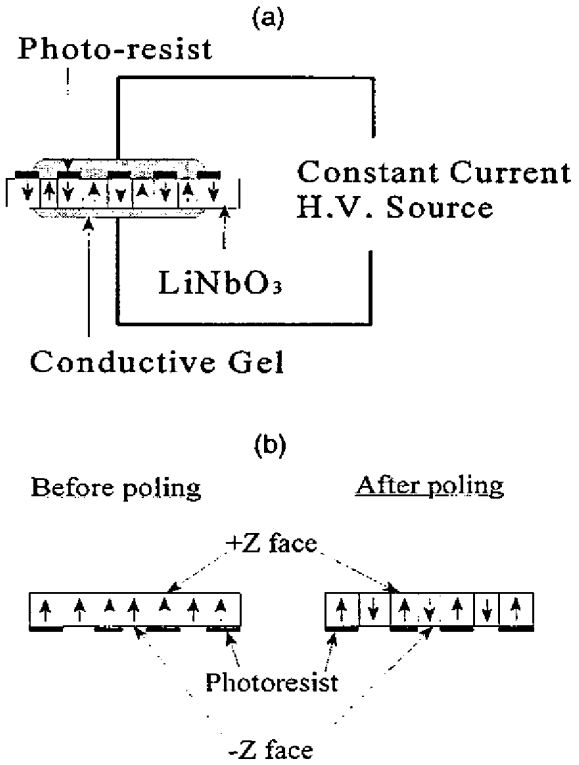

Fig. 1. (a) Schematic of the poling apparatus used. (b) Schematic of domain structure within the $LiNbO_3$ sample before and after poling.

and features parallel with the y direction. Other test patterns used were 200 μm diameter circles, randomly orientated lines of 100 μm width, and gratings with periods between 5 and 18 μm. These latter structures were etched only at room temperature. Once exposed the resist was developed for 50 s, washed in de-ionized water for 60 s and dried using dry compressed air.

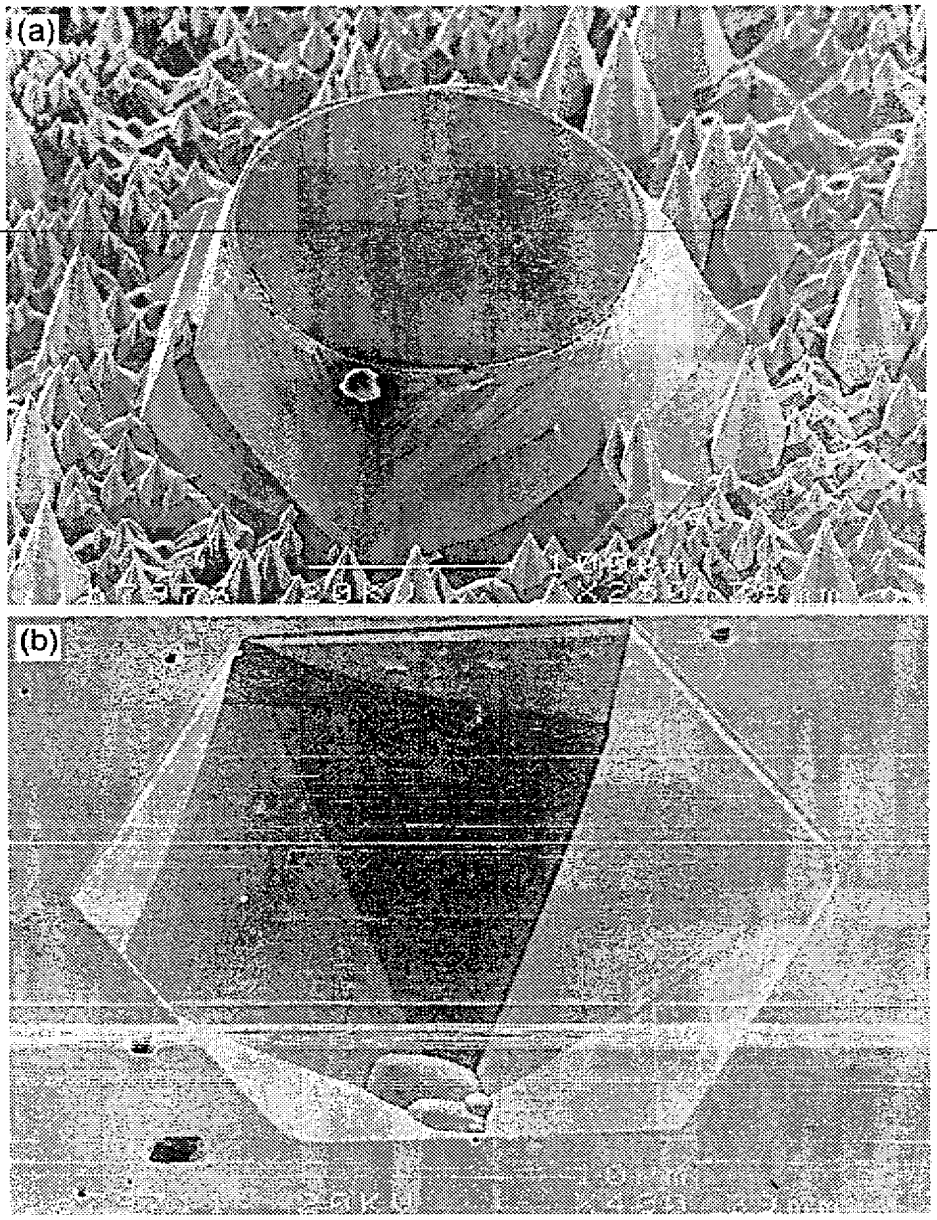

Fig. 2. (a) Circular feature patterned on the $-z$ face, after poling and etching. (b) Complementary structure produced on the opposite face after poling and etching.

The samples were poled by applying an external electric field of 22.5 kV/mm. Fig. 1a is a schematic of the apparatus used. Poling current was monitored, and controlled by varying the applied field. The expected displacement current, and hence total charge, was calculated in advance, and the poling process was terminated once the required degree of poling had been achieved. Liquid electrodes were used to ensure good electrical contact with the sample. After poling all samples were again cleaned using acetone and water.

The etchant consisted of HF and HNO_3 acids in a 1:2 ratio, where the HF was a 48% solution and the nitric acid was a 78% solution. The etchant was stirred constantly using a magnetic stirrer with an integral hotplate. The temperature of the hotplate was kept constant and the etchant allowed to reach equilibrium temperature before initiating the etch process. The etching time varied between 15 and 17 h for all samples. The etch depth was measured using a Tencor Alphastep profileometer. Additionally a JEOL JSM 6400 Scanning Electron Microscope (SEM) was used for visual inspection of the structures produced. Some samples were also set in low viscosity resin and then cut and polished in a plane normal to the z face to allow measurement of the etch depth from the SEM pictures obtained.

3. Results and discussion

Before poling, the lithium niobate wafers were all oriented single domain samples. After poling, samples had areas of induced domain reversal, as is illustrated schematically in Fig. 1b. Examination of the resultant etched structures revealed that opposing crystal z faces displayed quite different topology. The features on the photoresist patterned $-z$ face appear to faithfully replicate the areas of induced domain inversion. The features on the opposing z face (the $+z$ face), however, show some evidence of domain spreading, as revealed by the subsequent etching procedure. The underlying crystal $3m$ symmetry leads to features with characteristic triangular, and hexagonal shapes, and, as seen in the example of Fig. 2, an initially circular photoresist pattern will produce an equivalent circular etched structure on

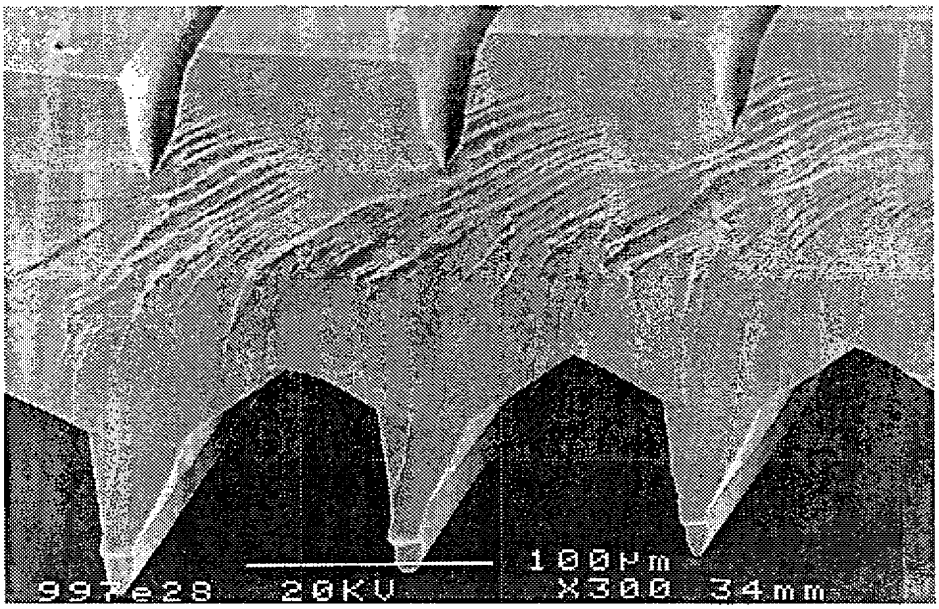

Fig. 3. Simultaneous view of both faces ($+z$ and $-z$), and different etch results. The edge of the sample appears rough, as this has been snapped prior to SEM viewing.

the $-z$ face, but a hexagonal structure on the etched $+z$ face.

Fig. 3 also shows such complementary structures, and illustrates the extent to which the etch process can be utilised to construct alignment aids, such as 'V'-grooves. It should be noted that the exact profile is not that of a 'V' in this case, but rather a tapered 'V'. The reasons for this exact structure are currently under further investigation, and are being studied as a function of both etchant concentrations and temperature. Under some conditions, very small (~ 100 nm) holes appear around features revealed on the $-z$ face. These are illustrated in Fig. 4, and are also under active study for possible uses in filtering, sieving, etc., but with the additional benefit of being in an *active* optical material. We are currently considering the modifications that can be expected in the nonlinear and electro-optic response of lithium niobate, by the inclusion of nanoscale particles of metals, or dielectrics. As a general observation, all structures produced via etching, and revealed on the $-z$ face display smooth walls, and vertical features. Under SEM examination, the smoothness persists at the highest resolution available with our SEM (~ 5 nm). The implication here is that crystal planes are being revealed via this technique and we are currently measuring individual facet orientations. Further studies will involve X-ray diffraction and topography analysis.

As etching proceeds, the facets produced appear to result in self-termination, or a much reduced rate of etching. This is of most use when alignment grooves are required, and an example of this is shown in Fig. 5. The facetting does not occur at the same depth in all cases however, and in Fig. 6 we show an example of a deep vertical walled ridge, suitable for waveguide applications, in which the etch has proceeded to a depth of ~ 20 μm, without any facets appearing. This behaviour is critical to the use of this technique for fabricating high aspect ratio structures. Finally we note the appearance of most of the etched samples so far in the near surface region. It is known that the domain inversion process is influenced by defects, and such structures as subsurface polishing damage. The first few micrometers of all etched samples shows a 'banded' appearance, the detailed structure of which may vary slightly, but which appears to be common to all etched samples.

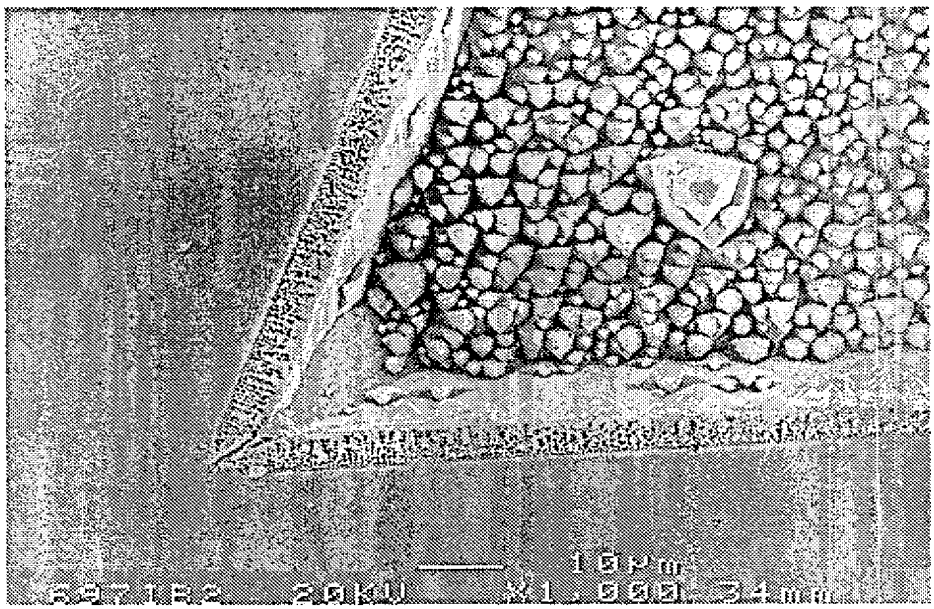

Fig. 4. Holes produced around edges of etched domain walls.

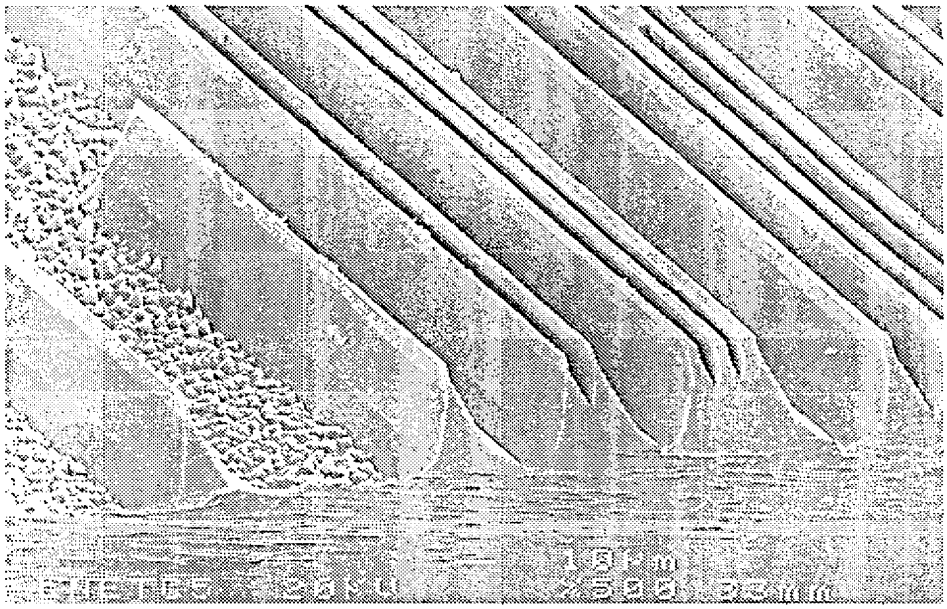

Fig. 5. Etched structure showing smooth walls, and V-groove features.

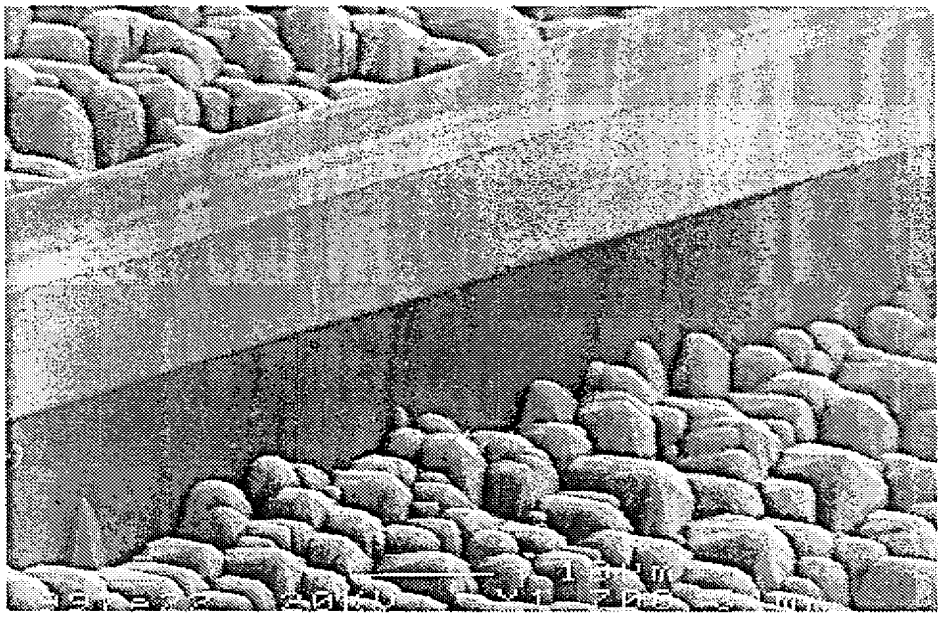

Fig. 6. Example of ridge structure suitable for waveguide applications. Note the smooth side-walls produced and clear evidence of surface 'banded' appearance.

Fig. 6 shows this particularly clearly. The surface smoothness seems unaffected however, and we are further investigating the origin of the contrast observed. A final example of the precision that can be achieved by this method is shown in Fig. 7. An isolated tip has been produced which may well prove useful in scanning microscopy applications, such as near field imaging.

Fig. 8 shows the results of etch rate obtained as a function of etch temperature. The mechanism by which etching proceeds faster at elevated temperatures can be considered from two perspectives. Firstly, such etching processes are expected to follow the normal Arrhenius law, (rate proportional to $A\exp[-E_a/RT]$), which would yield an exponential increase in etch rate. Secondly, however, there is another factor which might influence temperature dependent etch rates. Poling acts to displace both Li^+ and Nb^+ ions relative to the oxygen ions in the lattice. As this displacement is the key indicator of domain polarity, the exact positions of these ions must play an extremely important role in subsequent differential etch rates. Increased temperature will alter the metal ion positions within the lattice, and hence may well influence etch rate. Fig. 8 shows an

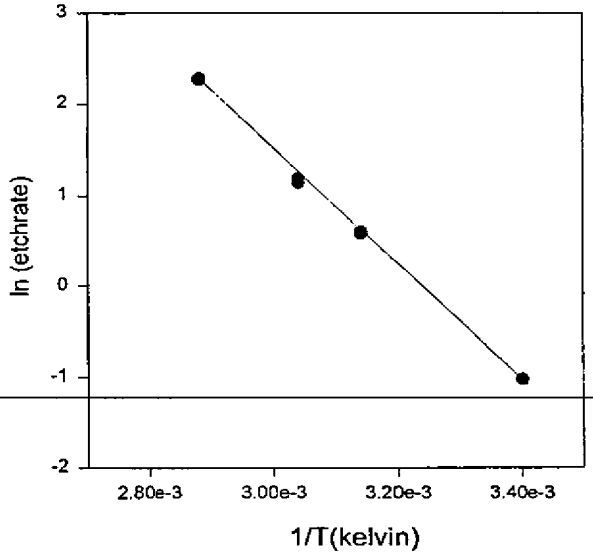

Fig. 8. Arrhenius plot showing natural log of etch-rate (measured in μm per hour), vs. 1/absolute temperature. The straight line fit shows no departure from the normal $\exp(E_a/RT)$ behaviour.

Arrhenius plot of ln (etch-rate), measured in μm per hour, vs. 1/absolute temperature, from which the linear gradient indicates no obvious departure from

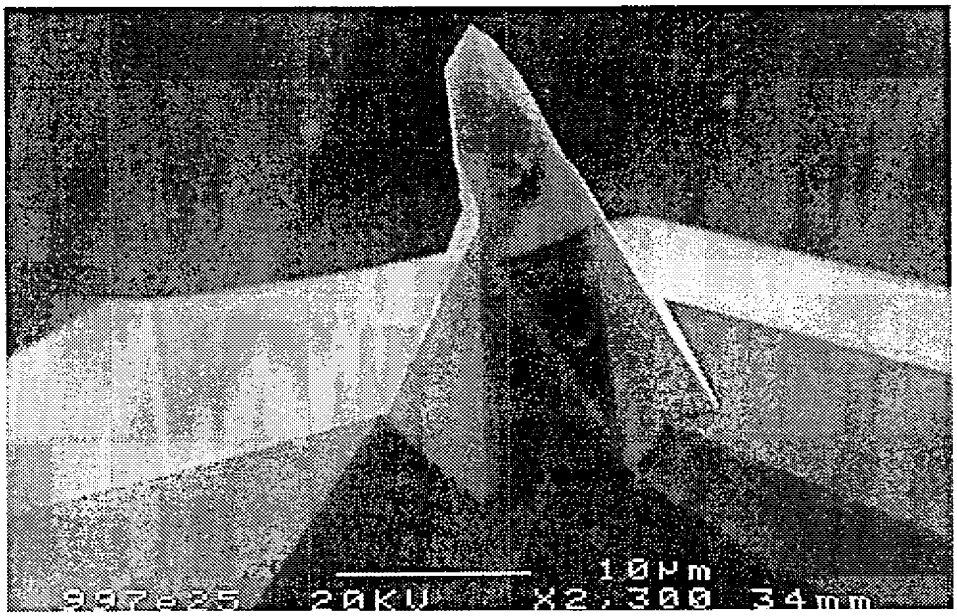

Fig. 7. Single crystal tip, for possible scanning microscopy applications.

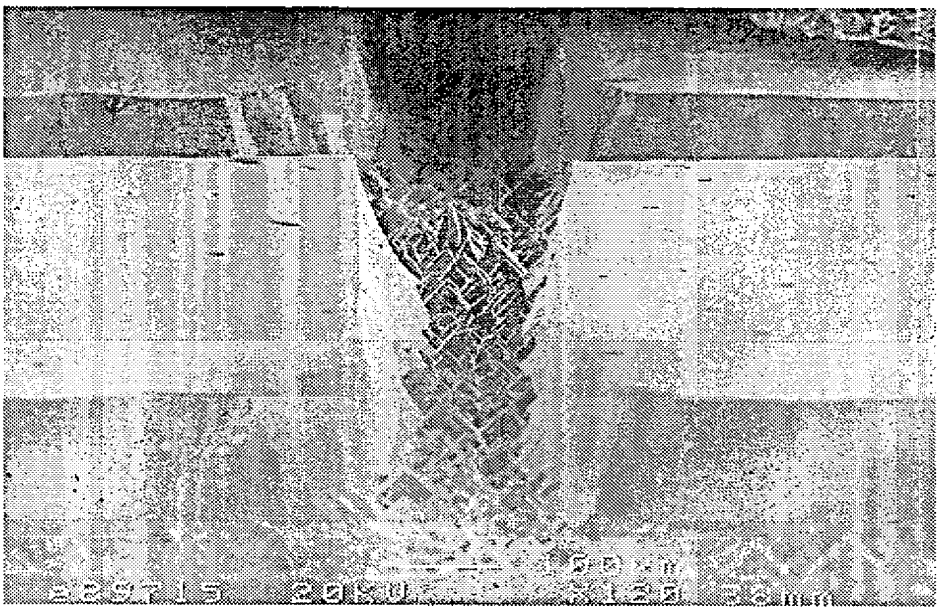

Fig. 9. Deep etching of trenches. The ~ 150 μm depth demonstrates independence of facet angle on number of separate etching steps, and feasibility of deep structures.

the expected Arrhenius law. Five temperatures from 21 to 95°C were used, but at the highest value, the etch rate was sufficiently fast to completely etch through the sample, preventing a quantitative determination of etch rate. Fig. 8 also indicates that at the highest temperature that can be used for boiling HF/HNO_3, which is 110°C, an etch rate of ~ 55 μm per hour is predicted. Repeated immersion of the sample did not affect the observed facet angles. The sample seen in Fig. 9 was immersed twice, and no change in etch behaviour was observed.

In summary therefore, a process consisting of domain patterning by electric field poling followed by etching in a 1:2 mixture of HF and HNO_3 acids has revealed a range of micro- and nanoscale structures. The surface quality appears extremely smooth and straight in directions parallel to the mirror planes of the crystal $3m$ symmetry, with surface roughness less than the 5 nm resolution available to us. The technique has produced ridge waveguides, alignment grooves, sharp tips and regular arrays of similarly shaped and equally sized holes. We are currently evaluating the technique for producing low loss ridge waveguides, and have defined a lower confinement layer using ion-beam implantation. The tip structures are under consideration for electro-optic sampling, near-field imaging microscopy, and other associated techniques.

Acknowledgements

The authors would like to acknowledge the Defence Evaluation Research Agency, and the Engineering and Physical Sciences Research Council for a postgraduate research award for Ian Barry. Thanks also go to Barbara Cressey, at the electron microscopy centre, for SEM facilities, and the microelectronics group for mask fabrication.

References

[1] A.M. Prokhorov, Yu. S. Kuz'minov, Physics and Chemistry of Crystalline Lithium Niobate' Adam Hilger, Bristol, 1990.
[2] L.E. Myers, R.C. Eckardt, M.M. Fejer, R.L. Byer, W.R. Bosenberg, J.W. Pierce, JOSA B 12 (1995) 2102.

[3] A.A. Oliver (Ed.), Acoustic Surface Waves, Topics in Applied Physics, Vol. 24, Springer-Verlag, 1978.
[4] J.L. Jackel, R.E. Howard, E.L. Hu, Appl. Phys. Lett. 38 (1981) 907.
[5] C.X. Ren, J. Yang, Y.F. Zheng, L.Z. Chen, G.L. Chen, S.C. Tsou, Nucl. Instr. Meth. B 19 (1987) 1018.
[6] F.K. Christensen, M. Müllenborn, Appl. Phys. Lett. 66 (1995) 2772.
[7] K.W. Beeson, V.H. Moulding, R. Beach, R.M. Osgood Jr., J. Appl. Phys. 64 (1988) 835.
[8] C.I.H. Ashby, P.J. Brannon, Appl. Phys. Lett. 49 (1986) 475.
[9] N. Niizeki, T. Yamada, H. Toyoda, Jpn. J. Appl. Phys. 6 (1967) 318.
[10] R.S. Cheng, W.L. Chen, W.S. Wang, IEEE Photon. Technol. Lett. 7 (1995) 1282.
[11] R.S. Weis, T.K. Gaylord, Appl. Phys. A 37 (1985) 191.

Jpn. J. Appl. Phys. Vol. 41 (2002) pp. 4825–4827
Part 1, No. 7B, July 2002

Fabrication of $LiNbO_3$ TE/TM Waveguides for 1.5 μm Wavelength Band by Zn/Ni Diffusion in Low-Pressure Atmosphere

Yasuaki SHIGEMATSU, Masatoshi FUJIMURA and Toshiaki SUHARA

Department of Electronics, Graduate School of Engineering, Osaka University, 2-1 Yamada-Oka, Suita, Osaka 565-0871, Japan

(Received December 17, 2001; accepted for publication March 8, 2002)

Zn-diffused waveguides can support both ordinary and extraordinary polarization modes and are expected to have high resistance to photorefractive damages. In this paper, fabrication of Zn:$LiNbO_3$ channel waveguides for 1.5 μm wavelength band by diffusing metallic Zn in low-pressure atmosphere is reported. The waveguides were fabricated under various conditions. It was found that pressure control during diffusion is crucial to obtain smooth diffused surface and to suppress Li_2O out-diffusion. Single-mode TE/TM waveguides with ~ 1 dB/cm propagation were obtained. The process is simple and has good reproducibility. [DOI: 10.1143/JJAP.41.4825]

KEYWORDS: lithium niobate, waveguide, Zn-diffusion, integrated optics, nonlinear optics

1. Introduction

$LiNbO_3$ waveguide quasi-phase-matched (QPM) nonlinear-optic (NLO) wavelength conversion devices have been studied for applications in optical communication systems, optical signal processing, etc. Annealed-proton-exchanged waveguides are widely used for such devices[1,2] because of their high resistance to photorefractive damage. However, they support only extraordinary guided modes, and they may suffer limitations in implementation of polarization-independent devices. Ti-diffused waveguides, which can support both ordinary and extraordinary guided modes, are also used.[3,4] But they involve notable photorefractive damage problem. The formation of unwanted domain inverted thin layer during the high temperature process for Ti diffusion may cause problems in fabrication of domain inverted gratings for QPM.[4]

Zn diffusion in $LiNbO_3$ takes place at relatively low temperature, and it can provide Zn-diffused waveguides which can support both polarization modes and are expected to have high resistance to photorefractive damages.[5] They are potentially suitable for applications to QPM-NLO devices.[6] We reported recently Zn-diffused $LiNbO_3$ waveguides for 1.5 μm wavelength band by diffusing from ZnO[7] and their application to QPM wavelength conversion devices.[8] There is also a report on the fabrication of the waveguides in y-cut $LiNbO_3$ for 1.32 μm wavelength by diffusing metallic Zn for applications to electrooptic (EO) devices.[9] However, fabrication techniques of Zn-diffused waveguides have not been fully established yet, especially for z-cut $LiNbO_3$.

In this study, we fabricated Zn-diffused $LiNbO_3$ waveguides for 1.5 μm wavelength band in z-cut $LiNbO_3$ by diffusing metallic Zn for applications to NLO devices. Pressure control during diffusion was crucial to obtain smooth surface after diffusion. We fabricated the waveguides under various conditions and clarified the condition to obtain TE/TM waveguides with good quality for 1.5 μm wavelength band.

2. Fabrication

Diffusion of metallic Zn into congruent optical-grade $LiNbO_3$ was examined. Although we tried to deposit Zn directly on the +z surface of $LiNbO_3$ crystal by thermal evaporation, the surface of the deposited Zn film was granular. Insertion of a thin Ni buffer layer was reported to allow deposition of the Zn film with uniform surface.[9] We first deposited Ni film of 5 nm thickness, and then deposited Zn on it. The Zn/Ni film was diffused using an ordinary quartz-tube electric furnace. The thermal diffusion in air of atmospheric pressure resulted in rough surface, as shown in Fig. 1(a). It was probably caused by Zn–$LiNbO_3$ reaction in the air. We tried the thermal diffusion in air of low-pressure atmosphere.[7] The quartz tube was evacuated by a rotary pump. The pressure was monitored with a Pirani gauge and was controlled by a throttle valve. We found that the smooth surface, as shown in Fig. 1(b), was obtained by diffusion in a low-pressure atmosphere of about 1.0 Torr. Thermal treatment in low-pressure accelerated Zn diffusion into $LiNbO_3$. Similar tendency was reported for Zn-diffused waveguide fabrication in vapor phase.[10] The pressure higher than 1.0 Torr resulted in rougher surface, and the lower pressure caused Li_2O outdiffusion.

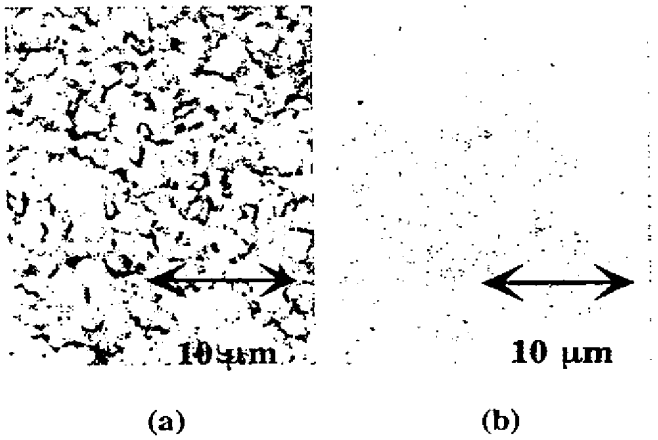

Fig. 1. Optical microscope photographs of the surfaces after diffusion at 890°C for 30 min in (a) atmospheric pressure and (b) 1.0 Torr.

Zn/Ni stripes of 4–8 μm width were patterned by lift-off technique, and diffused under various conditions for channel waveguide fabrication. The total thickness of Zn/Ni film, the diffusion temperature, the diffusion time ranged 100–200 nm, 830–950°C, 30–120 min, respectively. The pressure ranged from 1.0 to 30 Torr. After the thermal diffusion, the end facets

Table 1. Result of the optical guiding test of the fabricated channel waveguides.

	Fabrication conditions					Waveguiding characteristics					
	Diffusion			Zn/Ni stripe		Guiding mode s: single, m: multi		FWHM mode size Width/Depth		Throughput	
	Temperature,	Time,	Pressure	Width,	Thickness	TM	TE	TM	TE	TM	TE
#1	830°C,	30 min,	1.0 Torr	8.0 μm,	160 nm	m	s	8.0 μm/5.0 μm	8.5 μm/5.5 μm	21%	2%
#2	860°C,	30 min,	1.0 Torr	8.0 μm,	160 nm	m	s	7.5 μm/5.5 μm	8.5 μm/5.5 μm	22%	4%
#3	890°C,	30 min,	1.0 Torr	8.0 μm,	160 nm	m	s	8.6 μm/6.5 μm	8.6 μm/6.7 μm	31%	16%
#4	890°C,	120 min,	1.0 Torr	8.0 μm,	160 nm	—	—	14.6 μm/9.7 μm	13.7 μm/9.3 μm	20%	19%
#5	890°C,	30 min,	1.0 Torr	8.0 μm,	100 nm	m	s	13.0 μm/10.0 μm	19.5 μm/12.0 μm	17%	3%
#6	890°C,	30 min,	1.0 Torr	5.0 μm,	160 nm	—	—	—	—	—	—
#7	950°C,	30 min,	10 Torr	5.0 μm,	200 nm	s	s	13.3 μm/9.3 μm	13.3 μm/9.3 μm	17%	16%
#8	950°C,	30 min,	20 Torr	5.0 μm,	200 nm	s	s	9.7 μm/7.0 μm	9.7 μm/7.8 μm	42%	35%
#9	950°C,	30 min,	30 Torr	5.0 μm,	200 nm	s	s	—	—	9%	16%

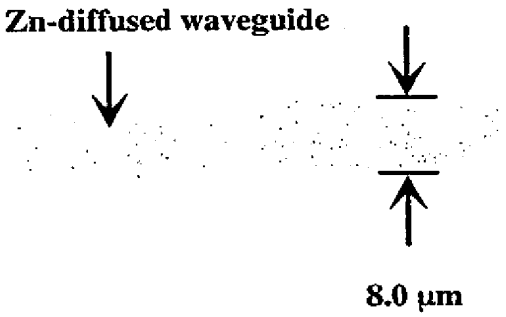

Fig. 2. The surface of Zn-diffused channel waveguide.

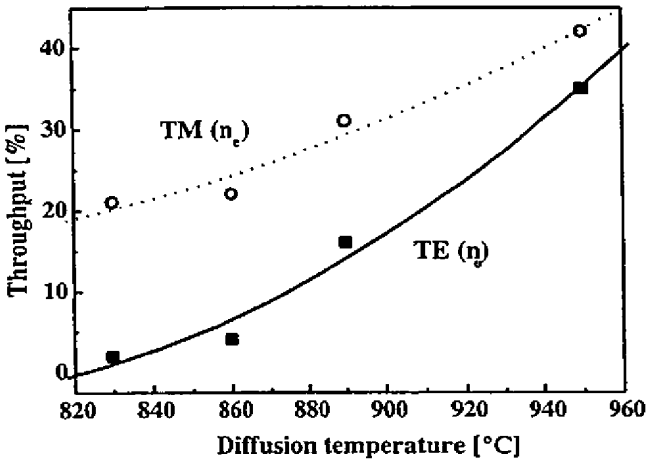

Fig. 3. The dependence of throughput on diffusion temperature.

were polished for end-fire coupling. The waveguide length was approximately 10 mm. The typical surface morphology of the crystal after diffusion is shown in Fig. 2. This sample was fabricated by diffusion at 890°C for 30 min in 1.0 Torr. Relatively smooth surface was obtained, though there was some residual that might cause a little propagation loss.

3. Characterization

The waveguiding characteristics at 1.55 μm wavelength were examined. A beam from a fiber-pigtailed laser diode was coupled into a waveguide using a 20× lens. We evaluated each waveguide by the full width at half-maximum (FWHM) mode size and throughput. The results are summarized in Table 1. In case of diffusion at 890°C, the waveguide #3 supported both polarization modes with relatively high throughput. In cases of diffusion at 830°C (#1) and 860°C (#2), TE mode showed quite low throughput. The waveguide #4 fabricated by diffusion for 120 min had larger mode size; they didn't have so good confinement as the waveguide #3 of 30 min diffusion. It seems to be because the diffusion was too deep. It was seen by comparing #3 and #5 that the Zn/Ni thickness should be about 160 nm. The waveguides diffused from Zn/Ni stripe of 8 μm width were multi-mode waveguides for TM mode. To make single-mode waveguides for both polarization modes, Zn/Ni stripe width should be about 5 μm. In case that the width is 5 μm, Zn/Ni stripe thickness needs to be about 200 nm. In addition, diffusion temperature has to be high. Under such conditions, the diffusion in 1.0 Torr progresses too rapidly and resulted in poor optical confinement. To make the diffusion rate slower, the pressure should be increased to approximately 20 Torr.

Figure 3 shows dependence of throughput on diffusion temperature. The higher the diffusion temperature was, the higher throughput and the smaller throughput differences between TM and TE modes we obtained. The reason for the dependence is under study. It is seen from Fig. 3 that the diffusion at higher temperature is favorable for the fabrication of waveguides with high throughput for both polarization modes. The best condition to fabricate single-mode channel waveguides with good confinement and high throughput for both polarizations is diffusion of Zn/Ni stripe with 5 μm width and 200 nm thickness at 950°C for 30 min in 20 Torr air.

Figure 4 shows the mode patterns in the waveguide fabricated by diffusion under the best condition. The FWHM mode sizes were 7.0 μm(depth) × 9.7 μm(width), and 7.8 μm × 9.7 μm for TM and TE modes, respectively. The propagation loss was measured as ~1 dB/cm for both modes

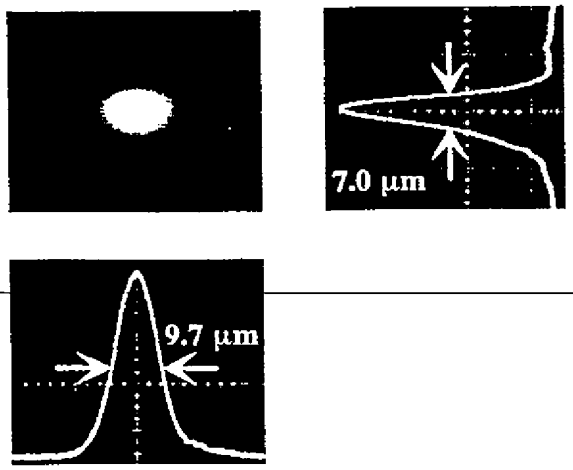

Fig. 4. Near field patterns of guided modes at 1.55 μm for (a) TM mode and (b) TE mode.

by the waveguide Fabry-Perót interference method using a temperature-tuned distributed feedback laser.

4. Conclusion

We studied fabrication of Zn-diffused $LiNbO_3$ waveguides by diffusing metallic Zn, and we found that diffusion in low-pressure atmosphere is crucial to fabricate the waveguides. We fabricated channel waveguides under various conditions and examined the waveguiding characteristics at 1.55 μm wavelength. Single-mode TE/TM waveguides for 1.5 μm wavelength band with $\sim$1 dB/cm propagation loss were obtained. The process is simple and has good reproducibility. Future work includes examination of the resistance of the Zn-diffused waveguides to photorefractive damages. More recently we applied these Zn-diffused waveguides for QPM wavelength conversion devices, and obtained encouraging results. The results will be reported elsewhere.

1) T. Suhara, H. Ishizuki, M. Fujimura and H. Nishihara: IEEE Photon. Technol. Lett. **11** (1999) 1027.
2) M. H. Chou, I. Brener, M. M. Fejer, E. E. Chanban and S. B. Christman: IEEE Photon. Technol. Lett. **11** (1999) 653.
3) H. Kanbara, H. Itoh, M. Asobe, K. Noguchi, H. Miyazawa, T. Yanagawa and I. Yokoyama: IEEE Photon. Technol. Lett. **11** (1999) 328.
4) D. Hofmann, G. Schreiber, C. Haase, H. Herrmann, W. Grundkotter, R. Ricken and W. Sohler: Opt. Lett. **24** (1999) 896.
5) W. M. Young, R. S. Feigelson, M. M. Fejer, M. J. F. Digonnet and H. J. Shaw: Opt. Lett. **16** (1991) 995.
6) T. Suhara: Microoptics News **18** (2000) No. 3, p. 19 [in Japanese].
7) T. Suhara, T. Fujieda, M. Fujimura and H. Nishihara: Jpn. J. Appl. Phys. **39** (2000) L864.
8) M. Fujimura, H. Ishizuki, T. Suhara and H. Nishihara: *Tech. Dig. CLEO/PR '01*, July 2001, Makuhari, ME1-5.
9) R. Twu, C. Huang and W. Wang: IEEE Photon. Technol. Lett. **12** (2000) 161.
10) B. Herreros and G. Lifante: Appl. Phys. Lett. **66** (1995) 1449.

15 February 2000

ELSEVIER

Optics Communications 175 (2000) 247–252

OPTICS COMMUNICATIONS

www.elsevier.com/locate/optcom

Studies of photorefractive crystals of double-doped Ce,Fe:$LiNbO_3$

Chunhui Yang *, Yequan Zhao, Rui Wang, Minghua Li

Department of Applied Chemistry, Harbin Institute of Technology, Harbin 150001, China

Received 29 July 1999; received in revised form 14 October 1999; accepted 6 December 1999

Abstract

In this paper, photorefractive crystals of Ce,Fe:$LiNbO_3$ are systematically studied. The crystals have been grown by the Czochralski method. Samples with various doping concentrations and oxidation/reduction treatment have been fabricated. Their photorefractive properties were experimentally investigated by using two-beam coupling. The results show that, compared with Ce:$LiNbO_3$ and Fe:$LiNbO_3$, the photorefractive effect of Ce,Fe:$LiNbO_3$ crystal was enhanced, and the photorefractive efficiency depends on the dopant concentration, oxidation/reduction treatment, and light wavelength. The doping mechanism is also discussed here.

Keywords: Photorefractive properties; Two-beam coupling; Ce,Fe:$LiNbO_3$ crystal

1. Introduction

Doped lithium niobate ($LiNbO_3$) crystals exhibit excellent photorefractive properties, and this attractive feature makes them important for applications in optical computing, image processing, phase conjugation, and laser hardening. Doping with transition metal or rare earth ions into crystals can affect efficiency, sensitivity, speed and spectral response of photorefractive effect. A great amount of studies on $LiNbO_3$ included crystals containing various dopants, such as Fe [1], Cr [2], Nd [3], Pr [4], Eu [5], Mg [6], Zn [7], Ce [8], and so on. Fe: $LiNbO_3$ crystal has been selected as one of holographic storage media for industrial use. It is due to the outstanding advantages as follows: (1) it can be easily grown from melt by Czochralski method; (2) its Curie temperature is very high (around 1200°C), so it is convenient during processing and applications; (3) its photorefractive effects are strong; and (4) there are some vacancies in the lattice, which makes it easy to introduce some dopants to tailor its photorefractive properties.

The effect of different dopants on the photorefractive effect of crystal is different. Two kinds of dopants were doped in $LiNbO_3$ in order to enhance its photorefractive effect, for example, the response time of Mg,Fe:$LiNbO_3$ is one magnitude faster than that of Fe:$LiNbO_3$ [9]. Double-doped Ce,Fe:$LiNbO_3$ crystal was grown in our lab in 1988, and has been proved as an excellent photorefractive material by

* Corresponding author. Fax: +86-451-622-1048; e-mail: yangchh@fmail.hl.cninfo.net

0030-4018/00/$ - see front matter
PII: S0030-4018(99)00753-1

the experimental results of two-beam coupling, four-wave mixing, and image processing [10–12]. In this paper, the growth and photorefractive properties are systematically reported.

2. Crystal growth and sample preparation

The starting materials used for crystal growth are ultra pure Li_2CO_3, Nb_2O_5, CeO_2 and Fe_2O_3. The congruent composition of Li:Nb = 0.946 was selected as melt and crystal compositions. Ce ions were added into the melts with the concentration of 0.1 mol.%, and Fe ions were with varying concentrations of 0.02 and 0.05 mol.%. The appropriately weighed materials were thoroughly mixed and calcined at 700°C and then sintered at 1150°C for 2 h, respectively.

Single crystals of Ce:$LiNbO_3$, Fe:$LiNbO_3$ and Ce,Fe:$LiNbO_3$ were pulled along c axis from the melt in a platinum crucible by Czochralski method. The sizes of crystals as grown are ~30–35 mm in diameter and 30–40 mm in length. Typical technique parameters for crystal growth are listed in Table 1.

All as-grown crystals show good symmetry and optical quality. The crystals were placed in a furnace where the temperature gradient is almost equal to zero for annealing and poling. After annealing at 1200°C for 8 h, the crystals were polarized with electric field at 5 mA/cm^2 for 30 min at the same temperature. Then the crystals were cut into samples with size of $12 \times 12 \times 2$ mm^3 ($a \times b \times c$).

As well-known, modest treatment of oxidation and reduction can change the valence state of the doped ions and the other defects' distribution, therefore affect the photorefractive effect of the crystal. In our experimental, in order to avoid introducing other impurities during oxidation and reduction, the powders of Nb_2O_5 and Li_2CO_3 were chosen as the oxidizing and reducing agents, respectively. The sample sheets were buried in the powdered Nb_2O_5 (or Li_2CO_3). The temperature of the oxidation was 1150°C, the treatment times were 24 h. The temperature of reduction and heavy reduction were 550°C, the treatment times were 24 and 36 h respectively. The treated samples were lapped and optically polished for characterization (see Table 2).

Table 1
Growth conditions for Ce:$LiNbO_3$, Fe:$LiNbO_3$ and Ce,Fe:$LiNbO_3$ crystals

Growth temperature	Temperature gradient	Growth atmosphere	Growth rate	Crystal rotation rate
1250°C	40°C/cm	air	2–3 mm/h	15–25 rpm

Table 2
Samples of Ce:$LiNbO_3$, Fe:$LiNbO_3$ and Ce,Fe:$LiNbO_3$ crystals

No.	CeO_2 (mol.%)	Fe_2O_3 (mol.%)	Treatment	Color
1	0	0	as grown	pale yellow
2	0.10	0	reduction	pale brown
3	0	0.05	reduction	red
4	0.10	0.02	as grown	rose red
5	0.10	0.02	reduction	heavy red
6	0.10	0.05	as grown	red
7	0.10	0.05	oxidation	pink
8	0.10	0.05	reduction	brown red
9	0.10	0.05	heavy reduction	red black

3. Optical absorption properties

The absorption spectra were obtained with non-polarized light and shown in Fig. 1. There is a broad absorption band located at 460–550 nm, which is induced by Fe^{2+} ions and oxygen vacancies $V_O^{\cdot\cdot}$ [13]. It is obviously that with more Fe ions in the crystal the absorption becomes heavier.

The influences of oxidation and reduction are also clearly observed. The intensity of the absorption

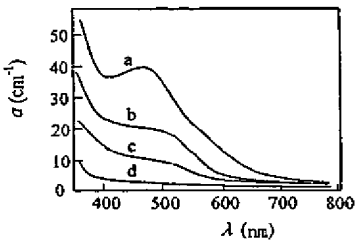

Fig. 1. Absorption spectra of CeO_2(0.10 mol.%),Fe_2O_3(0.50 mol.%):$LiNbO_3$ crystals: (a) No. 9 sample with heavy reduction; (b) No. 8 sample with reduction; (c) No. 6 sample as grown; and (d) No. 7 sample with oxidation.

band at 460–550 nm increases as reduction, and decreases as oxidation. That is resulted in the reactions that Fe^{2+} ions and oxygen vacancies $V_O^{\cdot\cdot}$ are induced by reduction treatment, but eliminated by oxidation treatment. The effects of these treatments on photorefractive properties will be studied and discussed later.

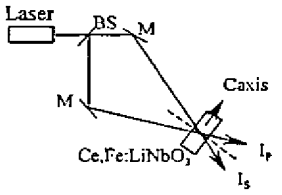

Fig. 2. Experimental set-up of two-beam coupling. BS: beam splitter, M: reflect mirror.

4. Two-beam coupling: theory

When two coherent laser beams incident into a photorefractive crystal, in which the C axis was oriented to be in the incident plane and perpendicular to the bisector of the two beams, beam coupling occurs, and causes one beam (signal beam) to gain intensity at the expense of the other beam (pump beam). The exponential gain coefficient of two-beam coupling Γ is experimentally measured through the relation [14,15].

$$\Gamma = \frac{1}{L}\ln\frac{I_s' I_p}{I_s I_p'} \tag{1}$$

where L is the interaction length of the two beams in crystal (taken as the thickness of the sample), I_s' (I_s) is the transmitted signal beam intensity with (without) coupling, and I_p' (I_p) is the transmitted pump beam intensity with (without) coupling. When the intensity of pump beam is much larger than that of signal beam, $I_p \gg I_s$, the two-beam coupling gain coefficient Γ becomes independent of the pump beam intensity (i.e. $I_p' \approx I_p$).

$$\Gamma = \frac{1}{L}\ln\frac{I_s'}{I_s}. \tag{2}$$

The two-beam coupling gain coefficient Γ is related to the photorefractive index grating amplitude δn (defined as one-half the peak-to-peak value) by [16]

$$\Gamma = 4\pi\,\delta n \sin\phi/m\lambda\cos\theta_I \tag{3}$$

where θ_I is the half angle between the beams inside the crystal, ϕ is the phase shift between the optical interference pattern and the photorefractive index grating, and m is the modulation depth of the incident optical interference pattern, $m = 2\sqrt{I_p I_s}/(I_p + I_s)$. The photorefractive index modulation δn is given by

$$\delta n = n^3 r_{\text{eff}} E_{SC}/2 \tag{4}$$

where E_{SC} is the space-charge electric field, n is the refractive index, and r_{eff} is the effective electro-optic coefficient. The photorefractive space-charge field E_{SC} is given by [17]

$$E_{SC} = m(k_B T/e)\left[K/(1+(K/K_0)^2\right]\zeta(K)\cos 2\theta_I \tag{5}$$

where $2\theta_I$ is the internal full crossing angle of the optical beams and $k_B T/e$ is the thermal energy per charge. The factor $\zeta(K)$ takes into account competition between holes and electrons.

An important parameter in Eq. (5) is the inverse Debye screen length K_0,

$$K_0^2 = e^2 N_{\text{eff}}/(\varepsilon\varepsilon_0 k_B T) \tag{6}$$

which depends on the effective density of photorefractive charge N_{eff} and the dc dielectric constant $\varepsilon\varepsilon_0$ along the direction of the grating wave vector K.

Combining Eqs. (1)–(6), the gain coefficient Γ can be written in the form:

$$\Gamma = \left[A\sin\theta/(1+B^{-2}\sin^2\theta)\right](\cos 2\theta_I/\cos\theta_I) \tag{7}$$

where θ is the external half angle and θ_I is the internal half angle between the two incident laser beams. Here we have assumed that the hole–electron competition factor $\zeta(K)$ in constant with K in order to simplify the data analysis.

The parameter A is proportional to the effective Pockels coefficient r_{eff}:

$$A = r_{\text{eff}}\zeta(K)\frac{8\pi^2 n^3 k_B T}{e\lambda^2} = \partial\Gamma/\partial\theta|_{\theta=0} \tag{8}$$

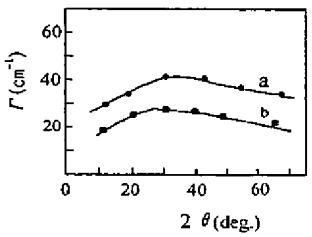

Fig. 3. Experimental curves of Γ vs. 2θ where the input beams wavelength is 488.0 nm. (a) No. 8 sample of CeO_2(0.10 mol.%),Fe_2O_3(0.05 mol.%):$LiNbO_3$; (b) No. 5 sample of CeO_2(0.10 mol.%),Fe_2O_3(0.02 mol.%):$LiNbO_3$ with reduction treatment.

and is determined by the slope of the plot of Γ vs. 2θ near $\theta = 0$. The parameter B is related to the effective photorefractive charge density N_{eff}:

$$B = \frac{\lambda K_0}{4\pi} = \frac{e\lambda}{4\pi}\sqrt{\frac{N_{\text{eff}}}{\varepsilon\varepsilon_0 k_B T}} \approx \sin\theta_{\text{peak}} \tag{9}$$

and is determined by $2\theta_{\text{peak}}$, the crossing angle at which the gain Γ (2θ) reaches its maximum value. We can obtain the effective photorefractive charge density N_{eff}, an important parameter, from the experimental curve of Γ vs. 2θ:

$$N_{\text{eff}} = \left(\frac{4\pi}{e\lambda}\right)^2 \varepsilon\varepsilon_0 k_B T \sin^2\theta_{\text{peak}}. \tag{10}$$

5. Two-beam coupling: experimental results and discussion

The experimental set-up is shown in Fig. 2. An Ar^+ ion laser and a He–Ne laser were used as light sources respectively. The two-beam coupling gain coefficient Γ was measured in Ce:$LiNbO_3$, Fe:$LiNbO_3$, and Ce,Fe:$LiNbO_3$ crystals to determine the effective charge density N_{eff}. The transmitted powers of both the weak signal beam and the strong pump beam were measured with and without coupling. The beam diameters were sufficiently large of 2.5 mm so that the interaction length L of the two beams was limited by the physical length of the sample. The pump/signal intensity ratio I_p/I_s was 3260, the pump beam intensity I_p is 4.62 W/cm^2. The input beams was extraordinary polarization. This range was a compromise that would minimize pump depletion. An iris with a diameter of 1.0 mm was placed in front of the power detector to minimize the influence of scattering light and to stop all higher diffraction lights.

5.1. Dopant dependence

Fig. 3 shows the dependence of the steady-state two-beam coupling gain coefficient Γ on the crossing angle between the two beams 2θ. They are not compared well with the theoretical plot. It is due to the stronger light crawling effect in the thinner samples [10]. So the crystals show a large angle range in which the gain coefficient is higher and the plots look flatter. The parameter N_{eff} can be determined from Eq. (10) by using some related parameters of doped $LiNbO_3$ crystals as follows: $e = 1.602 \times 10^{-19}$ C, $T = 300$ K, $\lambda = 4.88$ (or 5.145, or 6.328) $\times 10^{-5}$ cm, $k_B = 1.38 \times 10^{-23}$ J/K, and $\varepsilon\varepsilon_0 = 2.832 \times 10^{-12}$ C^2/J cm. N_{eff} values determined for double and singly doped crystals are listed in Table 3.

Compared with the Ce:$LiNbO_3$, the N_{eff} value of Ce,Fe:$LiNbO_3$ dramatically increases. While compared with that of Fe:$LiNbO_3$, the increase of that of Ce,Fe:$LiNbO_3$ is not so obvious. So Fe ions still as primary photorefractive centers play important roles in crystal, and Ce ions as assistants play roles. Overall, the photorefractive effect of Ce,Fe:$LiNbO_3$

Table 3
Photorefractive parameters of Ce,Fe:$LiNbO_3$ crystals

No.	Crystal	Treatment	Wavelength λ (nm)	Absorption α (cm^{-1})	Gain Γ (cm^{-1})	2θ (°)	N_{eff} (cm^{-3})
2	Ce:$LiNbO_3$	reduction	488.0	3.6	24.0	9.0	0.2×10^{15}
3	Fe:$LiNbO_3$	reduction	488.0	21.1	36.4	31.0	2.2×10^{15}
8	Ce,Fe:$LiNbO_3$	reduction	488.0	21.2	41.7	36.0	2.9×10^{15}

Table 4
Photorefractive parameters of Ce,Fe:$LiNbO_3$ crystals

No.	Treatment	Wavelength λ (nm)	Absorption α (cm^{-1})	Gain Γ (cm^{-1})	2θ (°)	N_{eff} (cm^{-3})
5	reduction	488.0	15.7	28.4	28.4	1.8×10^{15}
6	as grown	488.0	11.3	22.2	20.6	1.0×10^{15}
7	oxidation	488.0	1.6	9.8	18.8	0.8×10^{15}
8	reduction	488.0	21.2	41.7	36.0	2.9×10^{15}
9	heavy reduction	488.0	39.0	38.6	44.8	4.4×10^{15}
8	reduction	514.5	16.2	39.7	30.5	1.9×10^{15}
8	reduction	632.8	0.7	27.8	8.7	0.1×10^{15}

was enhanced compared with that of singly doped crystal.

Table 4 shows the effect of dopant concentration on the photorefractive properties of Ce,Fe:$LiNbO_3$ crystal. Comparing the experimental results of No. 5 and No. 8 samples, we can find that the larger the dopant concentration, the larger the N_{eff} value.

5.2. Oxidation / reduction treatment dependence

It is obviously that N_{eff} values are affected by the oxidation/reduction treatments greatly. The effective charge density N_{eff} can be written as [18]

$$N_{eff} = \frac{N_A(N_D - N_A)}{N_D}. \tag{11}$$

It actually is the relative concentrations of the donor center N_D and trap center N_A. Total dopant concentration $N = N_D + N_A$. So, proper oxidation/reduction treatment will change the photorefractive efficiency more effectively than the variety of the dopant concentrations, because the proper donors and traps are the key important factors in photorefractive process. And the photo-charge in crystal transports primarily by the diffusion when the concentration of Fe dopant is lower and the ratio of Fe^{2+} to Fe^{3+} is higher; While the photo-charge transports primarily by the photovoltaic effect when the concentration of Fe dopant is higher and the ratio of Fe^{2+} to Fe^{3+} is lower [19].

5.3. Absorption dependence

Photorefractive absorption coefficient α is defined as [18]

$$\alpha = \sigma_e N_D - \sigma_h N_A \tag{12}$$

where σ_e and σ_h are photoionization cross sections of electron and hole, respectively. If there is only one kind of charge carrier, Eq. (12) can be simplified as

$$\alpha = \sigma(N_D + N_A). \tag{13}$$

The effect of absorption on N_{eff} is due to the concentration difference between donor and trap $(N_D + N_A)$. As the wavelength becomes longer, the absorption of crystal is lower and lower, so, the value of N_{eff} decreases (Table 3).

6. Conclusion

In summary, we have grown a series of $LiNbO_3$ crystals co-doped with Ce- and Fe-ions in different levels and fabricated them into experimental samples available to photorefractive property measurement. The absorption spectra were studied in the wavelength range of 300–700 nm. Compared with the singly doped $LiNbO_3$, the photorefractive effect of Ce,Fe:$LiNbO_3$ was enhanced. With higher dopant concentration in the crystal, its absorption and two-beam coupling gain coefficients increase. Oxidation and/or reduction treatments have a significant effect on photorefractive properties of crystal. To get the optimal photorefractive properties, both the dopant concentration and proper oxidation/reduction condition must be taken into consideration. Double doped Ce,Fe:$LiNbO_3$ crystal shows itself a very promising photorefractive material.

Acknowledgements

This work was supported by High Technology Research and Development Program of China.

References

[1] G.W. Burr, D. Psaltis, Opt. Lett. 21 (1996) 893.
[2] A.P. Skvortsov, V.A. Trepakov, L. Jastrabik, J. Lumin. 72 (1997) 7116.
[3] G. Lifante, F. Cusso, F. Jaque, J.A. Sanz-Garcia, A. Monteil, B. Varrel, G. Boulon, J. Garcia-Sole, Chem. Phys. Lett. 176 (1991) 482.
[4] A. Lorenzo, L.E. Bausa, J. Garcia-Sole, Phys. Rev. B 51 (1995) 623.
[5] L. Arizmendi, J.M. Cabrera, Phys. Rev. B 31 (1985) 7138.
[6] K.L. Sweeney, L.E. Halliburton, D.A. Bryan, J. Appl. Phys. 57 (1985) 1036.
[7] V.R. Volk, V.I. Pryalkin, N.M. Rubinina, Opt. Lett. 15 (1990) 996.
[8] J. Liu, M. Li, Y. Xu, Ferrolectrics 168 (1995) 127.
[9] M. Li, J. Wang, Y. Zhao, A. Han, Chin. J. Infrared Millimeter Wave 14 (1995) 443.
[10] J. Zhang, W. Sun, H. Zhao, S. Bian, K. Xu, M. Li, Y. Xu, Opt. Lett. 18 (1993) 1391.
[11] M. Li, J. Wang, Y. Xu, K. Xu, Chin. J. Rare Earth 13 (1995) 302.
[12] M. Li, X. Jia, L. Liang, Acta Opt. Sin. 13 (1995) 229.
[13] O.F. Schirmer, O. Thiemann, M. Wohlecke, J. Phys. Chem. Solids 52 (1991) 185.
[14] M.D. Ewbank, R.R. Neurgaonkar, W.K. Cory, J. Feinberg, J. Appl. Phys. 62 (1987) 374.
[15] A. Marrakchi, J.P. Huignard, P. Gunter, Appl. Phys. 24 (1981) 131.
[16] P. Gunter, Phys. Rep. 93 (1982) 199.
[17] F.P. Strohkendl, J.M.C. Jonathan, R.W. Hellwarth, Opt. Lett. 11 (1986) 312.
[18] R.A. Vazquez, R.R. Neurgaonkar, M.D. Ewbank, J. Opt. Soc. Am. B 9 (1992) 1416.
[19] E. Kratzig, R. Orlowski, Ferroelectrics 27 (1980) 241.